PH and SPO^2 miniaturized sensors for fetal health monitoring

Thi Thanh Thuy Nguyen

Thesis

PH AND SPO_2 MINIATURIZED SENSORS FOR FETAL HEALTH MONITORING

Author
NGUYEN Thi Thanh Thuy

Supervisors
Gaëlle LISSORGUES and Hakim TAKHEDMIT (ESYCOM)

Advisors
Bernard JOURNET (ENS Paris Saclay) and Edouard Lecarpentier (IMRB, Inserm)

Jury

Reviewers	Mme Blanquet Elisabeth, SIMaP, DR
	M Feruglio Sylvain, LIP6, MCF HDR
Examinators	M Bernard Serge, LIRMM, DR
	M Henry Olivier, IMEC, CR
Director/Supervision	Mme Lissorgues Gaelle, ESYCOM, PR
Co-supervision	M Takhedmit Hakim, ESYCOM, MCF
Invited members	M Journet Bernard, ENS Paris Saclay, MCF
	M Lecarpentier Edouard, IMRB, HDR

Submitted in total fulfilment of the requirements of the degree of Doctor of Philosophy

May 2023.

Acknowledgements

This project has ignited a profound passion within me and its meaningful purpose has sustained my motivation from the very beginning to the end.

Sincere thanks to Prof. Gaelle LISSOGUES and prof Edouard LECARPENTIER, who came up with this very meaningful idea to aid a multitude of future babies and mothers.

First and foremost, I would like to express my deep gratitude to my supervisor/director Prof. Gaelle LISSOGUES. Her guidance, patience, and companionship have helped me overcome all difficult phases of the project. Additionally, I would like to express my deep appreciation to her very kind attention to my future career and her care in every other aspects of my life. I would like to give my warmest thanks to my co-supervisor Prof. Hakim TAKHEDMIT. Their advices and guidance made this work become possible.

I also could not have completed this journey without my defense committee, who generously provided me with their knowledge and expertise.

Thanks should also go to the support that I received in ESIEE/ESYCOM, clean room training by Lionel ROUSSEAU, Alexandre BONGRAIN, Serge DIDELON, Frederic MARTY and Nicolas PAVY, technical support by Julien PAGAZANI, and the contribution of Antoine BESSIERE. In ENS Paris Saclay, I would like to acknowledge the contribution from Quentin ROUSSET and Simon L'HORSET.

I would like to thank Prof Edouard LECARPENTIER for his follow-up and consultation on medical aspect, and the in vivo technical support from Audrey RIDOUX at Animal Facility of IMRB, Inserm – University Paris Est Créteil.

I would like to also give a heartfelt thanks to my office mates, Ummetabassum SARAH, Claudia WILFINGER, Antonella ALNAJJAR, Jaafar ALSINAYYID, Issam KURY, Jordan ROY, for their significant moral support and invaluable friendship.

A special appreciation to Prof. Bernard JOURNET, ENS Paris Saclay, for his very kind guidance and support to our research. Thank you for your continuous help since I was still a college student in Vietnam. I once said, thank you for making France so familiar and full of peace, from lecture halls to life. For me, you are family.

Last but not the least, thank to my family and my husband, Tu DUONG, the person who has loved me unconditionally, who has provided me with courage and good foods, who travels every weekend between Belgium and France to support my career. I would also like to thank my cat, Quyt, and my dog, Oi, for your companionship and emotional support. The love from my family for me was what sustained me this far.

This is a memorable journey in France, met the kindest people, and contributed to this meaningful work.

Résumé

CAPTEURS MINIATURISÉS DE PH ET DE SPO2 POUR LA SURVEILLANCE CONTINUE DE LA SANTÉ FŒTALE

La surveillance du bien-être du fœtus pendant le travail est une pratique courante dans les activités obstétricales quotidiennes. Assurer une bonne oxygénation du fœtus est important pour prévenir le risque d'asphyxie et ses conséquences les plus graves : la mort péripartum et les séquelles à distance, en particulier les troubles neurologiques. Dans ce travail, nous définissons l'importance de la mesure du pH et de la saturation en oxygène ou SpO_2 pour la santé humaine en général et la surveillance de la santé fœtale en particulier. L'aspect biologique du déséquilibre du pH et la pertinence de la SpO_2 sont expliqués, ainsi que la nécessité d'une mesure en temps réel afin de surmonter les limites de la technique actuelle d'analyse du sang. Un prototype, qui constitue une première tentative de surveillance continue de la santé du fœtus pendant le travail, est conçu et fabriqué dans cette thèse. Ce système est capable de mesurer simultanément le pH, la SpO_2 et de fournir un photopléthysmogramme (PPG) clair en temps réel. La microélectrode constitutive du capteur de pH a été fabriquée en utilisant du nitrure de titane (TiN) comme matériau de détection potentiométrique pour les variations de pH. Un capteur optique à réflectance a été utilisé pour la surveillance de la SpO_2. Les sondes de pH et de SpO_2 sont de dimensions réduites au minimum et fabriquées sur un substrat souple (polyimide) afin de respecter les contraintes futures de tests in-vivo.

L'exigence la plus critique du capteur de pH pour la surveillance de la santé du fœtus est une précision de 0.01 unité de pH, avec une conception miniaturisée appropriée. Les capteurs de pH potentiométriques sont les systèmes électrochimiques les plus courants en raison de leur conception simple et de la possibilité de les miniaturiser. Il existe évidemment différents groupes de matériaux sensibles aux variations de pH, par exemple les oxydes métalliques tels que l'oxyde d'iridium (IV) (IrO_2), l'oxyde de ruthénium (IV) (RuO_2), le trioxyde de tungstène (WO3) et le dioxyde de titane (TiO_2), les polymères conducteurs tels que la poly-aniline, le poly-pyrrole, etc. et, typiquement, l'électrode de pH en verre avec une sensibilité de Nernst idéale. Toutefois, ces dispositifs présentent encore quelques inconvénients en termes de dérive potentielle et de sélectivité (oxydes métalliques), de stabilité et de stockage à long terme (polymères), de fragilité et de non adaptation au contexte biomédical implantable (électrode de verre). Le nitrure métallique est un autre groupe de matériaux prometteur pour le développement d'un capteur de pH potentiométrique. Un exemple de la littérature a montré que des films minces de nitrure de titane pouvaient permettre

d'atteindre une précision de 0.01 pH, ce qui est essentiel pour notre application, mais ces films n'ont pas été conçus pour des électrodes miniatures. À notre connaissance, le nitrure de titane est le seul nitrure métallique rapporté pour les capteurs de pH potentiométriques, et il est considéré comme un matériau alternatif de détection du pH. Par conséquent, la première partie de notre travail se concentre sur le développement d'un micro-capteur de pH potentiométrique en TiN en salle blanche avec sa caractérisation complète in vitro.

En complément, un capteur de SpO_2 par réflectance a été conçu, utilisant deux LED à 630 nm et 940 nm de longueur d'onde avec une photodiode à large bande, le tout contrôlé par un microcontrôleur MSP432. Plusieurs versions du capteur SpO_2 ont été fabriquées. Les résultats enregistrés par le premier prototype du circuit imprimé classique de type PCB montrent un comportement proche de celui d'un dispositif commercial. Nous avons optimisé le circuit d'amplification et l'avons transféré sur un circuit imprimé flexible, en fabriquant un deuxième prototype. Enfin, nous avons mis au point un prototype de capteur SpO_2 miniature sur un substrat souple, qui pourrait enregistrer le signal PPG brut et être utilisé comme outil de mesure supplémentaire pour valider notre mesure du pH. À ce stade des travaux, les capteurs de pH et SPO_2 sont séparés, mais un ensemble intégré est envisagé pour la prochaine étape, en utilisant à la fois un circuit électronique flexible pour le SpO_2 et un substrat flexible pour le capteur de pH. Ce travail d'intégration devrait permettre d'obtenir un dispositif intégrant tous les capteurs mentionnés ci-dessus dans une solution flexible pour des tests in vivo ultérieurs, mais compatible avec les contraintes médicales (biocompatibilité des matériaux, stérilisation, manipulation aisée du dispositif final par le personnel médical...).

Les principales contributions et résultats sont les suivants :

- Un procédé de microfabrication développé et optimisé sur polyimide souple

- Un nouveau matériau d'électrode de travail testé (TiN standard et poreux)

- Plusieurs niveaux de masques conçus et mis en œuvre

- Un protocole complet de caractérisation in vitro développé et utilisé pour toutes les sondes (OCV, CV, PEIS, influence de la température)

- Le développement d'un capteur de SpO2 permettant l'enregistrement continu des données PPG

- Des tests préliminaires in-vivo effectués sur des souris montrant la preuve de concept

- Une sensibilité et une précision du capteur de pH proches de l'objectif attendu pour l'application fœtale (précision atteinte jusqu'à 0.02 unité selon les capteurs), compte tenu des contraintes de miniaturisation et de matériaux.

Résumé du chapitre 1

Cette thèse a été organisée en collaboration avec trois partenaires : Le laboratoire ESYCOM (UMR 9007 CNRS), où l'essentiel du travail a été réalisé ; l'ENS Paris Saclay, qui a assuré la supervision de la partie SpO_2 ; et le Centre Hospitalier Intercommunal de Créteil (CHIC) avec l'Institut Mondor de Recherche Biomédicale (IMRB) - UMR 955, qui a contribué aux aspects médicaux et in vivo. L'application médicale a été proposée par le Professeur Edouard Lecarpentier de l'INSERM et sera décrite en détail dans le chapitre d'introduction.

- La surveillance du bien-être fœtal pendant le travail est une pratique courante des activités obstétricales quotidiennes. Assurer une bonne oxygénation du fœtus est important pour prévenir le risque d'asphyxie et ses conséquences les plus graves : le décès péripartum et les séquelles à distance, en particulier les troubles neurologiques, y compris le handicap psychomoteur ou l'infirmité motrice cérébrale. Dans ce chapitre, nous définissons l'importance de la mesure du pH et de la SpO_2 pour la santé humaine en général et la surveillance de la santé fœtale en particulier. L'aspect biologique du déséquilibre du pH et sa pertinence pour la SpO_2 sont expliqués, ainsi que la nécessité d'une mesure en temps réel afin de dépasser les limites de la technique actuelle d'analyse du sang.

- L'objectif principal de la thèse est de concevoir un prototype, qui constitue une première tentative de surveillance continue de la santé du fœtus pendant le travail. Le système décrit dans cette étude est capable de mesurer simultanément le pH, la SpO_2 et de fournir un photopléthysmogramme clair en temps réel.

Résumé du chapitre 2

L'exigence la plus importante d'un capteur de pH pour la surveillance de la santé fœtale est une précision de 0.01 unité de pH, avec une conception miniaturisée appropriée. Les capteurs de pH potentiométriques sont les systèmes électrochimiques retenus en raison de leur conception simple et de la possibilité de les miniaturiser. Il existe évidemment différents groupes de matériaux sensibles aux variations de pH, par exemple les oxydes métalliques, les polymères conducteurs, etc. Toutefois, ces dispositifs présentent encore certains inconvénients en termes de dérive potentielle et de sélectivité (oxydes métalliques), de stabilité et de stockage à long terme (polymères), de fragilité et non adaptation aux tests in-vivo. Il est donc difficile de procéder à une validation médicale. Un autre groupe de matériaux prometteur pour le développement d'un capteur de pH potentiométrique est les nitrures métalliques. Certains matériaux tels que le nitrure de ruthénium (RuN), les nitrures de carbone (α-BC_xN_y) et le nitrure de silicium (Si_3N_4) ont été principalement utilisés pour les capteurs de pH de type transistor à effet de champ sélectif d'ions (ISFET). Fait remarquable, des films minces de nitrure de titane (TiN) ont été signalés une fois pour atteindre une précision de 0.01 pH, ce qui est essentiel pour notre application, mais ces films n'ont pas été

conçus pour des électrodes miniatures. À notre connaissance, le nitrure de titane (TiN) est le seul nitrure métallique rapporté pour les capteurs de pH potentiométriques, et il est considéré comme un matériau alternatif de détection du pH. Par conséquent, la première partie de notre travail se concentre sur le développement d'un micro-capteur de pH potentiométrique en TiN.

Résumé du chapitre 3

Dans ce chapitre, nous présentons un prototype qui est notre première tentative pour obtenir une mesure continue de la SpO_2 et fournir un photopléthysmogramme (PPG) clair en temps réel, considéré comme une mesure complémentaire de seconde ligne sur le fœtus pendant le travail. Ce travail vise à fabriquer un capteur de SpO_2 capable d'enregistrer les signaux bruts d'oxymétrie de pouls à des fins de recherche biologique. En outre, la mesure de la SpO_2 est utile pour évaluer notre mesure du pH car il existe une corrélation entre une faible oxygénation des tissus et un pH plus bas. Un capteur de SpO_2 par réflectance a été conçu, utilisant deux LED à 630 nm et 940 nm de longueur d'onde avec une photodiode à large bande, contrôlé par un microcontrôleur MSP432. Plusieurs versions du capteur SpO2 ont été fabriquées. Les résultats enregistrés par le premier prototype sur PCB montrent un comportement proche de celui d'un dispositif commercial. Nous avons optimisé le circuit, en fabriquant un deuxième prototype. D'autres développements visant à améliorer la précision du capteur ont été envisagés sur la base de cette étude préliminaire.

Conclusion

Dans ce travail, nous définissons l'importance de la mesure du pH et de la SpO_2 pour la santé humaine en général et la surveillance de la santé fœtale en particulier. L'aspect biologique du déséquilibre du pH et la pertinence de la SpO_2 sont expliqués, ainsi que la nécessité d'une mesure en temps réel afin de surmonter les limites de la technique actuelle d'analyse du sang. Un prototype, qui constitue une première tentative de surveillance continue de la santé du fœtus pendant le travail, est conçu, fabriqué et testé de façon complète in-vitro puis in-vivo. La microélectrode constitutive du capteur de pH a été fabriquée en utilisant du nitrure de titane (TiN) comme matériau de détection potentiométrique pour les variations de pH. Un capteur optique à réflectance a été utilisé pour la surveillance de la SpO_2. Les sondes de pH et de SpO_2 sont de dimensions réduites au minimum et fabriquées sur un substrat souple pour les derniers prototypes (polyimide).

La première partie du travail concerne sur le développement d'un micro-capteur de pH potentiométrique TiN en salle blanche avec sa caractérisation complète in vitro. La seconde partie est une étude complémentaire, dans laquelle nous présentons un prototype qui constitue notre première tentative pour obtenir une mesure continue de la SpO_2 et qui fournit un photopléthysmogramme clair en temps réel, considéré comme une mesure dite de seconde

ligne sur le fœtus pendant l'accouchement. Nous rappelons que la mesure de la SpO_2 est utile pour évaluer notre mesure du pH, car il existe une corrélation entre une faible oxygénation des tissus et un pH plus bas.

Nous avons également envisagé de nouvelles applications médicales, par exemple la détection de l'ischémie cardiaque. De nouveaux tests sont en cours sur différents modèles animaux à l'Ecole Vétérinaire d'Alfort pour compléter le travail dans un futur proche.

En tant que perspectives, dans la forme finale du dispositif, les électrodes pH flexibles pourraient être considérées comme étant attachées à une aiguille spécifique, qui est adaptable à l'insertion cutanée clinique. Cette aiguille de détection du pH sera fixée à la carte de détection de la SpO_2 à l'aide d'un substrat de polyimide flexible dans un boitier personnalisé.

Abstract

Monitoring fetal well-being during labor is a common practice of daily obstetrical activities. Ensuring the good oxygenation of the fetus is important to prevent the risk of asphyxiation and its most serious consequences: peripartum death and distant sequelae, in particular neurological disorders. In this work, we define the significance of pH and SpO_2 measurement to human health in general and fetal health monitoring in particular. Biological aspect of pH imbalance and the relevant to SpO_2 is explained, along with the need of real time measurement in order to get over the limitation of the current blood analyzing technique. A prototype, which is a first attempt to get continuous fetal health monitoring during labor, is designed and fabricated. This system is capable of simultaneously measuring pH, SpO_2 and provides a clear photoplethysmogram (PPG) in real time. Microelectrode was fabricated using Titanium nitride (TiN) as the potentiometric sensing material for pH variations. A reflectance optical sensor was used for SpO_2 monitoring. Both pH and SpO_2 probes are minimized and fabricated on flexible substrate (polyimide).

The most critical requirement of the pH sensor for fetal health monitoring is a precision of 0.01 in pH, with an appropriate miniaturized design. Potentiometric based pH sensors are the most favored electrochemical systems due to their simple design and possibility to be miniaturized. Evidently, there are different material groups that are sensitive to pH change, for example metal oxides such as Iridium (IV) oxide (IrO_2), Ruthenium (IV) oxide (RuO_2), Tungsten trioxide (WO_3) and Titanium dioxide (TiO_2), conductive polymers such as poly-aniline, poly-pyrrole, etc., and typically, the glass pH electrode with an ideal Nernstian sensitivity, etc. However, these devices still have some drawbacks in terms of potential drift and selectivity (metal oxides), stability and long-term storage (polymers), fragility and improbability of biomedical application (glass electrode). An alternative material group promising for developing a potentiomentric-based pH sensor is Metal Nitride. Remarkably, thin Titanium Nitride films have been reported once to reach 0.01 pH precision which is critical for our application but these films were not designed for miniature electrodes. To the best of our knowledge, Titanium nitride is the only metal nitride reported for potentiometric pH sensors, and is considered as an alternative pH-sensing material. Therefore, the first part of our work focuses on developing a TiN potentiometric pH micro-sensor in clean room with its complete characterization in vitro.

A reflectance SpO_2 sensor was designed, employed two LEDs at 630 nm and 940 nm wavelengths with one wideband photodiode and was monitored by a MSP432 microcontroller. Several versions of the SpO_2 sensor were fabricated. Result recorded of the first prototype of the classical hard-type PCB shows close behavior to a commercial device. We optimized the

analog front end (AFE) circuit and transferred it to a flexible PCB, fabricating a second prototype. Finally, we developed a prototype of miniature SpO_2 sensor on a flexible substrate, which could register raw PPG signal and could be used as a supplementary measurement tool to validate our pH measurement. At this stage, the sensors are separated but an integrated package is considered for the next step using both a flexible electronic circuit for SpO_2 and a flexible substrate fabrication for the pH sensor. This integration work is expected to provide a device embedding all above-mentioned sensors into a flexible solution for later in vivo testing but compatible with medical constraints (material biocompatibility, sterilization, easy manipulation of the final device by the medical staff…).

Main contributions and results:

- A microfabrication process developed and optimized on flexible polyimide
- A new working electrode material tested (TiN flat and porous)
- Several mask levels designed and implemented
- A full in vitro characterization protocol developed and used for all the probes (OCV, CV, PEIS, influence of the Temperature)
- A SpO_2 sensor developed allowing continuous PPG data recording
- Some in-vivo preliminary test done on mice showing the POC
- pH sensitivity and accuracy achieved close to the expected target for the fetal application (precision down to 0.02 unit) taking in consideration the miniaturization and material constraints

Contents

Glossary of terms

Term	**Definition**
Performance	Including sensitivity, stability, reproducibility, response time, hysteresis, precision
Accuracy	Sensitivity and precision
Sensitivity	Slope of the curve OCV vs pH
Precision	Hysteresis devided by sensitivity
Response time	Time for the electrode to reach 90% of stable potential
Reproducibility	Possibility to have similar OCV level in repreated measurement
Stability	OCV level over time at one pH
E_0	Standard potential, tendency for a given chemical species to be reduced
Pulse	A rhythmical throbbing of the arteries as blood is propelled through them

List of figures

List of tables

Chapter 1

INTRODUCTION

Abstract of Chapter 1

This thesis has been organized in collaboration with three partners: ESYCOM (UMR 9007 CNRS) lab, where the main part of the work was conducted; ENS Paris Saclay, which provided supervision for SpO_2 part; and the Intercommunal Hospital of Creteil (CHIC) with Institut Mondor de Recherche Biomédicale (IMRB) - UMR 955, which contributed to the medical and in vivo aspects. This work was partially supported by Comue University Paris Est. The medical application was proposed by Prof. Edouard Lecarpentier from INSERM and will be described in detail in this introduction chapter.

Monitoring fetal well-being during labor is a common practice of daily obstetrical activities. Ensuring the good oxygenation of the fetus is important to prevent the risk of asphyxiation and its most serious consequences: peripartum death and distant sequelae, in particular neurological disorders including psychomotor disability or cerebral palsy [1]. In this chapter, we define the significance of pH and SpO_2 measurement to human health in general and fetal health monitoring in particular. Biological aspect of pH imbalance and the relevance to SpO_2 is explained, along with the need of real time measurement in order to get over the limitation of the current blood analyzing technique.

The main goal of the thesis is to design a prototype, which is a first attempt to get continuous fetal health monitoring during labor. The system described in this study is capable of simultaneously measuring pH, SpO_2 and provides a clear photoplethysmogram (PPG) in real time. The in vitro and in vivo validation will be discussed in chapters 2 and 3.

Content of chapter 1

1.1 Detection of pH and practical issue of fetal health monitoring

1.1.1. Definition of pH and effect of temperature on pH measurement

The pH of a solution represents the power of Hydrogen ion (H^+), expressing the acidity or alkalinity of a solution and defined by (1-1):

$$pH = - \log [H^+] \tag{1-1}$$

where $[H^+]$ is the proton concentration in the solution in moles per liter (mol/l). A solution, which has a neutral pH, is said to be pH 7, a lower pH indicates a more acidic solution and a higher pH indicates a more alkaline solution (Figure 1-1). Some well-known pH solutions are illustrated on Figure 1-2.

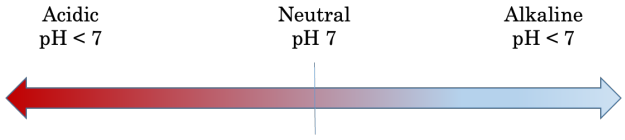

Figure 1-1 pH of a solution.

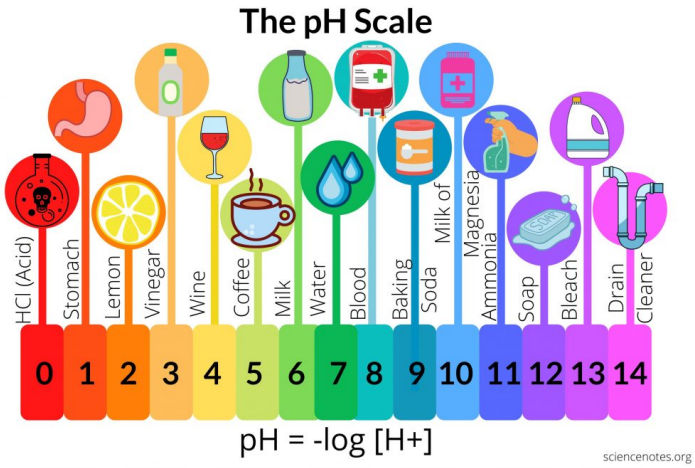

Figure 1-2 The pH Scale of Common Chemicals.
https://sciencenotes.org/the-ph-scale-of-common-chemicals/

It is notable that pH measurement is temperature-dependent, due to two factors: the increase of ion concentrations and the change of potential of working electrode when the temperature changes. Indeed, the water autoproteolysis is expressed as (1-2):

$$H_2O \leftrightarrow H^+ + OH^- \tag{1-2}$$

Since free hydrogen ions cannot exist in aqueous solution, $[H^+]$ denotes the activity of hydronium ions H_3O^+ and higher associates $[H_3O.nH_2O]^+$, n = 1, 2, 3, 4, 5, 6. The more the temperature increases the more water dissociates into ions, leading to a higher concentration

of hydrogen ions (or H_3O^+). A higher concentration of H_3O^+ results in lower pH, but it does not mean the sample has changed.

The second factor is the dependance of electrode potential (E) to temperature (T). Consider this chemical equation (1-3) happens at the electrode:

$$xA + ne^- \leftrightarrow yB \tag{1-3}$$

In which, A is oxidized form of the considered species and B is corresponding reduced form. According to Nernst Equation (1-4):

$$E = E^0 - \frac{RT}{nF} \ln K_{eq} \tag{1-4}$$

Or also equivalent to:

$$E = E^0 - \frac{RT}{nF} \lg(10) \frac{[B]^y}{[A]^x} \tag{1-5}$$

In which, E is the electrode potential in Volt (V); E^0 is the standard potential (V); R is ideal gas constant, equal to 8.314 462 1 $Jmol^{-1} K^{-1}$; n is the number of electrons transferred in the half-reaction; F is Faraday's constant, equal to 96.485 $Cmol^{-1}$; K_{eq} is the equilibrium constant of reaction; [A] and [B] are molar concentration of oxidant and reducing agents respectively.

A potentiometric pH sensor indicates pH level based on the change in the potential difference between the reference electrode and the working electrode, therefore the measurement is also affected.

At room temperature (25 °C = 298.15 K), the potential of electrode can be calculated as:

$$E = E^0 - 0.05916 \frac{[B]^y}{[A]^x} \tag{1-6}$$

which demonstrate that a working electrode which oxidation-reduction chemical reaction involved ideally one transfer electron (n = 1) has 59.16 mV sensitivity at room temperature (25°C). This is also called Nernstian sensitivity. In particular, glass pH electrodes, based on their potentiometric membrane which selectively sensitive to hydrogen ion, show ideal Nernstian response of 59 mV independent of redox interferences [2].

1.1.2. Significance of pH in biological systems and impact of pH imbalances on health

In human body, each part operates optimally at a specific pH level. There are a lot of biological process being pH dependent, since the activity of most chemical reactions mediated by enzyme proteins depends on the pH of the body fluid [3]. Human blood has a pH level at 7.4 within a very small variation between 7.386 - 7.462 [4]. Meanwhile, pH level in different position of healthy organs or tissues could be found ranging from 6 to 8, for example: pH

6.0 - 7.0 in saliva, pH 6.2 - 8.0 in urinary tract or 7.3 - 7.7 in healthy tear [5]. In diagnosis of abnormal condition and disease, an acidic pH level was discovered in extracellular tumor (6.5 - 7.2), inflamed tissue (4.5) or cardiac ischemia (5.7) [5]. Figure 1.2 and Figure 1-3 recited pH level of different locations in human body and pH value of human body fluids.

Level	Location		pH
Intracellular	Early endosome		6.0-6.5
	Late endosome		5.0-6.0
	Lysosome		4.5-5.0
	Golgi complex		6.0-6.7
Tissue or organ	Gastrointestinal tract	Saliva	6.0-7.0
		Gastric fluid	1.0–3.5
		Bile	7.8
		Pancreatic fluid	8.0-8.3
		Small-intestinal fluid	7.5-8.0
		Large-intestinal fluid	5.5-7.0
	Urinary tract		6.5–8.0
	Vagina		3.8–4.5
	Eye	Ocular surface	7.1
		Healthy tear	7.3-7.7
	Plasma		7.4
Pathological microenvironment	Extracellular tumor		6.5–7.2
	Inflamed tissue		5.4
	Fracture-related hematomas		4.7
	Cardiac ischemia		5.7

Figure 1-3 pH of different locations in human body.[5]

	pH	
Fluid	Mean	Range
Blood, arterial	7.424	7.386–7.462
Blood: red cells	7.209	7.175–7.243
Blood: plasma, arterial	7.39	7.35–7.43
Blood: plasma, venous	7.398	7.378–7.418
Bile, hepatic	7.5	6.2–8.5
Bile, gall bladder	6.0	5.6–8.0
Breast milk	7.01	6.4–7.6
Cerebrospinal fluid	7.349	7.327–7.371
Faces, adult	7.15	5.85–8.45
Faces, infant	4.9	4.6–5.2
Gastric juice, male	1.92 ± 1.28	
Gastric juice, female	2.59 ± 2.08	
Gastric juice, child	3.27	0.9–7.7
Gastric juice, newborn	2.52	1.2–7.4
Pancreatic juice		7.5–8.8
Saliva	6.4	5.8–7.1
Semen		7.2–8.0
Sweat		4.0–6.8
Synovial fluid	7.434	7.31–7.64
Tear		6.5–7.6
Urine	5.75	4.8–7.5
Vaginal secretions		3.5–4.0

Figure 1-4 pH value of human body fluids.[4]

Level of pH in the body is a fundamental indicator to evaluate abnormal status of organs and alert various illnesses (acidosis status, tumor diagnostic, drug delivery, wound and fetal

health monitoring). pH also affects skin barrier function, lipid synthesis and aggregation, epidermal differentiation and desquamation [6]. A slight imbalance in pH level can create a disorder functioning at the cell level and to the overall health, or lead to a serious consequence such as:

- Respiratory disorders such as acidosis or alkalosis
- Metabolic disorders such as diabetic ketoacidosis or lactic acidosis
- Kidney failure
- Liver diseases
- Cardiovascular problems
- Seizures and muscle weakness
- Impairment of enzymes and other proteins
- Poor immune function and increased risk of infections
- Disturbance of the nervous system and brain function
- Coma or death in severe cases.

Acidosis is a condition in which there is too much acid in the body fluids, which is the opposite of alkalosis. There are two types of acidosis: respiratory acidosis and metabolism acidosis.

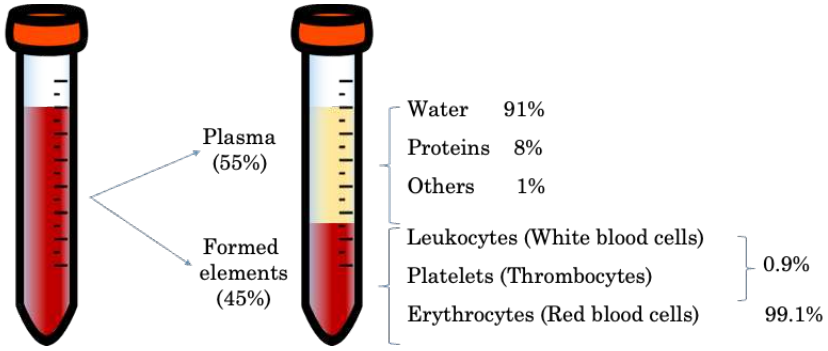

Figure 1-5 Percentage of blood components.

Respiratory acidosis happens when the ventilation is disrupted, which means the lung could not functionally remove CO_2 out of the body. This failure leads to overly accumulating CO_2 inside the body. According to Henderson-Hasselbach reaction, CO_2 comes from the breakdown of glucose contained in food that occurred in mitochondrial (a compartment of the cell). This reaction releases chemical energy and produces CO_2 and H_2O as waste (7).

$$\underset{\text{(Glucose)}}{C_6H_{12}O_6} + \underset{\text{(Oxygen)}}{6O_2} \xrightarrow{\text{Energy released}} \underset{\text{(Carbon dioxide)}}{6CO_2} + \underset{\text{(Water)}}{6H_2O} \quad (1\text{-}7)$$

The released energy is stored in an energy-rich compound Adenosine triphosphate (ATP) to drive other cellular processes. It was acknowledged that there is 91% of water in blood plasma

and plasma is accounting for 55% of the whole blood. CO_2 molecules easily interact with water to form acid carbonate (H_2CO_3) which is dissociated in the form of bicarbonate (HCO_3^-) and hydrogen ion (H^+). Majority of CO_2 amount is transported to lung in the form of bicarbonate, the other is in combination with hemoglobin (Hb) and in the form of bicarbonate in blood plasma. When this bicarbonate-rich blood reaches the lungs, the bicarbonate is converted to carbon dioxide according to the reverse reaction described above. The carbon dioxide will then diffuse from the blood into the lungs and be exhaled. Therefore, when the respiratory acidosis happens, the amount of CO_2 kept inside the body increases which led to the right shift of reaction (according to Le Chatelier's principle), thus increasing the amount of bicarbonate (HCO_3^-) and hydrogen ion (H^+). Consequently, the pH of the blood decreases.

Metabolic acidosis happens when the body produced too much acid or when the kidneys fail to remove enough acid out of the body. It could be in the form of diabetic acidosis developed when substances called ketone bodies (which are acidic) buildup. It could also concern lactic acidosis when lactate level elevates and pH of the individual's blood serum decreases to equal to or less than 7.38, hyperchloremic acidosis (which caused by the loss of sodium bicarbonate due to severe diarrhea).

1.1.3. Explanation of fetal acidosis and the relevance to the dropping of pH in skin tissue

In case of fetal acidosis, respiratory acidosis is not caused by the dysfunctionality of the lung, but of the placenta, which ensures oxygen and CO_2 exchange between the fetus and the mother. This can occur very fast in a few minutes and can be rapidly restored as soon as the fetus is delivered and can breathe the air. With only a few exceptions, the respiratory acidosis does not cause a long-term consequence including neurological sequelae for the infant. On the other hand, metabolic acidosis might induce irreversible organ damage. It appears slower after a long period of fetal tissue hypoxia. Production of lactic acid leads to a decrease in pH and the formed lactic acid levels may remain high several hours after hypoxia correction. Ensuring the good oxygenation of the fetus is of high importance to prevent the risk of intrapartum hypoxic-ischemic encephalopathy (HIE) and neonatal encephalopathy [7].

1.1.4. The need of high accuracy pH measurement for fetal health mornitoring and pH detection in real time

Measuring pH levels of fetuses requires a critical precision of 0.01 in pH in the range of pH from 6 to 8. The first line examination to monitor fetal status is heart rate via a cardiotocograph. However, it was reported that even the fetal heart rate was shown normal, one half of these fetus was in hypoxia state. Therefore, scalp blood sampling to determine pH

and lactate were referred as the second line examination to reduce false positives rate for predicting fetal intrapartum asphyxia. However, the technique to collect capillary samples from fetal scalp has many limitations in term of discontinuity and high rate of failures. Figure 1-6 describes the blood sampling by capillary tube, in which a small cut on the fetal scalp is occurred to collect blood droplets for analysis. In addition, the skills from operators can cause patient discomfort or reluctance to repeat the test, which limits the ability to observe a trend in fetal pH measurement throughout labor. Indeed, the variation in pH capillary per minute from 0.02 to 0.05 is potentially critical from a decision point of obstetric view (continued labor vs. birth within 30 minutes vs. immediate birth, table 1-1) [8]. Thus, taking a discontinuous sample every 30 minutes appears obviously non efficient in some obstetrical situations.

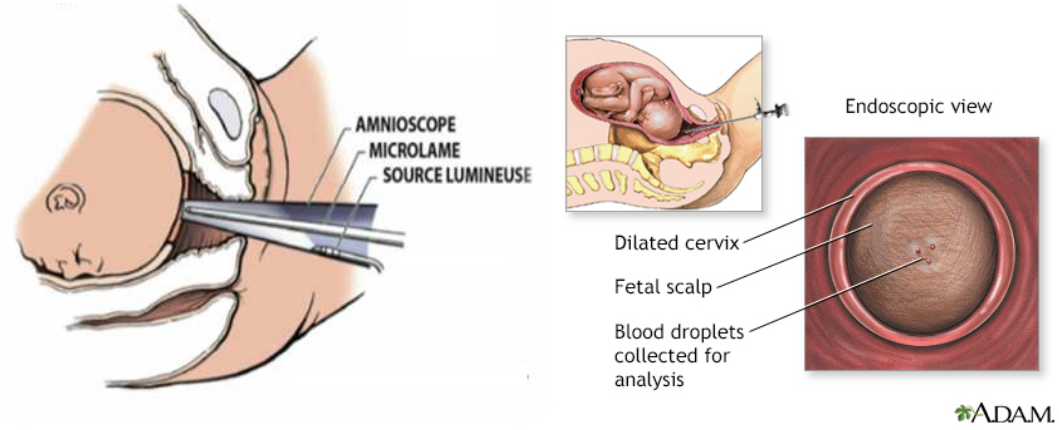

Figure 1-6 Blood sampling to analyze pH of fetus during labor. [1]

Table 1-1 Interpretation bases on pH level during labor. [8]

	Measurands	Interpretation
Fetal scalp blood pH level	≥ 7,25	Normal
	7,21 – 7,24	Borderline
	≤ 7,20	Abnormal

Analyzing the blood pH from fetal scalp was first proposed by Saling in 1963 [9]. The first experience with continuous pH measurement on 22 cases fetus was reported in 1978, showed eight failures, seven were acceptable quality and seven of poor quality, which indicates that the pH electrode was not suitable for routine use. Probable reasons for these failures were related to the drawback of the size of the electrodes in relation with the excessive depth of penetration. It was also concluded that perpendicular position of the electrode in the fetal scalp is an important condition for obtaining reliable pH values [10].

It was testified that the correlation between tissular pH and capillary blood at birth is good. In 1978, clinical evaluation of tissue pH monitoring was obtained on 61 cases during labor, determining a correlation coefficient between tissular pH and capillary blood pH being 0.94 and the correlation coefficient between the last intrapartum tissue pH and the umbilical arterial blood pH being 0.84. This study opened a research strategy toward continuous measurement of tissular pH on the scalp of fetus during labor as an alternative method to blood sampling. However, the research on this topic stopped after the 80s as it was challenging for miniaturization due to limitation of technology in that period.

Not only in fetal health monitoring, but accuracy of pH detection is also critical in general medical application. It was found that intracellular pH falls by 0.5–1 unit during cerebral ischemia [11]. The extracellular space begins to go acid within 20 s of beginning anoxia or global ischemia. Intracellular pH follows a similar time course, beginning to fall within 1 min and reaching a minimal value after 2 min [12]. An important determinant is that the pH fall usually correlates with increased lactate concentration as blood glucose is increased.

Therefore, spatially and temporarily addressed pH measurements in vivo are of considerable clinical interest, which lead to the need of real-time pH sensing in medical application. Miniaturized pH sensors have also become a necessary equipment to be developed and processed in clinical studies. Nowadays, the development of micro-fabrication technology and the notable growing in the industry of materials allows to potentially originate the miniaturized sensors for in vivo experiments. Thanks to our collaboration with the CHIC, our work focuses on fetal health mornitoring application, to prevent the risk of acidocis for the fetus during laboring process, but it can be extended to more medical applications.

1.1.5. Overview of pH sensors for fetal health monitoring

Potentiometric based pH sensors are the most favored electrochemical systems due to their simple design and possibility to be miniaturized [13]. A potentiometric based sensor includes one working electrode (WE) and one reference electrode (RE). In principle, when the sensor is immersed in the test solutions, a potential difference between the WE and the RE (open circuit voltage) is produced and proportional to the pH variation. The most common material of RE is Ag/AgCl, due to its stable potential. Some pH-sensitive materials have been reported for the WE including metal oxides such as Iridium (IV) oxide (IrO_2), Ruthenium (IV) oxide (RuO_2), Tungsten trioxide (WO_3) and Titanium dioxide (TiO_2) etc., conductive polymers such as poly-aniline, poly-pyrrole, etc., and typically, the glass pH electrode with an ideal Nernstian sensitivity. However, these devices still have some drawbacks in terms of potential drift and selectivity (metal oxides), stability and long-term storage (polymers), fragility and improbability of biomedical application (glass electrode), and the difficulty of miniaturization and conformation for the in vivo test. Since 1976, some teams have developed continuous

measurement systems for tissue pH at the fetal scalp during labor, using miniaturized [14], optical fiber and indicator pH colorimetric [15]. The methodologies set out in these publications seemed promising, yet despite progress, it was eventually stagnant because of technical limitations mainly related to the fabrication technique of miniaturization of the measuring device.

An alternative material group promising for developing a potentiomentric-based pH sensor is Metal Nitride. Remarkably, thin Titanium Nitride (TiN) films have been reported once to reach 0.01 pH precision [16] which is critical for our application but these films were not designed for miniature electrodes. To the best of our knowledge, Titanium nitride (TiN) is the only metal nitride reported for potentiometric pH sensors [17], and is considered as an alternative pH-sensing material. Therefore, the first part of our work (chapter 2) focuses on developing a TiN potentiometric pH micro-sensor in clean room with its complete characterization in vitro.

1.2 Relevance of SpO_2 measurement for pH measurement

As mentioned in session 1.1, heart rate has been used as the first line examination to surveillance fetal status and scalp blood sampling were referred as the second line examination to reduce false positives rate for predicting fetal intrapartum asphyxia. When the fetus suffocates, both pH and SpO_2 will decrease.

Beside heart rate, oxygen saturation is also relevant to oxygen level of our body. Oxygen saturation in arterial blood (SaO_2) is a parameter indicating the amount of hemoglobin carrying oxygen (HbO_2) in the blood relative to the amount of hemoglobin not carrying oxygen (Hb). SaO_2 is calculated as in (1-8):

$$SaO_2 = \frac{[HbO_2]}{[HbO_2] + [Hb]} \tag{1-8}$$

In which, $[HbO_2]$ and [Hb] are concerntration of hemoglobin carried oxygen and not carrying oxygen, respectively.

SpO_2 is the oxygen saturation measurement conducted by pulse oximetry technique. It was reported that SpO_2 measurement has an accuracy of 2%, reflects an expected error of 4% to 5% of the examinations done simultaneously with SaO_2 measurement in healthy individuals. This is said to be sufficient for the detection of a significant decline in respiratory function and thus pulse oximetry has been accepted as a reliable technique [18]. Principle of pulse oximetry is based on the different absorption spectra of the oxygenated and deoxygenated hemoglobin at two different wavelengths. Optical probe of a SpO_2 sensor is made of two LEDs and one photodiode. By emitting the light to the skin and measuring the reflected or transmitted light, the percentage of oxygen in the red blood cell can be determined.

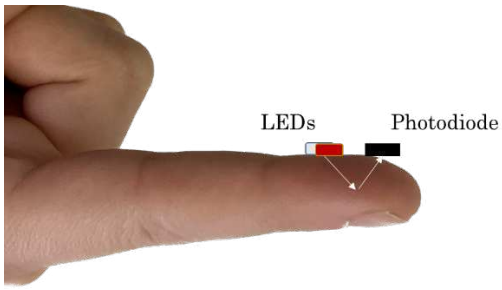

Figure 1-7 Reflectance SpO_2 probe.

Is it reported that SpO_2 measured at different positions on our body provides information in certain medical condition. SpO_2 measured by transmittance technique is widely used in daily health care, for example to position the sensor on finger, toes, and ears or at nasal alar if the patient is peripherally shut down and on Inotropes. Meanwhile, reflectance principle is required in some specific positions, such as force head, temple, and belly of pregnant woman to determined heart rate, respiratory rate, and pulse oxygenation of the fetus. In our work, we try to design a SpO_2 probe to put on the scalp of the fetus (in contact with skin) during laboring process. Therefore, it requires a reflectance sensor (example on Figure 1-7). This part of the work will be detailed in chapter 3.

1.3 A miniaturized device model proposal to fulfill medical requirements

In this thesis, we design a prototype for the first time to continuously monitor fetal tissue pH during labor, combined with fetal oxygen saturation (SpO_2) as control. Microelectrode was fabricated using Titanium nitride (TiN) as the potentiometric sensing material for pH variations. A reflectance optical sensor was used for SpO_2 monitoring. The signal waveform also known as photoplethysmogram can be useful to determine pulse wave characteristics, such as dicrotic notch, systolic and diastolic phases, and was also made available.

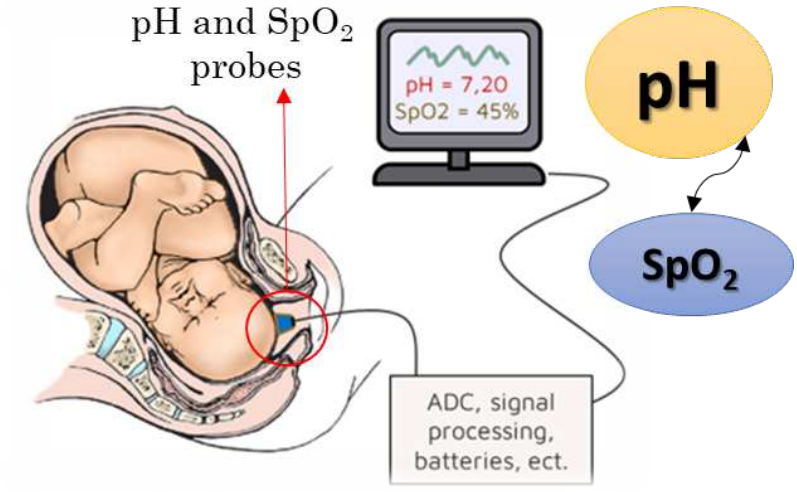

Figure 1-8 Idea of prototype device capable of measuring fetal tissue pH and fetal SpO_2 continuously in real time.

Figure 1-8 illustrates the idea of our prototype device capable of measuring fetal tissue pH and fetal SpO_2 continuously in real time. Both pH and SpO_2 probe sizes are minimized and fabricated on flexible substrate (polyimide) to be inserted through birth canal of the mother and attached to the scalp of the fetus. It is notable that during labor stage, the fetus is ensured to have turn the head facing the opening of the birth canal, so that it is possible to attract the device. The rigid and bigger components, in particular batteries, electronic components for signal processing (analog front end, microcontroller, filters, SD card, etc.) are placed externally. The data acquired from these sensors including pH, SpO_2, heart rate and PPG are saved in a SD card and be displayed on an LCD touchscreen for real time monitoring needs. It is our target to have the 2 values at the same time continuously, and no need of high accuracy for spO_2 but only the trends of decrease or increase in SpO_2 is enough. System is designed to be compact, however wireless communication between the sensor probes and the external elements is forbiden because it is unacceptable to lose the device inside the mother.

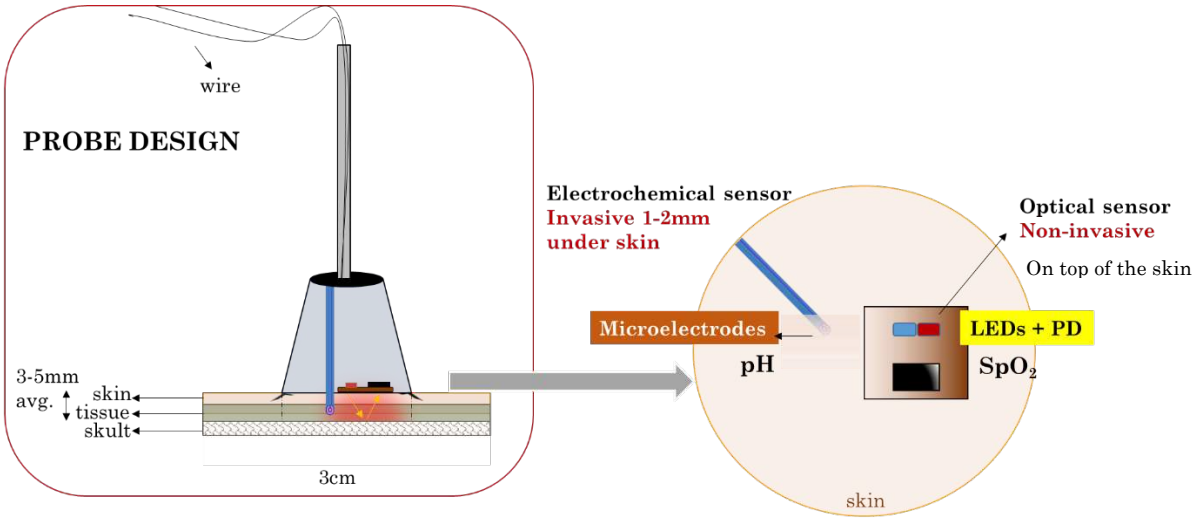

Figure 1-9 Prototype idea for miniaturized pH and SpO_2 sensors for fetal health monitoring.

Figure 1-9 describe the idea of the probe head, which will be inserted inside the mother. Considering the size of the guide tube used in blood sampling technique (Figure 1-10), we expect to achieve a probe with a size smaller than 3 cm x 3 cm, making it easy to manipulate by the doctor. It is important to note that the sensing part in contact with the fetus will be significantly smaller that it could adapt to 1-2 mm insertion (for the pH probe) and 5 mm^2 on the scalp surface (for the SpO_2 probe).

Figure 1-10 Image of the guide tube to insert equipment to the birth canal for blood sampling.

This prototype is proposed to fulfill the medical requirement in term of size and usage. The additional constraints will be on the sensitivity, accuracy and reproducibility of both developed sensors (pH ans SpO_2).

1.4. Thesis objectives and manuscript structure

This section outlines the objectives of the thesis and provides an overview of the manuscript's structure. It establishes the research goals and highlights the organization of the subsequent chapters.

1.4.1. Thesis Objectives

The primary objectives of this thesis are as follows:

1. To investigate a new material (TiN) to pH sensing and its microfabrication process
2. To develop an in vitro characterization protocol and conduct a complete characterization of the fabricated pH sensors
3. To archive a high sensitivity and accuracy of pH sensor, targeting the fetal health monitoring application (accuracy of 0.01)
4. To develop a SpO_2 sensor which can provide a clear raw PPG recording
5. To attempt to test the fabricated sensors in vivo

1.4.2. Manuscript Structure

The thesis is structured as follows:

Chapter 1: Introduction

This chapter provides an overview of the research background, problem statement, and significance of the study. It also outlines the research objectives, research questions, and the structure of the thesis.

Chapter 2: pH sensors

This chapter includes a bibliography study on the state of art of pH sensors and a detailed presentation on our work on producing a prototype of pH sensor with high accuracy. Methodology including materials, fabrication process and characterization protocol in vitro and in vivo is explained, followed by a complete characterization result on the performance of the sensor (sensitivity, stability, hysteresis, reproducibility, response time) and the properties of TiN material (geomorphology study, PEIS, CV). An evaluation of uniformity of fabrication process is also provided. Preliminary in vivo demonstration of pH sensors will be presented and challenge faced during the tests will be discussed. Additionally, it discusses the limitations and potential biases of the methodology.

Chapter 3: SpO_2 sensors

This chapter first provides the state of art for SpO_2 sensors and then described our study to develop SpO_2 sensors. The system to measure SpO_2 will be described, including the optical probe design, analog front end (AFE) circuit design and data collection methods. It outlines our achievement to collect raw PPG and SpO_2 signal.

Chapter 4: Conclusion and Perspective

The final chapter summarizes the key achievements of the two sensors (pH and SpO_2), draws conclusions based on the research objectives, and highlights the contributions of the study to the field. It also provides recommendations for future research and practical applications.

Annex

Some supplementary materials, such as bibliography study, or additional data, are included in the annex.

References

Chapter 2

PH SENSORS

Abstract of Chapter 2

The most critical requirement of a pH sensor for fetal health monitoring is a precision of 0.01 in pH, with an appropriate miniaturized design. Potentiometric based pH sensors are the most favored electrochemical systems due to their simple design and possibility to be miniaturized. Evidently, there are different material groups that are sensitive to pH change, for example metal oxides such as Iridium (IV) oxide (IrO_2), Ruthenium (IV) oxide (RuO_2), Tungsten trioxide (WO_3) and Titanium dioxide (TiO_2), conductive polymers such as poly-aniline, poly-pyrrole, etc., and typically, the glass pH electrode with an ideal Nernstian sensitivity, etc. However, these devices still have some drawbacks in terms of potential drift and selectivity (metal oxides), stability and long-term storage (polymers), fragility and improbability of biomedical application (glass electrode). Hence, it is difficult for medical validation process. An alternative material group promising for developing a potentiometric-based pH sensors is Metal Nitride. Some materials such as Ruthenium Nitride (RuN), Carbon Nitrides (α-BC_xN_y), and Silicon Nitride (Si_3N_4) have been mainly used for Ion Selective Field Effect Transistor (ISFET) type of pH sensors. Remarkably, thin Titanium Nitride (TiN) films have been reported once to reach 0.01 pH precision which is critical for the fetal scalp tissue pH measurements but these films were not designed for miniature electrodes. To the best of our knowledge, Titanium nitride (TiN) is the only metal nitride reported for potentiometric pH sensors, and is considered as an alternative pH-sensing material. Therefore, the first part of our work focuses on developing a TiN potentiometric pH micro-sensor.

Content of Chapter 2

2.1. Bibliography study/ State of art of pH sensor

2.1.1. Overview on methods to measure pH – State of Art

In the early 14th century, Arna ldus de Villa Nova invented litmus paper for studying acids and bases. In 1909, Søren Peter Lauritz Sørensen developed the pH scale from 0 to 14 and for the first time introduced the concept of pH and pH paper. Over the last one hundred-years, detection technique to measure pH has been investigated from conventional glass electrode to optical-based pH sensor, acoustic-based pH sensor and electrical-based sensor. Within these approaches, electrical-based pH sensors are the most dominantly-studied type of pH sensor because of the diversity of materials which are electrochemically sensitive to pH, and the development of miniaturized technology. There exist electrical-based pH sensors such as ion sensitive field induced transistors (ISFET), conductiometric, amperometric, AC impedance spectroscopy-based, capacitive pH sensor and potentiometric sensor. Among them, potentiometric sensors are the most accurate type of measurement and are widely used due to its simple design and easy adaptation for miniaturization. The following section provides a brief explanation of the principles behind the above-mentioned types of pH sensors, allowing us to better understand why a potentiometric pH sensor was chosen in our study.

Conventional glass electrode (Figure 2-1) is the earliest electrochemical method-based pH sensor which was first developed in 1906 by Max Cremer and first commercially successful by Arnold Orville Beckman in 1934 [19], [20]. Remains to this day, this is considered as a gold standard in pH measurement thanks to the silicate glass used in pH electrodes is primarily sensitive to hydrogen ions (H+). It is noteworthy to mention that glass can also respond to other ions present in the solution to a certain extent, such as Na+, K+, and Ca^{2}+, However, due to the presence of silanol (Si-OH) groups on the surface of the glass, which can readily exchange with H+ ions in the solution, the sensitivity to these ions is much lower than the sensitivity to H+. Therefore, the sensitivity of silicate glass to other ions is relatively low compared to its sensitivity to H+ and the effect of these ions on pH measurement is typically negligible. Despite the high accuracy and selectivity, a conventional glass pH meter is fragile, shows a sluggish response and especially presents unstable response for miniaturized system [21]. It also requires frequent calibration. For the biological application, its mechanical stiffness prevents from use effectively in vivo. This limitation pushed the research field towards alternative sensitive devices and materials.

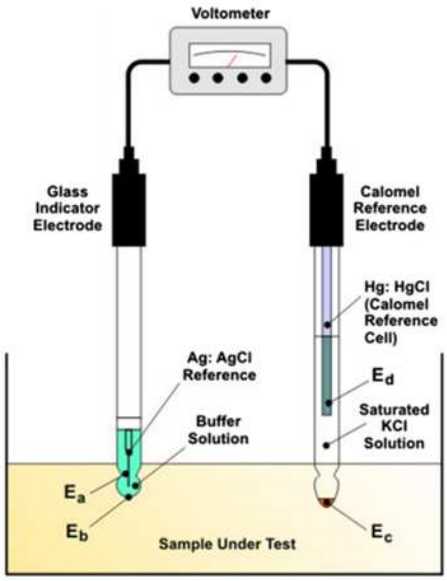

Figure 2-1 Working principle of a glass pH meter.
https://www.azosensors.com/article.aspx?ArticleID=34

Other methods which were also early studied in the 20 centuries for pH sensing is optical methods. In the 1970s and 1980s, researchers began to develop new optical pH sensing methods, such as fluorescence and luminescence-based sensors, which offered several advantages over traditional glass electrodes, including higher selectivity, sensitivity, and flexibility. These methods which also called fluorometric-, ratiometric- pH sensors, utilized pH-sensitive dyes, perform both excitation and fluorescence and measure the absorbance or fluorescence change due to the effect of pH. In the 1990s, the development of fiber optic pH sensors enabled the remote sensing of pH in harsh or hard-to-reach environments. These sensors utilized fiber optic cables to transmit light between the sensor and the detector, enabling real-time, in situ pH measurements. An example of the principle of optical fiber pH sensor based on polymers that can sense color change is showed in Figure 2-2. Today, there are a wide variety of optical pH sensing methods available, including surface plasmon resonance, surface-enhanced Raman spectroscopy, holographic pH sensor (to send UV laser to induce a specific arrangement of nanoparticles, which cause gratting effect and lead to a difference wavelength (color) of the out-going light, from that change, the change in fluoresence is measured) and CCD camera. The main problem of these type of optical-based sensors is that they include optical devices that might be unsuitable for miniaturized and movable systems.

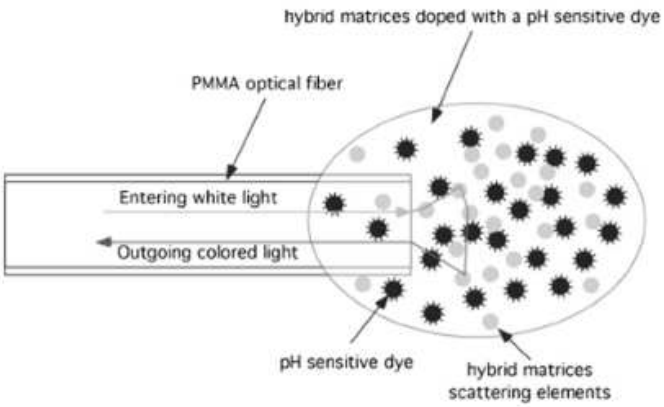

Figure 2-2 Working principle of an optical fiber pH sensor based on polymers that can sense color change. [15]

Acoustic phenomena is also applied in pH detection. pH sensors designed with a cantilever and microcantilever was reported in [22] (Figure 2-3a). Based on pH, the aqueous solution produces shrinking or swelling of the hydrogel, which produces deformation in the cantilever. A magnetoelastic pH sensor was introduced by Cai and Grimes, 2000 (Figure 2-3b) [23]. This sensor sensed the vibrations induced by magnetic field on the magneto-elastic ribbons coated with pH responsive hydrogel. It is obvious that it is not suitable for implantable application.

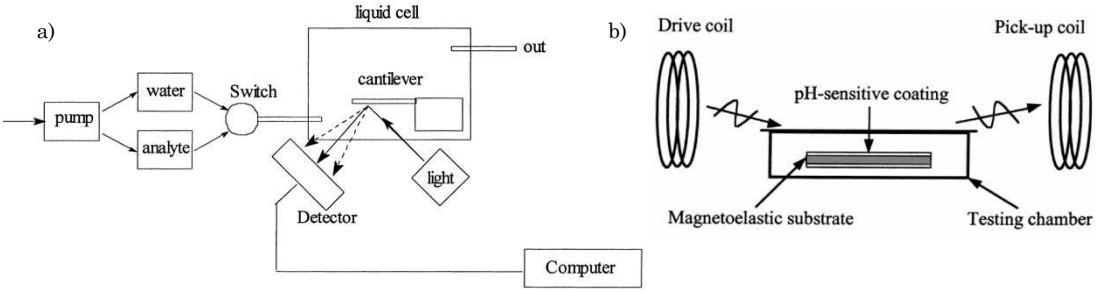

Figure 2-3 a) Shcematic of microcantilever.[22] ; b) Schematic of magnetoelastic sensor.[23]

ISFET-based pH sensor measures the current through a conduction channel between source and drain originating from pH dependent threshold voltage due to sensing gate-liquid surface potential. Figure 2-4 illustrates an ISFET sensor integrated with a temperature sensor on flexible polyimide substrate used to measure pH in sweat. Disadvantages of this type of sensor is that it requires high power for FET operations and the fabrication process is sophisticated. It is also sensitive to electrostatic damage of the gate oxide and it is difficult to integrate into a miniaturized system due to floating gate configuration.

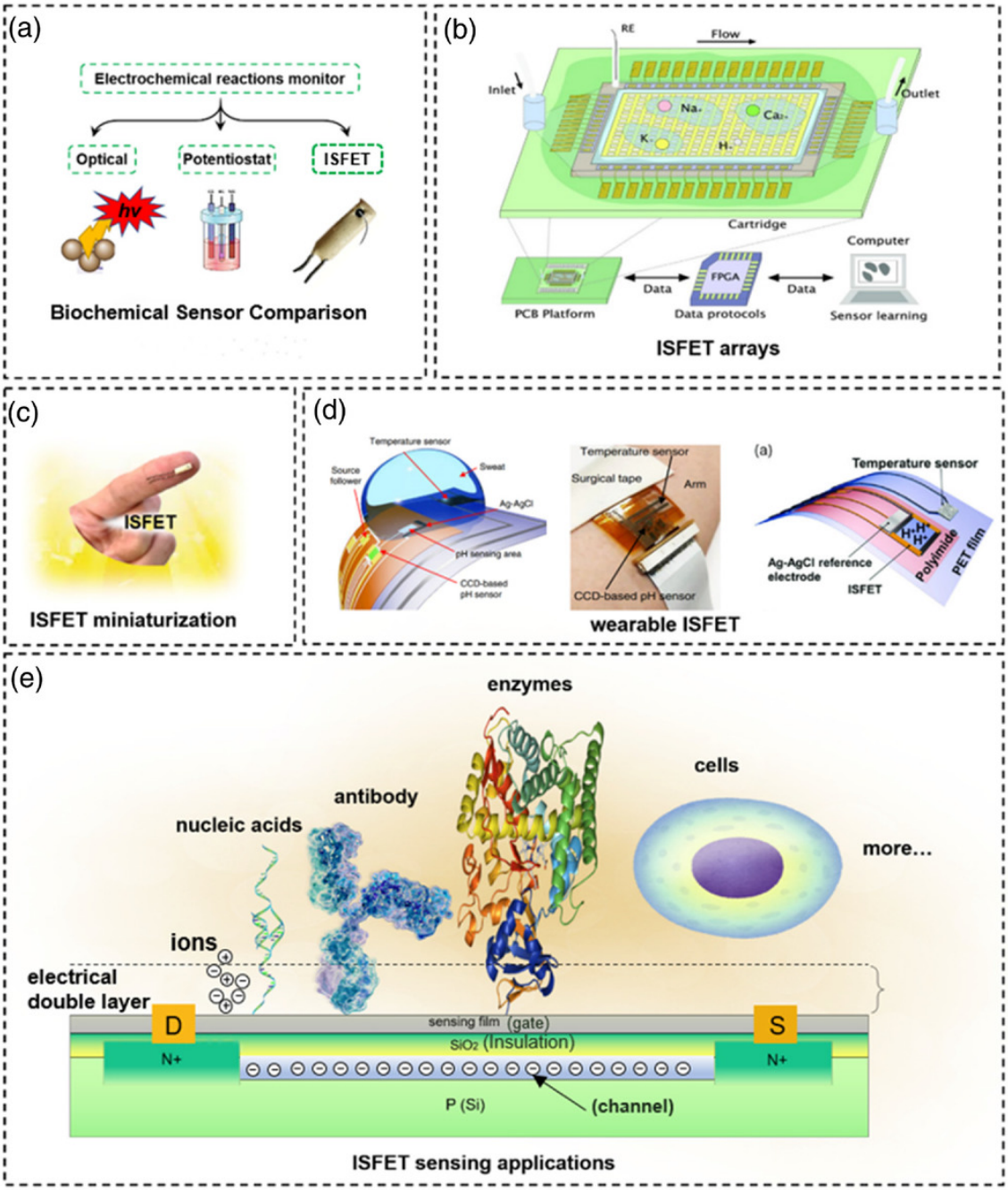

Figure 2-4 The wearable sensor based on the ISFET technique.[24]

Figure 2-5 illustrates a conductimetric pH sensor which has interdigitated electrode (IDE) arrays coated with poly-aniline (PANI) as the pH sensitive material. PANI is a conducting polymer and has shown its suitability as a pH sensing material in many applications.

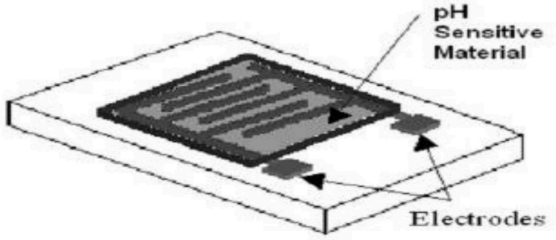

Figure 2-5 Example of a conductimetric pH sensor.[25]

The majority of pH sensing systems use either amperometric or potentiometric devices [26], [27]. Precise pH measurements rely on the potentiometric method rather than on optical methods [28]. It is also the most popular among the pH sensors due to its simple device structure and facility to be miniaturized.

A potentiometric pH sensor is a type of electrochemical sensor that measures the pH of a solution by detecting the potential difference between two electrodes (a reference electrode and a pH-sensitive electrode) in contact with the solution (example in Figure 2-6). Principally, conventional glass electrode and ISFET can also be classified as potentiometric pH sensor since they operate on the principle of measuring the voltage generated by a pH sensitive electrode when it is in contact with a solution of known pH.

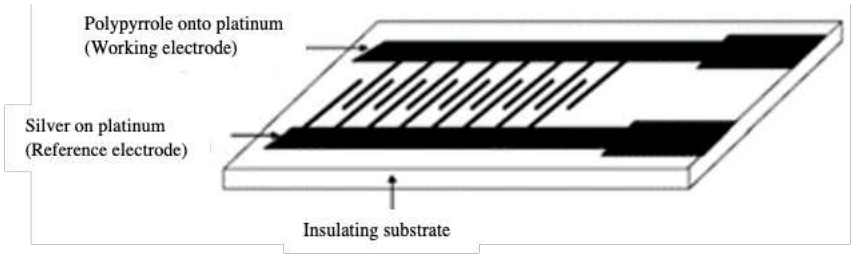

Figure 2-6 Example of a potentiometric pH sensor containing a reference electrode from silver on platinum and a working electrode from conductive polymer on platinum in an interdigited design.

The reference electrode has a stable and known potential that does not vary with changes in the pH of the solution. It is typically made of a silver/silver chloride (Ag/AgCl) electrode. The pH-sensitive electrode, on the other hand, is designed to respond to changes in the pH of the solution. It can be made of different materials, such as glass or a combination of metals. When the two electrodes are placed in contact with the solution being measured, a potential difference is established between the two electrodes due to the difference in the electrochemical reactions at the electrode/solution interface. This potential difference is directly related to the pH of the solution according to the Nernst equation. The Nernst equation relates the electrode potential to the concentration of hydrogen ions in the solution and the temperature of the solution (as this was explained in chapter 1).

By measuring the potential difference between the two electrodes, the pH of the solution can be calculated. In a potentiometric pH sensor, the open circuit potential (OCP) or open circuit voltage (OCV) is the voltage difference between the pH-sensitive electrode and a reference electrode when no current is flowing between them. The OCP is directly related to the pH of the solution being measured.

Materials which are sensitive to pH change used in electrical-based pH sensors comprise a broad and extensively researched field. This area of study encompasses a wide range of materials, including but not limited to metals, metal oxides, metal nitrides, and conductive polymers, which will be subject to further, detailed review on advantages and disadvantages of these materials in Section 2.1.2.

Overall, the choice of pH sensor depends on the specific needs of the application, including factors such as cost, accuracy, precision, response time, and ease of use. Potentiometric pH sensors are well-suited for applications which require miniaturized system where a high degree of accuracy is required. Therefore, we decided to develop a prototype of potentiometric pH sensor for our application.

To summarize, a review on advantages and drawbacks of different types of pH sensors is presented in Figure 2-7 [28].

	Range of application	Challenges
Glass electrode	Temperature: < 80...130 °C Pressure: < 60 bar (with counter pressure) Stability: ± 1 mV week^{-1}	▪ Interaction of surfactants and film formation on the glass surface in reaction mixtures ▪ Mechanical instability of the glass membrane ▪ Individual calibration of each electrode; ▪ Destruction by fluoride and highly hydroscopic solutions. ▪ Sodium error in alkaline solutions ▪ Expensive manufacture
ISFET	Temperature: < 85 °C Pressure: < 2 bar	▪ Film formation on the surface ▪ Bad long-term stability ▪ Poor stability of the reference electrode
Antimony electrode	e.g. strong caustic solutions (no sodium error), fluoride containing waste water	▪ High degree of asymmetry ($pH_{iso} \approx -3$) ▪ Chloride causes potential shift ▪ Deleterious effect of sulfides, and citrates (which form complexes with Sb^{III})
Optical sensors	Transparent liquids Small and flexible (fiber sensors) No reference element required Signal transmittance over large distances	▪ Change of transparency of the solution ▪ Photobleaching and wash-out of indicator phases ▪ Non-linear calibration curve with immobilized indicators

Figure 2-7 Advantages and drawbacks of different types of pH sensors.[28]

2.1.2. Review on materials for pH sensors as potentiometric sensors

The performance of potentiometric pH (including sensitivity, accuracy, stability, hysteresis, reproducibility, which are explained in Glossary of terms) sensors largely depend on the materials used to construct the pH-sensitive electrodes. These materials must have specific characteristics, such as high sensitivity, stability and selectivity towards hydrogen ions, in order to accurately measure the pH of a solution. Additionally, the materials used to construct the reference electrode must also be carefully chosen to ensure accurate and reliable pH measurements.

Some groups of material have been reported to be sensitive to pH such as metal oxides (iridium oxide IrO_2 : 51-70.5mV/pH, ruthenium oxide RuO_2: 56.6mV/pH, tungsten trioxide WO_3 41mV/pH, titanium dioxide TiO_2 55mV/pH, zinc oxide ZnO 59mV/pH, lead dioxide PbO_2 88-112 mV/pH, etc.[28], [29], [30]), conducting polymer (poly aniline 50-70 mV/pH, poly pyrrole: 48 mV/pH, polyaniline/zeolite blend: 310 ± 40 mV/pH, polypyrrole/zeolite blend: 1300 ± 100 mV/pH, etc. [27], [30]) and typically, the glass pH electrode with ideal Nernstian sensitivity. However, these types of devices still have some drawbacks in term of stability, potential drift and selectivity [7] and the difficulty of miniaturization and conformation for the in vivo test. A list of metal oxides and conductive polymers which have been reported for pH sensors is presented in annex along with their reference.

Beside glass electrode that have been discussed in previous section, metal oxides and polymers are both majority and widely used materials for pH sensors, but the choice of sensing material depends on the specific need of the application. For example, metal oxide sensors may be preferred in harsh or high temperature environments, while polymer sensors may be better suited for biomedical applications where biocompatibility and flexibility are important factors. Most oxides are sensitive to pH in a large range of pH 2 to pH 11, and show a noticeable hysteresis, i.e., the electrode potential suffers a shift if the solution changes from pH 2 to pH 12, and back to pH 2 again. RuO_2 and OsO_2 (Osmium dioxide) show good accuracy (± 2 mV) [28]. It is important to note that various fabrication methods can result in differing performance factors, such as sensitivity, hysteresis, and drift effects (table 2-1 and table 2-2). Also, metal oxide detects pH change based on its capacity of redox reactions, for example:

$$Ir^{IV}O_2 + e^- + H^+ \rightarrow Ir^{III}O(OH) \quad [13]$$

Therefore, the performance of such systems in pH measuring is limited because they are undesirably sensitive to several redox agents and exhibit a systematic deviation from the expected behavior.

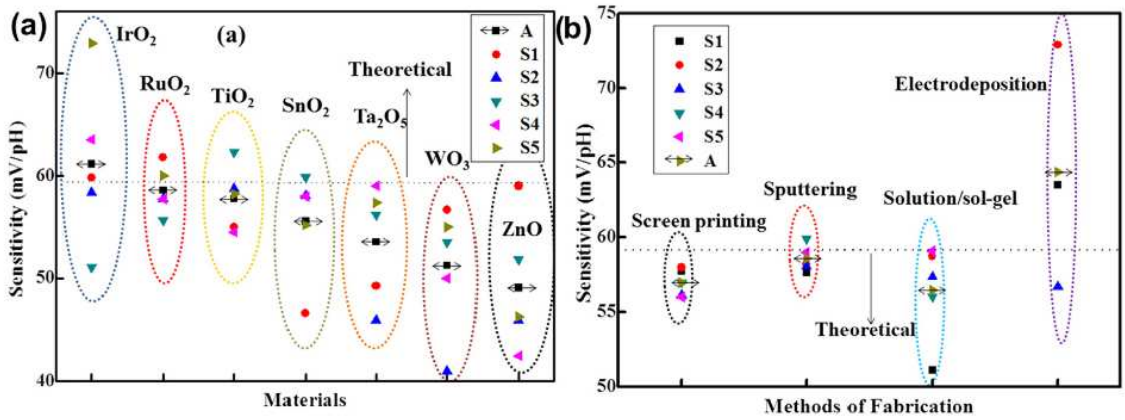

Figure 2-8 Comparison of potentiometric pH sensitivity of different metal oxide materials. [31]

Table 2-1 Drift effect for a few metal oxide based pH sensors. [31]

Materials	Method of fabrication	Drift Effect	Ref
RuO_2	radio frequency sputtering	pH 4: 0.13 mV/pH; pH 7: 0.38 mV/pH; pH: 10 7.31 mV/pH	[58]
RuO_2	screen printing	± 1.5 mV/month (after 15 days of measurement)	[59]
IrO_2	electrodeposition	pH 1: 0.02 pH/h pH 7: 0.003 pH/h pH 11: 0.07 pH/h	[57]
IrO_2	sol–gel	3–10 mV	[40]
Ta_2O_5	radio frequency sputtering	pH 7: 0.03–0.05 mV/day	[71]
Ta_2O_5	electron-beam evaporation	pH 7: < 0.5 mV/h (after 3 h); 0.2 mV/h (after 10 h)	[142]
WO_3	radio frequency sputtering	pH 1: 1.5 mV/h pH 3: 3.6 mV/h pH 5: 6.6 mV/h pH 7: 15.7 mV/h	[143]
WO_3	magnetron sputtering	< 3 mV	[73]
TiO_2	sol–gel	pH 7: 1.97 mV/h	[61]
TiO_2	radio frequency sputtering	1.67 mV/h	[144]

Table 2-2 Hysteresis effect of metal oxide based pH sensors. [31]

Materials	Method fabrication	pH loop/values	Hysteresis (mV)	Ref
RuO_2	radio frequency sputtering	7-4-7-10-7	4.36	[58]
		7-10-7-4-7	2.2	
RuO_2	magnetron sputtering	7-4-7-10-7	6.4	[38]
		7-10-7-4-7	5.1	
		2-8-12-8-2	10.2	
IrO_2	sol-gel	1.50, 2.81, 3.75, 6.28, 7.86, 9.52 and 10.50	23.7, 9.5, 0.3, 14.5, 16.5, 6.7, and 11.5	[40]
IrO_2	Electrodeposition	2-10-2	2.5 ± 0.6	[56]
IrO_2	electrodeposited	7	1.5-0.5	[57]
WO_3	magnetron sputtering.	2-12	< 13	[73]
WO_3	radio frequency sputtering	3-1-3-5-3	7.2	[143]
		5-3-1-3	12.5	
		4-1-4-7-4	12	
		4-7-4-1-4	26	
		3-1-3-5-3	7.2, 9.7 and 15.4 (10, 20 and 40 min)	
Ta_2O_5	radio frequency sputtering	7-4-1-4-7-10-7	~5	[70]
Ta_2O_5	electron-beam evaporation	3-10	1.5-9	[142]
Ta_2O_5		6-2-6-12-6	15.2 and 0.3 (without and with post annealing)	
			6.3 and 0.7 (without and with post annealing)	
		6-12-6-2-6		
SnO_2	radio frequency sputtering	7-10-7-4-7	< 3	[145]
		7-4-7-10-7	< 7	
		7-2-7-12-6	7.3	
SnO_2	sol-gel	5-1-5-9-5	3.74	[83]
		4-1-4-7-4	1.3	

The phenomenon known as hysteresis effect occurs when a pH electrode, previously used in the same pH buffer solution multiple times, produces a shift in output voltages. The hysteresis known to be smaller in acidic solutions compared to alkaline solutions due to the faster diffusion of H^+ ions compared to OH^- ions. Notably, in MO_x-based sensors, it has been observed that the hysteresis width is dependent on the measurement loop time, with an increase in hysteresis width as the loop time increases. Consequently, the hysteresis width of MO_x pH sensors is reported to be strongly influenced by factors such as the pH measurement loop and time, as well as the surface area and crystalline properties of the materials used. [31]

In general, polymers are more sensitive to pH changes than metal oxide [27]. In a polymer-based pH sensor, the functional group is introduced and selectively swells and shrinks according to pH. This leads to a change in mass and elasticity. Other phenomenon encountered is a controlled surface reaction, in which reaction of H+ onto amino groups created local charge density excess at the electrode surface.

The main advantage of using polymers for sensor applications is their relative low cost and ease of fabrication, meanwhile the drawbacks are the long-term stability and storage [25].

Overall, Figure 2-9 illustrate an overlook of advantage and limitation of the main material groups for pH sensor.

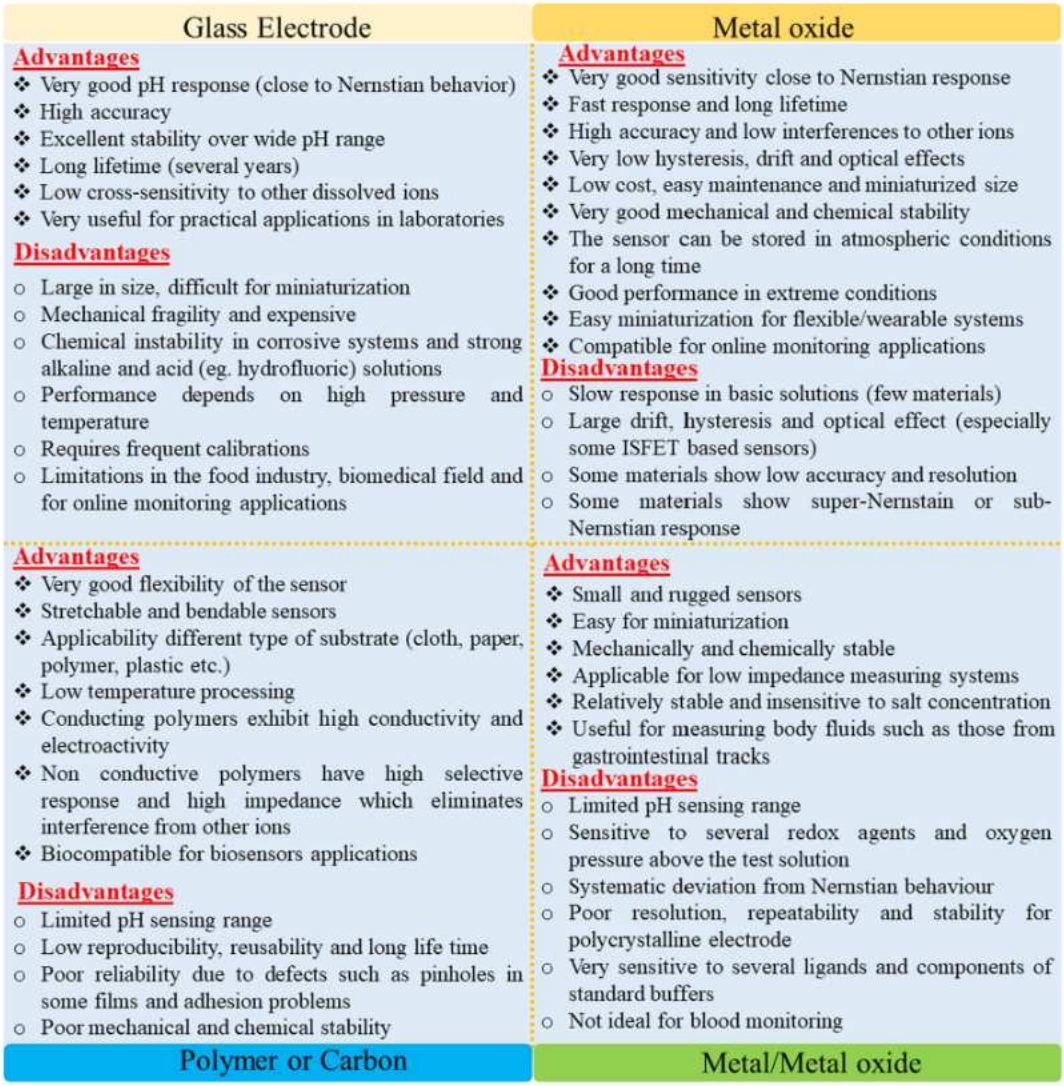

Figure 2-9 Advantages and disadvantages of the major material groups used for electrochemical pH sensor[31]

Metal nitrides – an alternative approach to potentiometric pH sensors

In our work, we would like to investigate the capability of an alternative material, titanium nitride, for the potentiometric pH sensors. Titanium nitride belongs to metal nitride group, which to the best of our knowledge, has been employed mostly for the development of Ion sensitive field induced (ISFET) based pH sensors. Previous studies conducted on metal nitrides, i.e., RuN, Br-C-N, SiN, TiN, ZiN, and HfN, as re-cited in Table 2-3 below [32]. In addition, Aluminum nitride (AlN) and Gallium nitride (GaN), 54mV/pH - 57. mV/pH [33], [34] have been described as a H+ ion-sensitive field-effect transistor (ISFET).

Table 2-3 Metal nitride based pH sensors. [32]

Application Matrix	pH Sensitive Material	Fabrication Method	Sensitivity (mV/h)	pH Range	Reference
Redox matrix	RuO_2	RF sputtering	−56.6	2–12	[7]
Biological and environmental application	RuN	Magnetron sputtering	−58.3	1–12	[23]
Phosphate buffer solution	Br-C-N	Dual gun sputtering	−46	1–13	[28]
Aquaculture	SiN	ISFET package	−53.6	4–10	[29]
Chemical applications	InN	ISFET	−58.2	2–12	[32]
Chemical application	IrO_2 + Nafion	Cryogenic sputtering	−60.2	2–12	[21]
Fresh Orange juice	TiN	RF Magnetron sputtering	−59.1	2–12	[21] previous work
Common drinks with redox species	TiN + Nafion	RF Magnetron sputtering	−56.6	2–12	* This work

TiN is the only metal nitride reported for potentiometric pH sensors [35]. Thin TiN films are reported once to have 0.01 precision and sensitivity of 59.1 mV/pH, which is critical in our case for the fetal scalp tissue pH measurement [16]. The same group recently reported a nafion modified titanium nitrides for pH sensor to minimize the redox shift of the potential E0 value from 30 mV to 2 mV [32].

2.1.3. Overview on the flexible substrate for pH sensor

A recent review in 2020 by L. Manjakkal et al about properties of the substrates and platforms used for wearable/flexible electrochemical sensor provides us an overlook to consider different possibilities for the final design and packaging. Polyimide and parylene C are considered equivalently as a biocompatible substrate for medical application [36], [37]. In our work, we chose polyimide to be the flexible substrate due to convenience in fabrication. Polyimides have shown their judiciously certified biocompatible characteristics, which can accommodate in vivo conditions and function for a long time [36], [37]. Flexible polyimide was investigated to have rather better accommodation to tissue reaction, reduced inflammation and destruction caused by motion compared to the rigid-type substrate. pH sensors employing polyimide as flexible substrate have been reported with various pH-sensitive materials. Yang et al introduced their potentiometric pH sensor using zinc oxide (ZnO) and aluminum-doped zinc oxide (AZO) on polyimide substrate, showing a sensitivity of 34.82 mV/pH and 42.99 mV/pH, respectively [38].

Table 2-4 Substrates and platforms used for wearable/flexible pH sensor [39].

Table 2 Properties of the substrates and platforms used for wearable/flexible electrochemical sensor fabrication

Substrate	Properties	Ref.
Polyimide (PI) (Apical, Kapton, UPILEX films, *etc.*)	• Bendable • Low transparency • Dielectric constant 2.8–3.5 • Resistant to temperature <450 °C • Coefficient of thermal expansion $\approx 5 \times 10^{-5}$ K^{-1} • Resistant to weak acids and alkalis • Resistant to ethanol and acetone	124, 138–141
Polyethylene terephthalate (PET)	• Bendable • >85% transparency • Dielectric constant 2.5–3.5 • Resistant to temperature <100 °C • Coefficient of thermal expansion $\approx 7 \times 10^{-5}$ K^{-1} • Dissolvable in acetone	123, 142 and 143
Polyethylene naphthalene (PEN)	• Bendable • >85% transparency • Dielectric constant 2.9–3.2 • Resistant to temperature <180 °C • Coefficient of thermal expansion $\approx 2 \times 10^{-5}$ K^{-1} • Easily permeated by oxygen and water	124 and 144
Polydimethylsiloxane (PDMS)	• Stretchable • >95% transparency • Dielectric constant 2.3–2.8 • Resistant to temperature <100 °C • Coefficient of thermal expansion $\approx 30 \times 10^{-5}$ K^{-1} • Mostly resistant to ethanol and acetone, may cause swelling	145–148
Fibers, textiles & fabrics	• Stretchable & bendable • Low transparency/opaque • Resistant to temperature <100 °C • Easily permeated by oxygen and water	132, 133 and 149
Tattoos	• Bendable • Stretchable • Opaque • Resistant to temperature <100 °C	135 and 150
Paper	• Bendable • Opaque • Resistant to temperature <100 °C • Dielectric constant 2.3–3.0 • Absorbs moisture • Dissolves in strong acids	103 and 151
Bandage	• Stretchable & bendable • Opaque • Resistant to temperature <100 °C • Easily permeated by oxygen • Absorb moisture • Water soluble/waterproof	10 and 152

2.1.4. An overview on in vivo research of pH sensor

Although there is a lot of pH sensors reported, to the best of our knowledge, only few works reported on real applications involving the in vivo determination of pH [40].

In 2014, Chung et al reported their demonstration on a real-time measurement of a stretchable, multiplexed pH sensor in IrO_2 on the surfaces of explanted rabbit hearts and a donated human heart during ischemia–reperfusion (Figure 2-10). In this paper, a balloon catheter that incorporates three pH sensors and a stretchable sheet that incorporates a matrix array of thirty pH sensors were introduced. An average sensitivity of 69.9 ± 2.2 mV/pH over 30 sensors was reported with 24 out of 30 sensitivity value were between 69 and 74 mV/pH. Influence of temperature and influence of extra-cellular ions were also reported to be -1.63 ± 0.02 mV/pH and (< 3.5 mV), respectively.

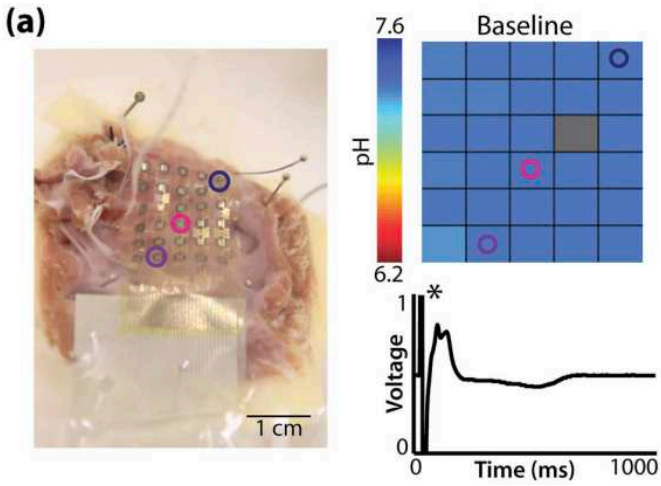

Figure 2-10 Human right ventricular wedge preparation with endocardial surface in contact with pH array (left). Opened colored circles (navy, pink, purple) highlight the location of pH sensors. [41]

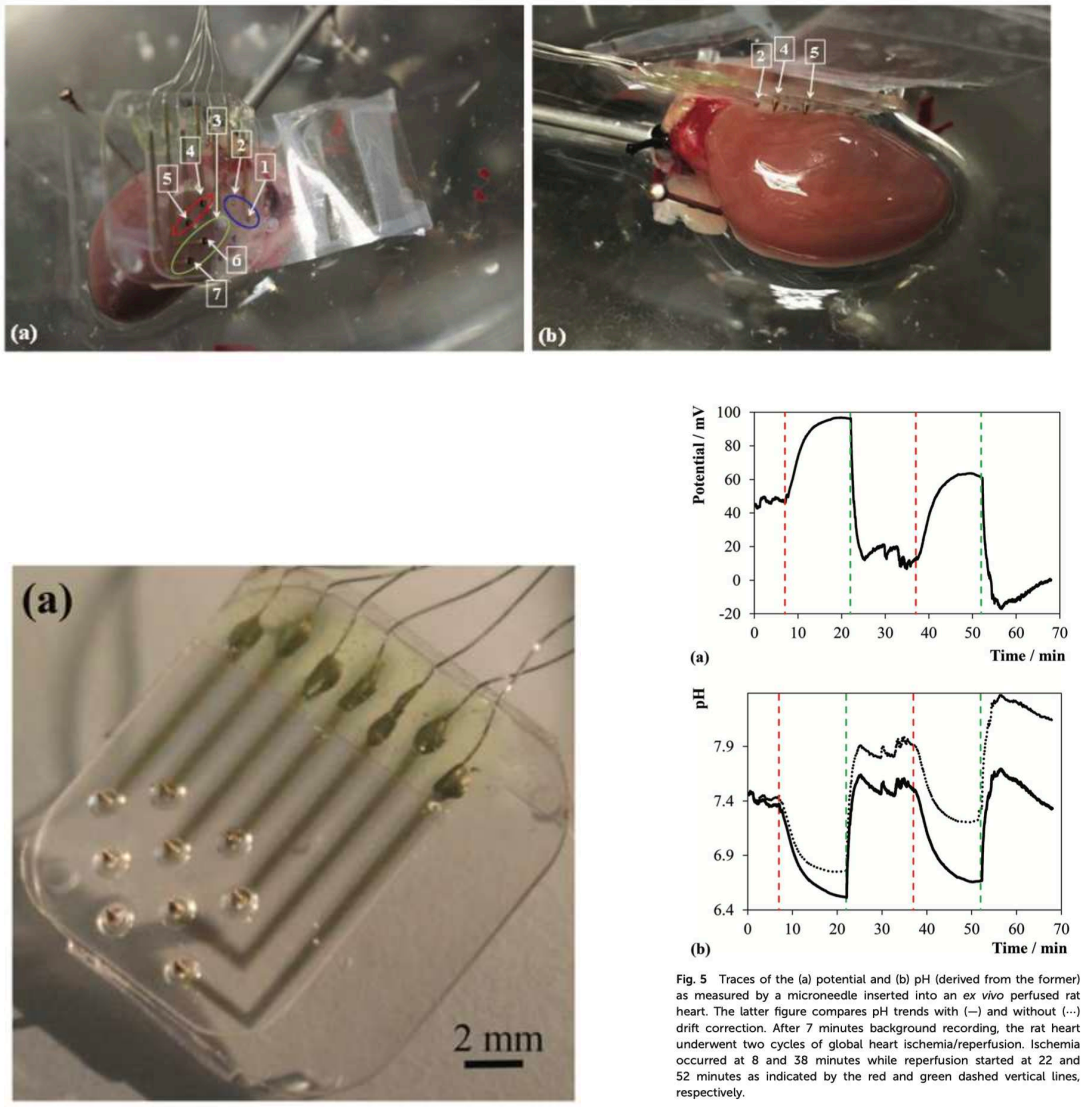

Fig. 5 Traces of the (a) potential and (b) pH (derived from the former) as measured by a microneedle inserted into an *ex vivo* perfused rat heart. The latter figure compares pH trends with (—) and without (···) drift correction. After 7 minutes background recording, the rat heart underwent two cycles of global heart ischemia/reperfusion. Ischemia occurred at 8 and 38 minutes while reperfusion started at 22 and 52 minutes as indicated by the red and green dashed vertical lines, respectively.

Figure 2-11 Demonstration of IrO_x-coated microneedle array on an explanted heart undergoing cycles of global ischemia/reper- fusion. [42]

Zuliani et al presented a complete biological protocol regarding the demonstration of their IrO_x-coated microneedle array on an explanted heart undergoing cycles of global ischemia/reper-fusion allowing mapping the pH distribution across multiple sites of the heart and showing the regional dynamics of the ischemic response (Figure 2-11). The radius and height of the needles are 0.8 mm and 1.6 mm, respectively, and the tip diameter at the apex is 50–80 µm [42].

Mani et al in 2017, presented their microneedle pH sensor incorporated with a reference electrode from Ag/AgCl thick film and a working electrode from ZnO thin film on tungsten (W) microneedle. This system exhibited the Nernstian response of -46 mV/pH and demonstrated in vivo in mice cerebrospinal fluid (CSF) and bladder (Figure 2-12), which was found totally reversible and results were reproducible after several routine testing [43].

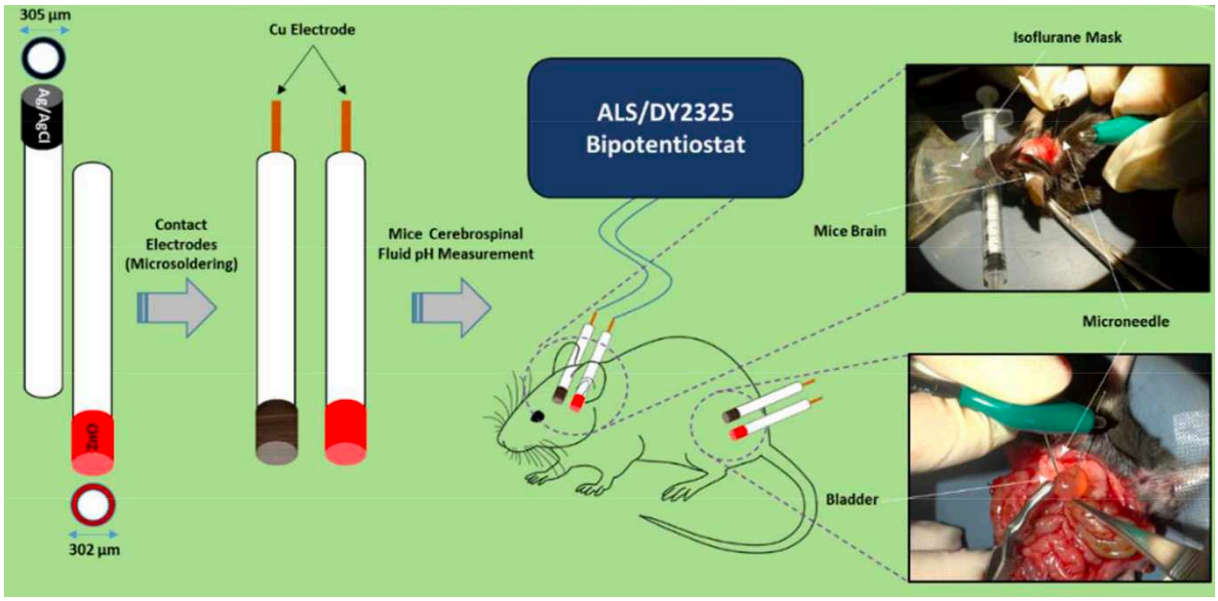

Figure 2-12 Schematic of complete fabrication and testing of microneedle pH sensor. [43]

Zhou et al. created a highly sensitive pH sensor utilizing molybdenum disulfide (MoS2) nanosheets and polyaniline (PANI)-functionalized acupuncture needles, enabling real-time tracking of pH fluctuations in the rat brain (Figure 2-13). The PAN/MoS2/AN composite exhibited a high Nernstian response of −51.2 mV/pH over a wide pH range from 3.0 to 9.0 [44].

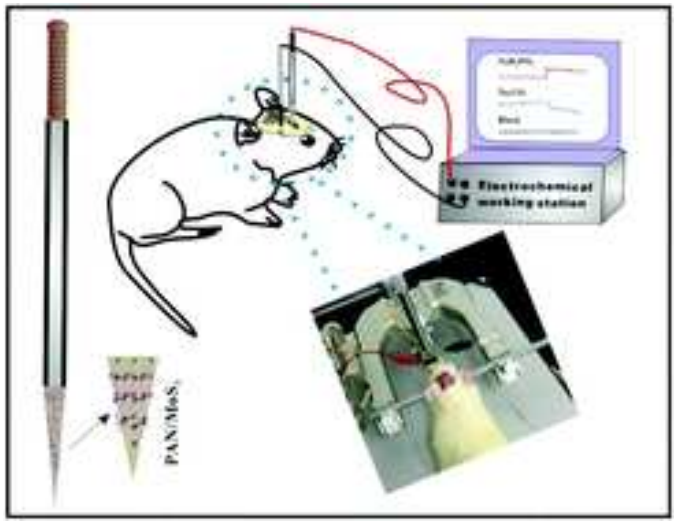

Figure 2-13 pH sensor utilizing molybdenum disulfide (MoS2) nanosheets and polyaniline (PANI)-functionalized acupuncture needles, enabling real-time tracking of pH fluctuations in the rat brain. [44]

Within the concept of microneedle, the most recent publish of García-Guzmán et al., 2021, presented a potentiometric microneedle sensor, for the first time, measure pH in transdermal. The ability to resist skin insertions was evaluated and calibrated in several ex vivo setups using three different animal skins (i.e., chicken, pork, and rat). Subcutaneous measurement of pH was also performed using a micro-pH meter (Figure 2-14) [40].

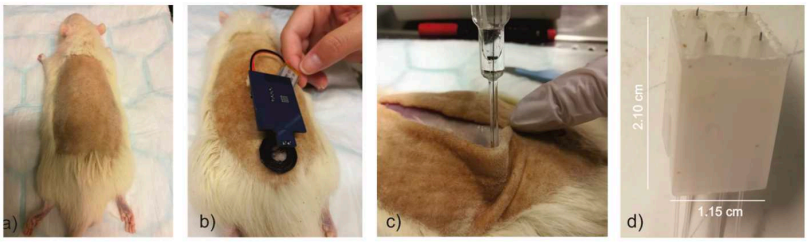

Figure 2-14 Pictures of on-body measurements in a euthanized rat specimen: (a) shaved rat prepared for the insertion of the MN patch. (b) pH MN patch coupled with the potentiometric electronic board and providing transdermal measurements in the rat back. (c) Subcutaneous measurement of pH using a micro-pH meter. (d) Home-made tool for ISF collection based on a hollow MN hub connected to a peristaltic pump. [40]

2.1.5. Overall summary

A bibliography study on the state of the art of pH sensors was presented, providing an overview on different aspects including pH sensing principle, pH sensitive materials, flexible substrate possibility. This is the base to consider and decide the design of our targeted pH sensor.

Indeed, to summarise, measuring pH levels of fetuses ideally requires a critical precision of 0.01 in pH (≥7.25: normal, continued labor vs. 7.21-7.24: borderline, birth within 30 minutes vs. ≤ 7.20: abnormal, immediate birth) in the range of pH from 6 to 8, as the human pH range.

Some pH-sensitive materials have been reported including metal oxides such as Iridium oxide (IrO_2), Ruthenium oxide (RuO_2), Tungsten trioxide (WO_3) and Titanium dioxide (TiO_2) etc., conductive polymers such as poly-aniline, poly-pyrrole, etc., and typically, the glass pH electrode with an ideal Nernstian sensitivity. However, these types of devices still have some drawbacks in terms of stability, potential drift and selectivity and the difficulty of miniaturization and conformation for the in vivo test. Since 1976, some teams have developed continuous measurement systems for tissue pH at the fetal scalp during labor, using miniaturized glass electrode, optical fiber and indicator pH colorimetric as presented in Chapter 1. The methodologies set out in these publications seemed promising, yet despite progress, it was eventually stagnant because of technical limitations mainly related to the fabrication technique linked to the difficult miniaturization of the measuring device.

To the best of our knowledge, Titanitum Nitride (TiN) is the only metal nitride reported for potentiometric pH sensors. Thin TiN films were reported to have 0.01 precision in very specific conditions. Since potentiometric based pH sensors are the most favored electrochemical systems due to their simple design and possibility to be miniaturized, our work focuses on developing a miniaturized potentiometric pH sensor using TiN as sensing material. This work is targeting a real time detection of pH in fetal tissue positioned on the scalp.

We also presented, to the best of our knowledge, all the in vivo experiments that have been reported. Despite abundant research in the field, only a few papers were found with the in vivo and ex vivo demonstration protocols. This information helps us to identify our work in the real up-to-date situations.

2.2. Methodology

2.2.1. Materials and fabrication methods

The WE of our pH sensor is constructed from multiple layers of different materials to optimize sensitivity, conductivity and consistancy of the sensor. At the same time, the design must ensure the biological compatibility and ease for sterilization. TiN is employed as the pH-sensing layer which will be in contact with the tested fluids, and TiN was reported to be biocompatible for human health. Gold which is well known as the most malleable of all metals, was selected as the metalic based layer to contruct the tracklines and the contact pads due to its high conductivity and also to avoid cracking the structure under bending stress. In the final prototype, we used polyimide as flexible substrate due to its biocompability and ease for sterilization. Platinum and Gold were used to test the possibility to be the integrated reference electrodes. The other layers of material such as TiW or Ti are seed layers to enhance then adhesion of the metalic layer such as Au or Pt, respectively.

Following the improvement of the pH micro-sensor prototype during the PhD period, there are four models of pH sensors that were designed and developed from 2020 to 2023. The subsequent section will provide a brief description of each model, encompassing their characteristics and advantages, as well as a rationale for the development of each model. A complete study on the characterization and demonstration results on these models will be later presented in chapter 2, section 2.3.

Model 1 – Glass strip/ Flat TiN

This model was initially fabricated to evaluate the sensitivity to pH of TiN, because the process on glass substrate is less complicated compared to flexible substrate. The design contains only the working electrode and without integrated reference electrode (Figure 2-15). The working electrode has sensitive area of a circle shape with various diameter: 100 µm, 200 µm, 400 µm and 600 µm to preliminarily evaluate the performance by size. This model was fabricated based on available masks in clean room and was tested later with an external commercial Ag/AgCl reference electrode from World Precision Instruments.

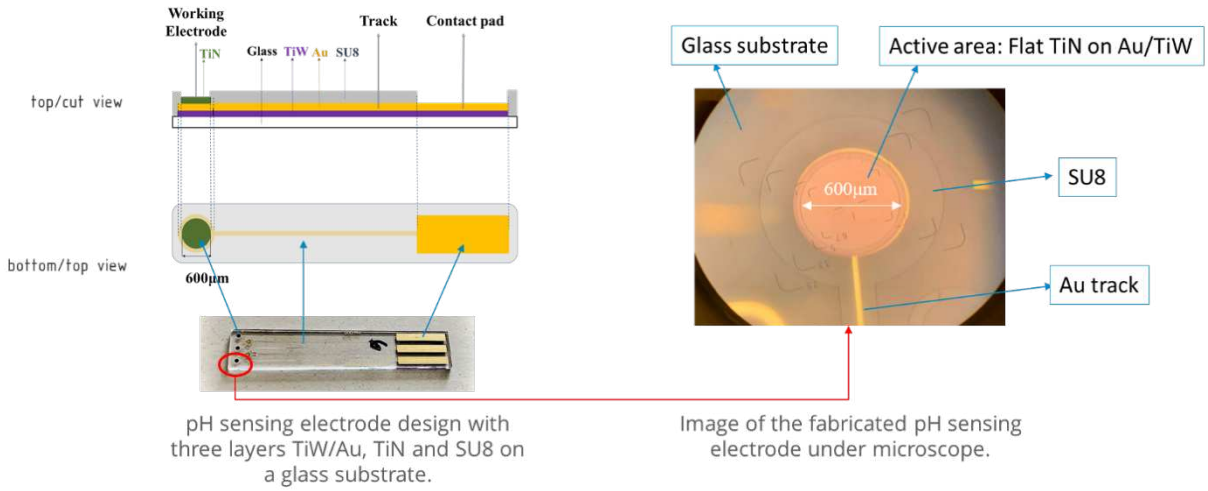

Figure 2-15 pH sensor Model 1 – Glass substrate/ Flat TiN.

Model 2 – Glass strip/ Porous TiN

The porosity of TiN was created by applying a specific treatment (see chapter 2, section 2.3.2) to the surface of the working electrode with the same design as model 1. The purpose of having porous TiN is to reduce hysteresis and increase the precision of the pH measurement. Result demonstrated that *the sensitivity is maintained the same as the flat TiN, however the precision is improved from 0.14 to 0.02 in pH* (see chapter 2, section 2.3.2.2). The porous TiN could be recognized by the darker color of the surface area as in Figure 2-16, and was confirmed by the impedance spectroscopy measurement (see section 2.3.2.2).

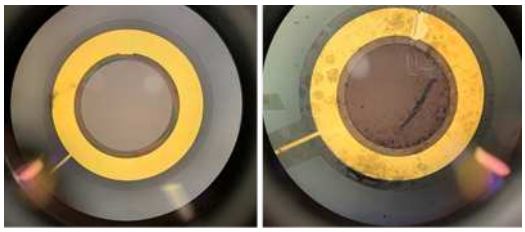

Figure 2-16 pH sensor Model 2- Glass substrate/ Porous TiN. Picture taken under microscope. Flat TiN (model 1) on the left and porous TiN (model 2) on the right.

Model 3: Flexible polyimide substrate/ Flat TiN

- Model 3-a**:** After validating our fabricated TiN can be sensitive to the pH change at a high precision (0.02 in pH), a prototype of flexible pH microsensor was designed and fabricated, which contains a working electrode and an integrated pseudo reference electrode from Platinum (Figure 2-17). Specific mask levels were designed before fabrication. Result on the characterization of this model 3 will be presented in chapter 2, section 2.3.3, and be later compared with the next model of porous TiN on flexible substrate (model 4-a).

- Model 3-b: On this model, *the geometric structure was improved* (see Figure 2-18) and made the fabrication process more complete. This model 3-b employed flat TiN and new masks were designed for this optimization (Figure 2-19). During optimization process, we changed the thickness of TiN layer from 200nm to 300nm to evaluate the sensitivity to this parameter. We also attempted to integrate a reference electrode (RE) from various materials such as Platinum, Gold and Ag/AgCL. A supplementary study about the sensitivity of the pH sensor while using the integrated RE will be presented in chapter 2, section 2.3.3.

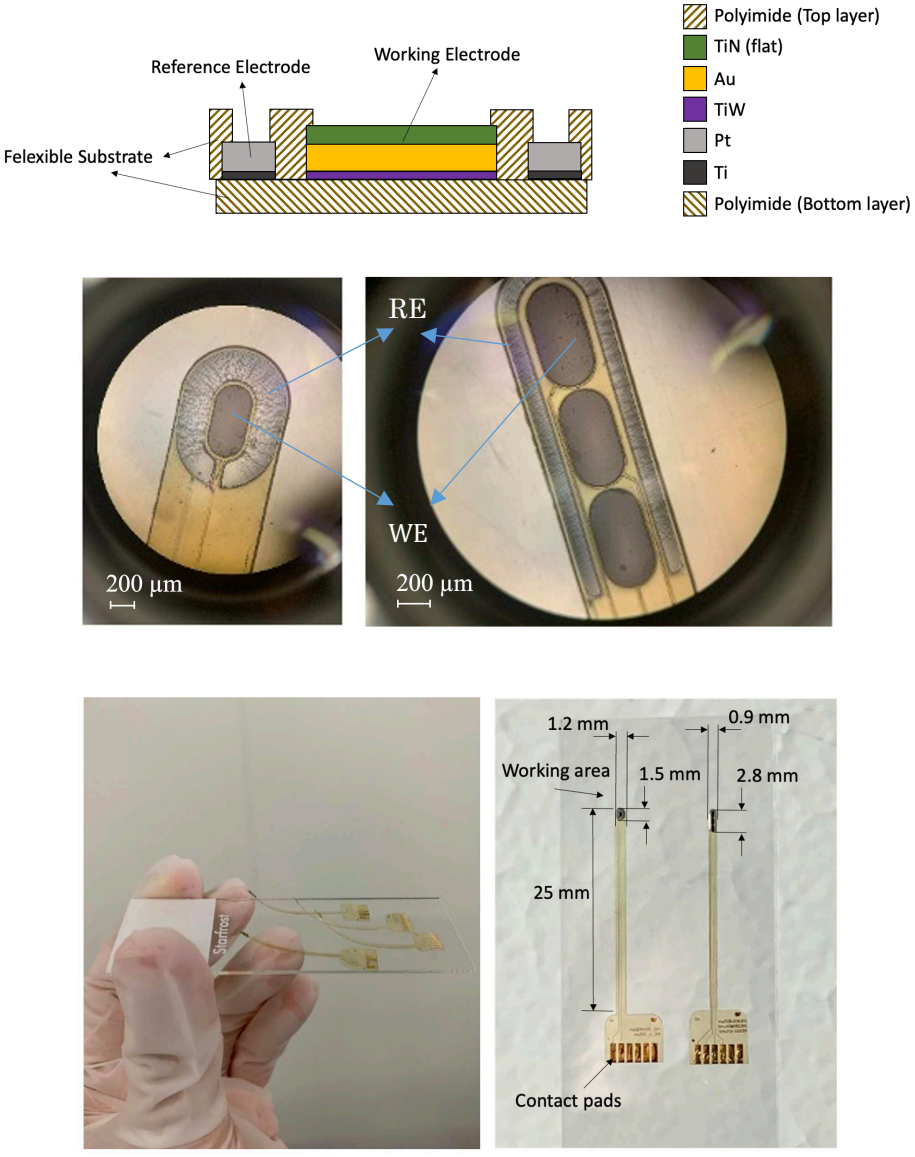

Figure 2-17 Sensor Model 3a Flexible polyimide substrate/ Flat TiN. Reference electrode is Platinum.

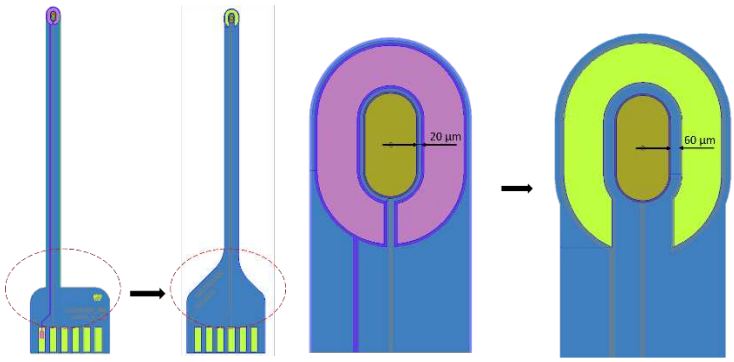

Figure 2-18 Improvement in geometric structure of model 3-b.

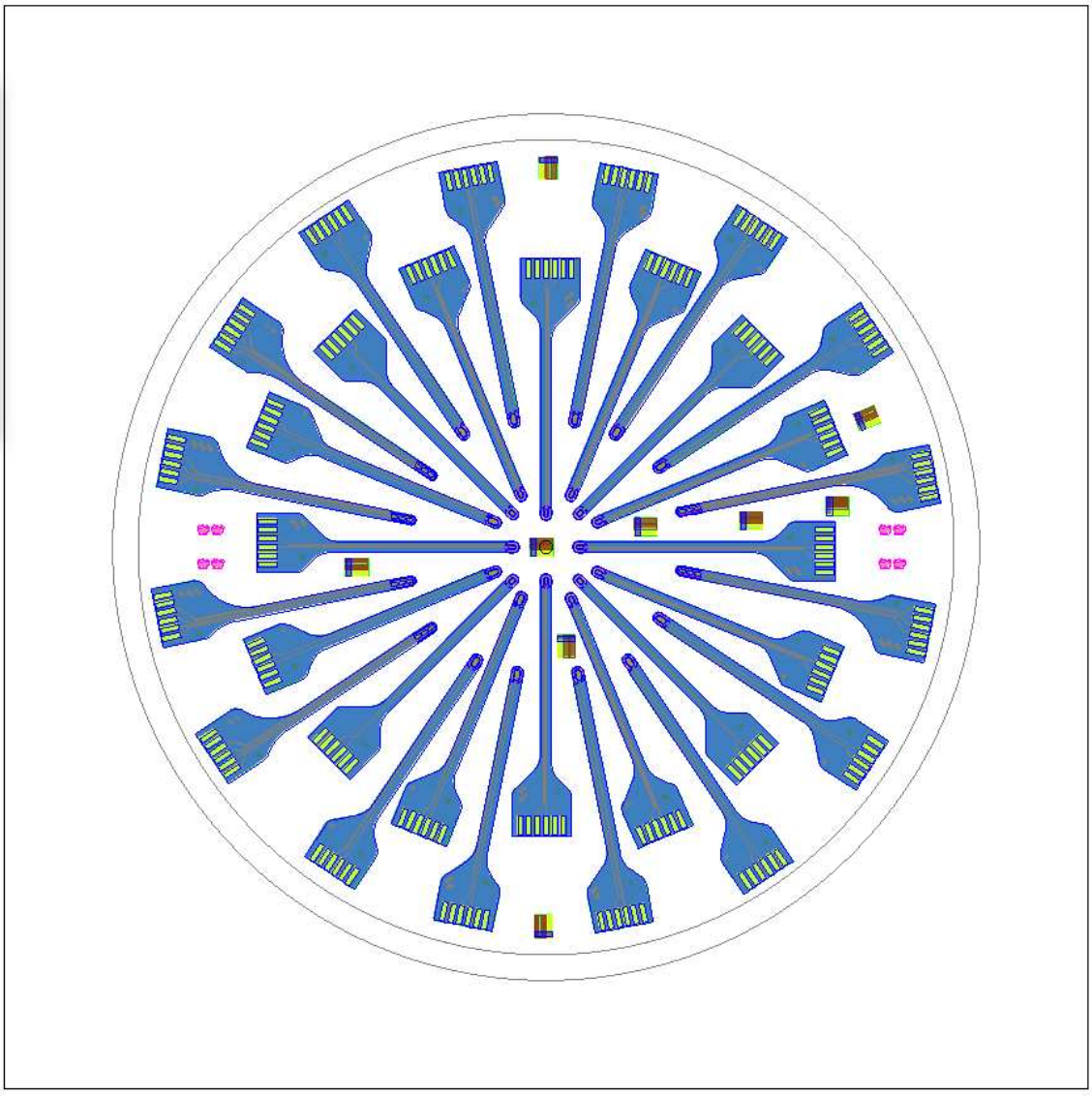

Figure 2-19 Mask design of model 3-b.

Model 4: Flexible polyimide substrate/ Porous TiN

The final prototype is introduced with an improvement from model 3, from flat TiN to porous TiN working electrode, using the same geometries and mask levels. In this model 4, we

introduced 2 sub-models to optimize the performance and suitability of design for practical application, which was re-evaluated after a few trials of demonstration on mice at Animal Facility of the Mondor Institute for Biomedical Research (IMRB, U955 Inserm –Université Paris Est Créteil, UPEC).

- Model 4-a: This is basically the *same design as model* 3-a but *with a porous TiN surface*. We fabricated a similar TiN layer of 200nm thick and then applied the treatment to create the porosity. This model 4-a is tested and compared to model 3-a, which shows an advantage in precision from 0.1 to 0.05 while mantaining the same sensitivity. This is in agreement with the above-mentioned models on glass substrate.
- Model 4-b: This is basically the *same design as* model 3-b but with *a porous TiN surface*. We fabricated a similar TiN layer and then applied the treatment to create the porosity. This model 4-b employed porous TiN in an optimized geometric design (Figure 2-20). Results on this model will be presented in chapter 2, section 2.3.4.

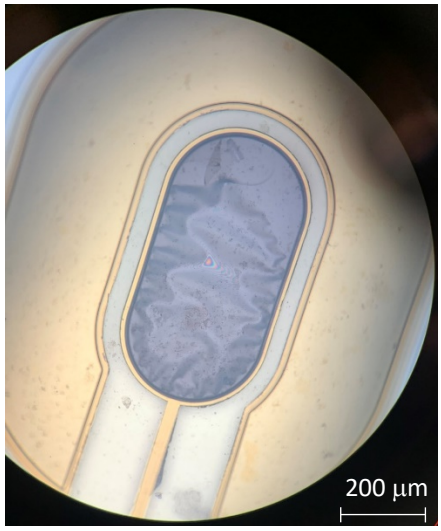

Figure 2-20 Photo under microscope of etched TiN flexible – new mask. Reference electrode is Gold.

The detailed structure of each model and its characterization results and comparisons will be presented in chapter 2, section 2.3. This is however demonstrated that our final model 4-b is the optimized prototype for a pH microsensor.

The materials used in these models and their fabrication methods are listed in table 2-5. Principle of each fabrication methods are explained in annex. The fabrication methods step by step of each model are detailed in chapter 2, section 2.3.

Table 2-5 Materials and equipment used in pH sensor fabrication.

Component	*Material*	*Formula*	*Fabrication method*	*Equipment/supplier*
WE	Titanium Nitride	TiN	Sputtering	Plassys
WE/RE	Gold/ Titanium Tungsten	Au/TiW	Sputtering	Alcatel
RE	Titanium/Platinum	Ti/Pt	Sputtering	Plassys
RE	Silver/Silver Chloride	Ag/AgCl	Commercial	From World Precision Instruments
RE	Silver/Silver Chloride	Ag/AgCl	Paste	From Sigma Aldrich
Flexible substrate	Polyimide	PI	Spin coating	SÜSS
Insulator layer	SU-8	SU-8	Spin coating	SÜSS
Wafer	Glass	SiO_2	Commercial	From Plan Optik/Wafer Universe
Wafer	Silicon	Si	Commercial	From Sil'Troni
Sacrificial layer	Aluminum	Al	Sputtering	Plassys

2.2.2. Methods to study material properties

Morphology of our TiN surfaces was studied by using Scanning Electron Microscopy (SEM, Neon 40, Zeiss).

Potentiostatic Electro Impedance Spectroscopy (PEIS) and Cyclic Voltammetry (CV) were carried out to study electrochemical properties of materials, using a three electrodes potentiostate (SP-200 from Biologic Science Instrument), Figure 2-21. A Silver/Silver Chloride (Ag/AgCl) and a Platinum (Pt) wire were used as an external reference electrode and counter electrode, respectively. PEIS measurements were conducted in Phosphate Buffer Saline (PBS) 0.01 M. CV measurements were carried out in Lithium Perchlorate (LiClO4) 0.1 M, with potential window from - 0.8 V to 0.8 V and at different scan rates (from 50 mV/s to 500 mV/s).

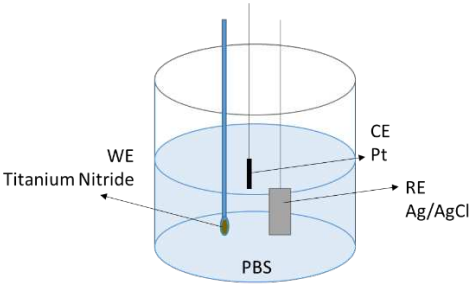

Figure 2-21. Experimental setup to measure CV and PEIS.

Experimental results including a comparison of PEIS and CV between flat TiN and porous TiN in case of glass strip and flexible substrate is presented accordingly in chapter 2, section 2.3.

2.2.3. Method to study the performance of our pH sensors

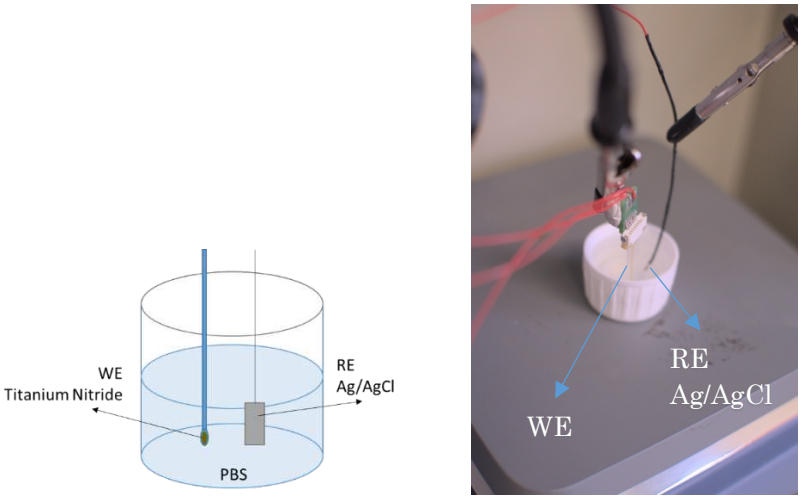

Figure 2-22 Experimental set up to test sensitivity of flexible TiN electrode in PBS solution at different pH levels.

The pH sensing performance of the fabricated electrodes was studied by measuring open circuit voltage (OCV) or open circuit potential, also using the potentiostat SP-200 from Biologic Science Instrument. OCV was measured in phosphate-buffered saline (PBS) test solutions with pH ranging from 6 to 8 at room temperature, with 0.2 pH step to determine sensitivity, stability, response time, hysteresis and reproducibility of the pH sensor. pH solutions, Figure 2-24, were prepared from DPBS 10X, Gibco 14200-067, diluted to 1X with distilled water; NaOH 1N, VWR 28222-290 and HCl 3,7 %, VWR 20252-290, by INSERM. An Ag/AgCl electrode was used as an external RE (Figure 2-23). The WE and the RE were submerged sequentially in the test solutions disregarding cross-contamination. A commercial glass electrode from Atlas Scientific was used to confirm the pH level of the solution under testing.

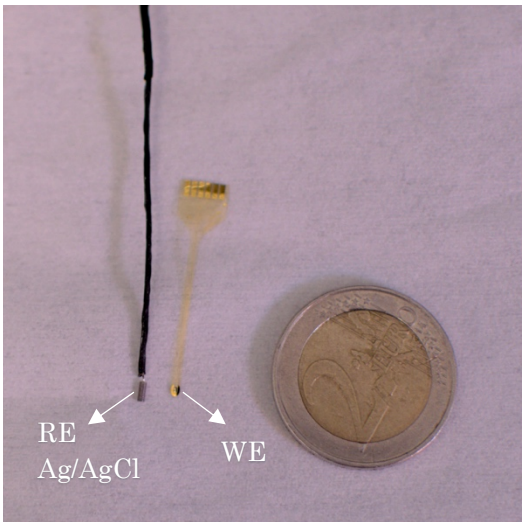

Figure 2-23 RE (Ag/AgCl) and fabricated pH probe.

Measuring the OCP with a potentiometric pH sensor has some remarks during manipulation:

1. Make sure that the electrodes are in close proximity to each other but are not touching while immerse both the pH-sensitive electrode and the reference electrode in the solution being measured.

2. Measure the voltage difference (without current) between the pH-sensitive electrode and the reference electrode. In some cases, the electrodes need to be equilibrated in the solution for a few minutes to ensure that the OCP has stabilized.

Figure 2-24 Test solution PBS at different pH levels.

We also tested the performance of our fabricated sensors at 37°C (body's temperature). The experimental set up is described as in Figure 2-25. Hot plate 2 (5) is used to heat and maintain the PBS test solutions at different pH levels at 37°C during the experiment. The measurements are performed sequentially in each PBS solution placed on hot plate 1 (2). Thermometer 1 (3) and 2 (4) are used to check the temperature of the solutions heated by the two hot plates to ensure they have the same temperature of 37°C. The RE and WE are fixed above the test solution and are connected to the input of potentiostat SP-200 (9) in order to

register the signal. Output of potentiostat is connected to a computer which has installed EC-Lab software (8) to monitor the data acquisition of multiple experimental protocols (e.g. OCV, PEIS, CV).

The system to measure pH of the test solutions (6) is showed on Figure 2-26, in which the above-mentioned commercial glass electrode from Atlas Scientific (7) is connected to an EZO™ pH Chip from Atlas Scientific. A customized LCD screen is controlled via Arduino (programed by Antoine Bessiere, Intern, ESIEE) for data visualization and data storage in a SD card. This system could be also used for OCV measurement by replacing the EZO™ pH Chip by the EZO™ ORP Chip from Atlas Scientific and the corresponding connection pins to Arduino.

A homemade Faraday cage is used to avoid noise from electronic equipment in the lab, or the contact to tissue during experiment conducted by potentiostat SP-200. Practical experiments show that the EZO™ ORP Chip could filter the noise better than the potentiostat, especially in case measuring in vivo, while the electrode is placed with the skin of animal.

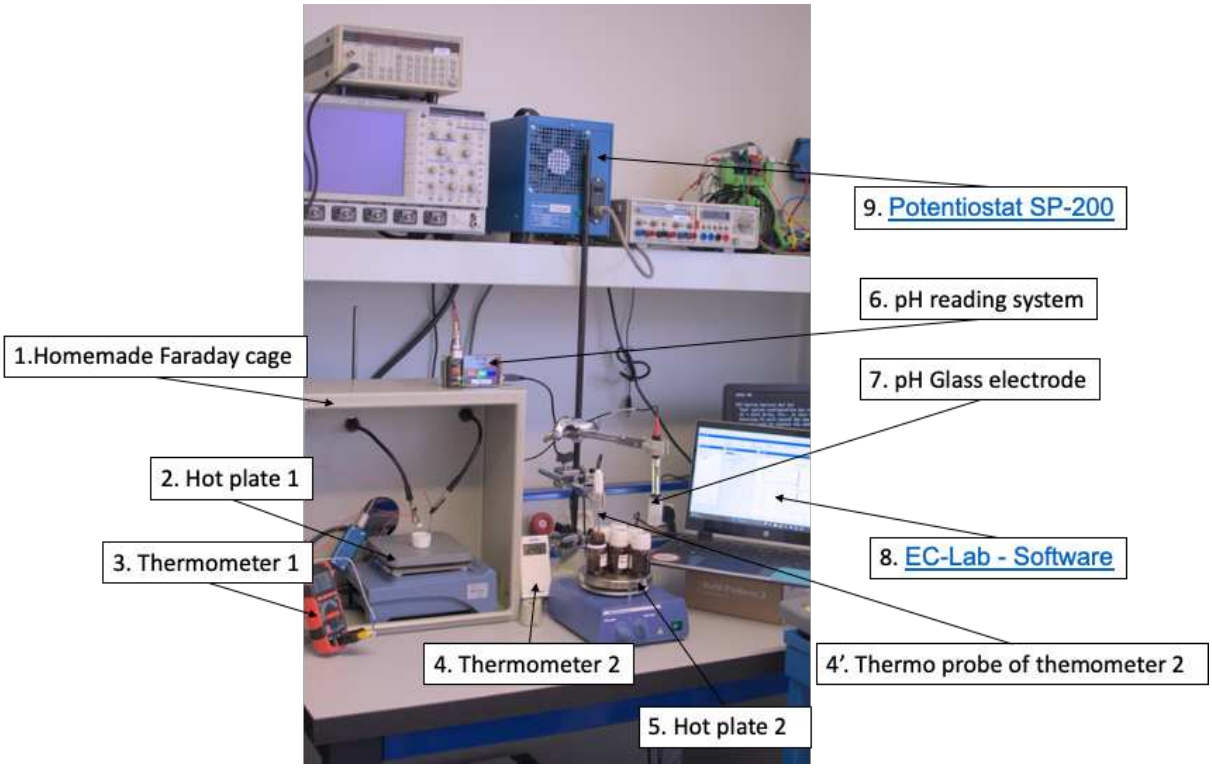

Figure 2-25. Experimental setup to run experiment at higher temperature.

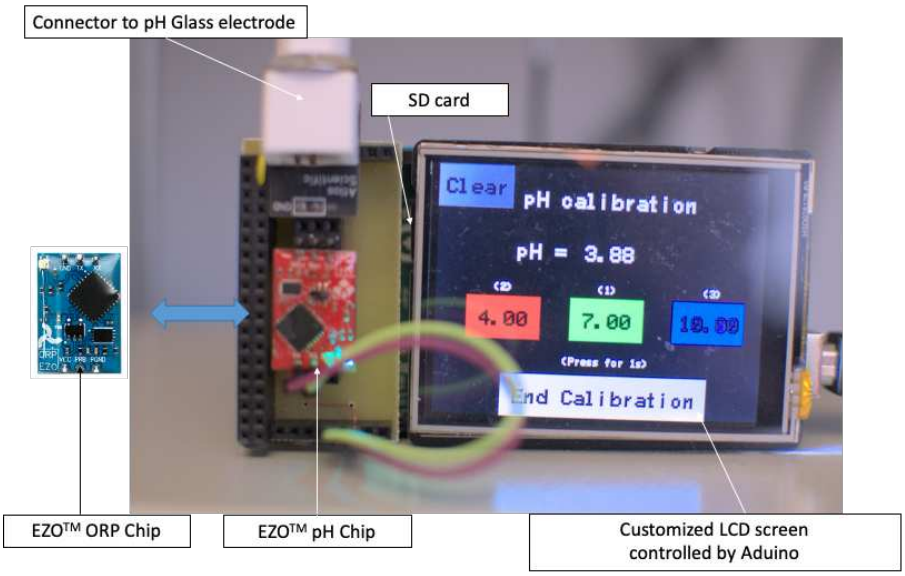

Figure 2-26. pH reading system using EZO™ pH Chip connected to a customized LCD screen controlled via Arduino and data storage in a SD card. EZO™ ORP Chip could be replaced incase measuring OCV.

Experimental result will be given in chapter 2, session 2.3.

2.2.4. In vivo demonstration procedure

Three demonstrations on mice were conducted at Animal Facility of the Mondor Institute for Biomedical Research (IMRB, U955 Inserm –Université Paris Est Créteil , UPEC) during the development of the prototype, as follow:

- Demonstration 1: included 2 sessions occured on 20th and 27th, June, 2022. Demonstrated on model 3, wafer 1, 2 sensors on 5 mice (4 male, 1 female).
- Demonstration 2: included 3 sessions occured on 29th September, 6th and 13th October, 2022. Demonstrated on model 3 and model 4 wafer 2, 5 sensors on 6 mice (2 male, 4 female).

The in vivo test was conducted on mice with the pH probe implanted under the skin either at the tail or the leg, under #35095-2022013116589573 v11 authorisation. OCV signal was recorded under anesthesia conditions. For the anesthesia protocol, buprenorphine at the concentration of 0.05 mg/kg was injected subcutaneously 30 min before the general anesthesia, which is performed under 2% isoflurane.

A compact measurement system was designed with a customized LCD screen for real time signal visualization, an EZO™ ORP Circuit for data acquisition and an integrated SD card for data storage.

2.3. Fabrication and characterization results

2.3.1. Model 1 – Glass strip/ Flat TiN

A microelectrode of 600 µm diameter was fabricated using Titanium nitride (TiN) as the potentiometric sensing material for pH variations.

2.3.1.1. Fabrication process of model 1

Electrodes of 600 µm diameter in size were fabricated following the process illustrated on Figure 2-27: (1) a gold/titanium tungsten (Au/TiW) layer of 520 nm in thickness was deposited on a glass substrate (Alcatel sputtering), (2) a positive photoresist was spin coated on top of the gold layer for photolithography, development and etching, (3) the photoresist was removed, (4) the process was repeated with the second layer which is then TiN of 200 nm thick (Plassys sputtering) and (5) completed with the third layer of 1.7 µm thick photoresist SU8 used as an insulator with the openings on the electrode and contact pad areas. Figure 2-28 illustrates the design of the electrode with the corresponding microscope image on Figure 2-29.

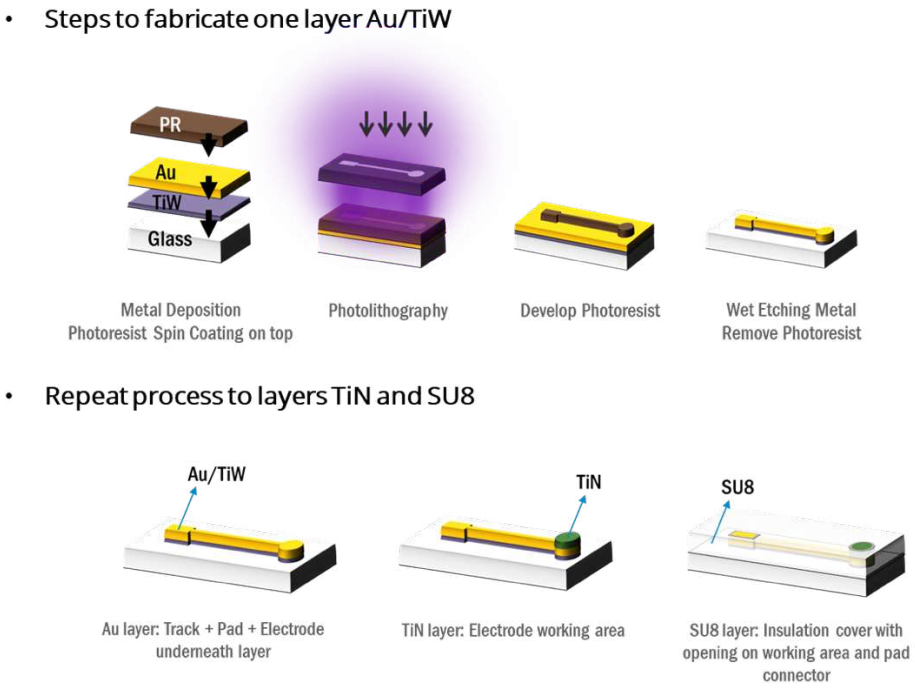

Figure 2-27 Fabrication steps of pH sensor model 1 - Glass strip/ Flat TiN.

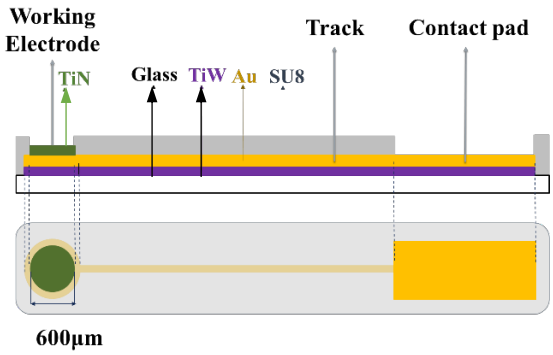

Figure 2-28 pH sensing electrode design with three layers TiW/Au, TiN and SU8 on a glass substrate, top/cut view, bottom/top view.

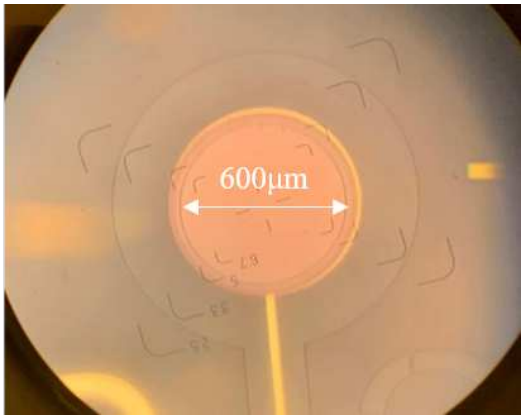

Figure 2-29 Image of the fabricated pH sensing electrode under microscope.

2.3.1.2. Results and discussion on model 1

TiN electrode characterization for pH sensing application.

The sensitivity of the TiN electrodes fabricated with the above-described clean room process as a potentiometric sensor was determined by measuring the OCV values at different pH levels of the test solutions during 100 s. The recorded data from 50 s to 100 s were averaged to calculate the sensitivity of TiN electrode as shown in Figure 2-30. The slope of the curve is 62.8 mV/pH corresponding to the sensitivity of the TiN electrode. The correlation coefficient was calculated to be 0.998 and the standard reduction potential E is 402.6 mV, corresponding to the intercept of the curve.

This sensitivity is higher than the reported results of sputtered TiN film with the same thickness of TiN layer (57.5 mV/pH, $R^2 = 0.9999$), [16], TiN nanotube array (TiN NTA, 55.33 mV/pH, $R^2 = 0.995$), and TiN nano powder (TiN NP, 46.48 mV/pH, $R^2 = 0.992$), (Liu et al., 2016).

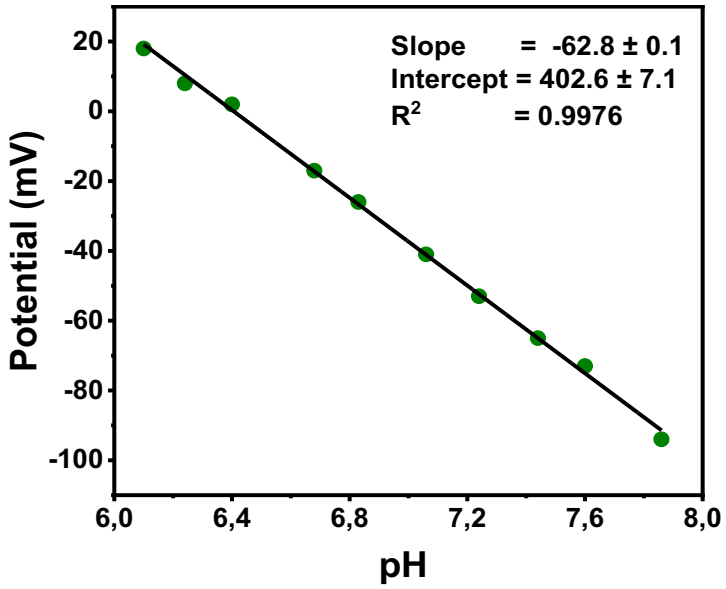

Figure 2-30 OCV curve and sensitivity of our fabricated TiN electrode.

Data from Table 2-7 show that we should achieve a better sensitivity than most of the other materials. Especially compared to IrO_2, which has been developed for in vivo and in vitro applications, our TiN electrode has shown a comparable sensitivity. It was however reported a greater sensitivity in conductive polymer - based sensors such as polyaniline and polypyrrole blends (310 ± 40 mV/pH and 1300 ± 100 mV/pH, respectively) [27]. Yet, their application is still limited due to its tendency to become unstable over time.

Table 2-6 Potentiometric pH sensor performance of different materials.

Material	Sensitivity (mV/pH)	Response time (s)	Reference
TiN NP	46.48	5.2	[35]
TiN NTA	55.33	4.4	[35]
TiN thin film	57.5	-	[16]
IrO_2	69.9 ± 2.2	0.5 s	[45]
IrO_2	51	0.9 to 2 s	[46]
Polyaniline	58 ± 0.3	20	[47]
Polyaniline	62.4	12.8	[48]
Polyaniline/Zeolite blend	310 ± 40	-	[49]
Polypyrrole/Zeolite blend	1300 ± 100	-	[49]

The response time of the TiN electrode was measured by immersing the WE and the RE continuously in PBS solutions with pH levels from 6.10 to pH 7.74. The time for the signal to reach 90 % of equilibrium value is 10 s (Figure 2-31) which is comparable and even better than some reported polymer-based potentiometric pH sensors (Table 2-6). This response time is slower than that of TiN NTA (4.4 s), TiN NP (5.2 s) [35] and IrO_2 (0.5 s to 2s) (Manjakkal

et al., 2020). This can be explained by the low porosity of the surface of our TiN layer (ability to trap more ions in a certain area), which is expected to be improved in the next fabrication process after a specific surface treatment.

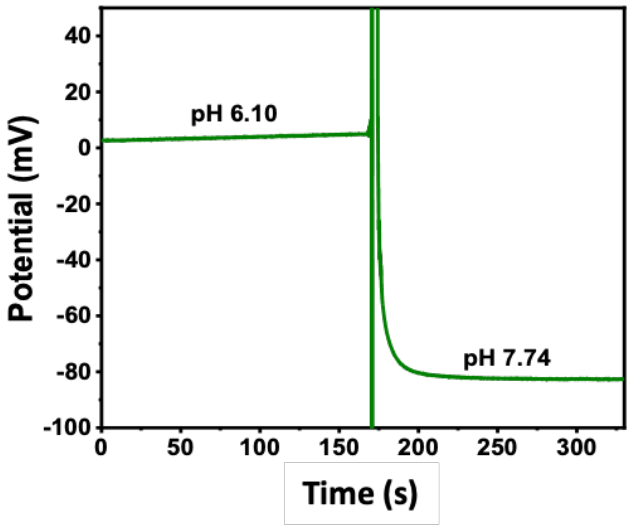

Figure 2-31 The response time of TiN in PBS. The parasite signal in between two pH levels is only due to manipulation during the experiment.

Figure 2-32 shows the stability of the open circuit potential of the same electrode in different pH levels during 200 s. A potential drift of less than 3 mV was observed during the first 50 s but stabilized after that. This drift might have been caused by the hydrogen ion trapping and diffusion phenomena into the lattice of the material.

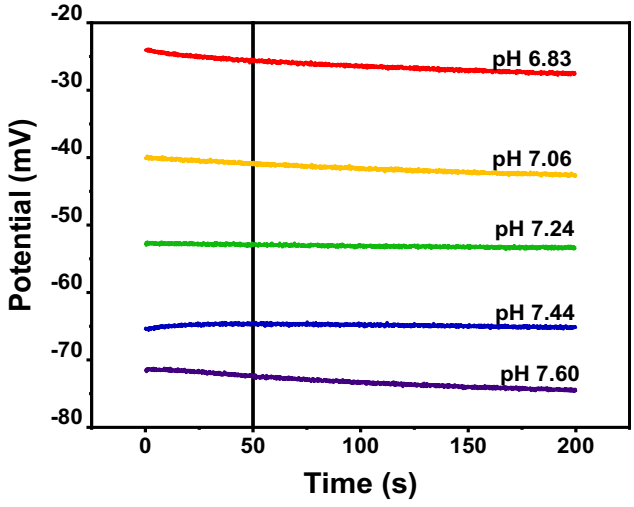

Figure 2-32 The stability of one TiN electrode at different pH levels of PBS solutions during 200 s.

A hysteresis of 10 mV was observed with the pH range from 6 to 7.6 during 6 cycles, as shown in Figure 2-33. The hysteresis could be caused by the cross-contamination and possibly by condition differences in the testing process, such as the stability of pH test solutions, temperature and connection problems. Since we are looking at a small variation of pH in a

narrow clinical-related pH range, the experiment still needs to be improved to evaluate accurately the performance of the electrode including operation at 37°C. This temperature dependence will be detailed in section 2.3.3.2c.

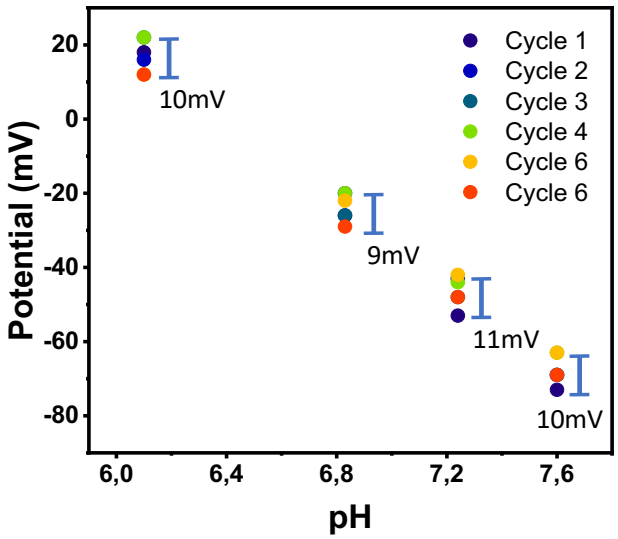

Figure 2-33 OCV of one TiN electrode during 6 cycles.

Reproducibility during 3 loops of measurements on the same electrode is presented in Figure 2-34. The variation of the pH value was calculated to be 0.14 (by hysteresis over sensitivity), which represented the precision of our electrode. It is not yet sufficient for the fetal tissue pH monitoring application but already interesting for other applications. The optimization was then proposed by varying the TiN fabrication parameters, changing its surface properties (roughness) and creating porous TiN to improve the performance of the TiN electrodes.

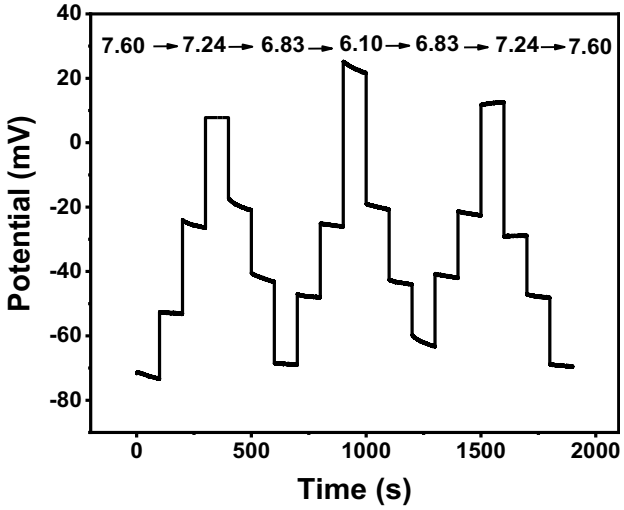

Figure 2-34 The reproducibility of one TiN electrode during 3 loops measurements in 4 pH levels: 6.10, 6.83, 7,24, 7.60.

2.3.1.3. Conclusion on model 1

A prototype, model 1, capable of measuring pH has been developed showing promising initial performance. To summaries, a 600 µm diameter pH sensing electrode that was constructed from Titanium nitride (TiN), performed a linear Nernstian sensitivity of 62.8 mV/pH within the pH range from 6 to 8 with a precision of 0.14.

2.3.2. Model 2 – Glass strip/ Porous TiN

As the precision of pH measurement of model 1- flat TiN - based prototype (0.14 in pH) has not yet reached the medical requirements, this section presents the development of porous TiN as pH sensing material on glass substrate. The idea is to enhance the precision of the sensor. By applying an additional wet etching process, the porosity of TiN surface can be controlled. Improvements in chemical properties and performances are presented and compared to flat TiN.

2.3.2.1. Fabrication process of model 2

The flat TiN electrodes of 600 µm diameter and 200 nm in TiN thickness were prepared on glass substrate with the technique described in the previous section. Electrodes were prepared by O2 plasma cleaning and then etched in a mixture solution of H2O2 30% + TBR, at 40° C. Porosity of the TiN surface has been obtained after 6-minutes etching time (Figure 2-35). Electrodes were then rinsed in DI water during 3 minutes.

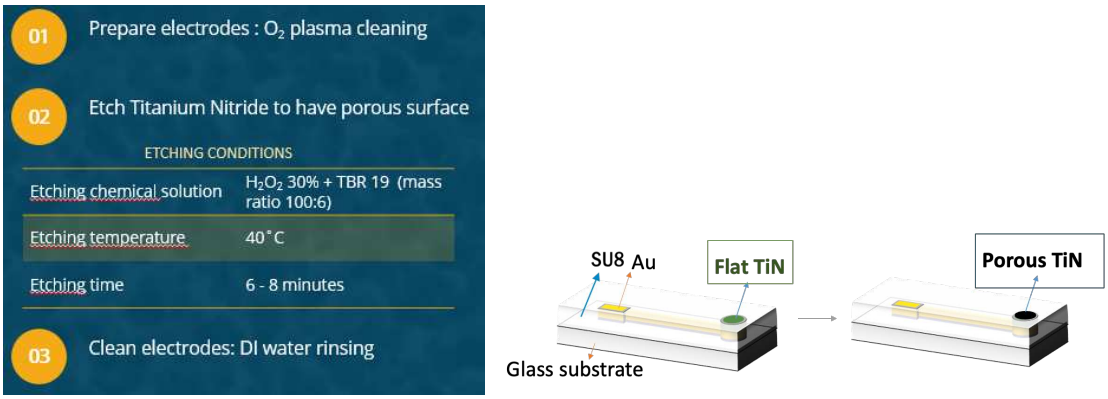

Figure 2-35 Fabrication process of a porous TiN electrode.

2.3.2.2. Results and discussion on model 2

Morphology Study

SEM images of TiN surface etched 6 minutes and flat TiN surface are shown in Figure 2-36. Porosity of the TiN surfaces appeared obviously on the etched electrode.

a) b)

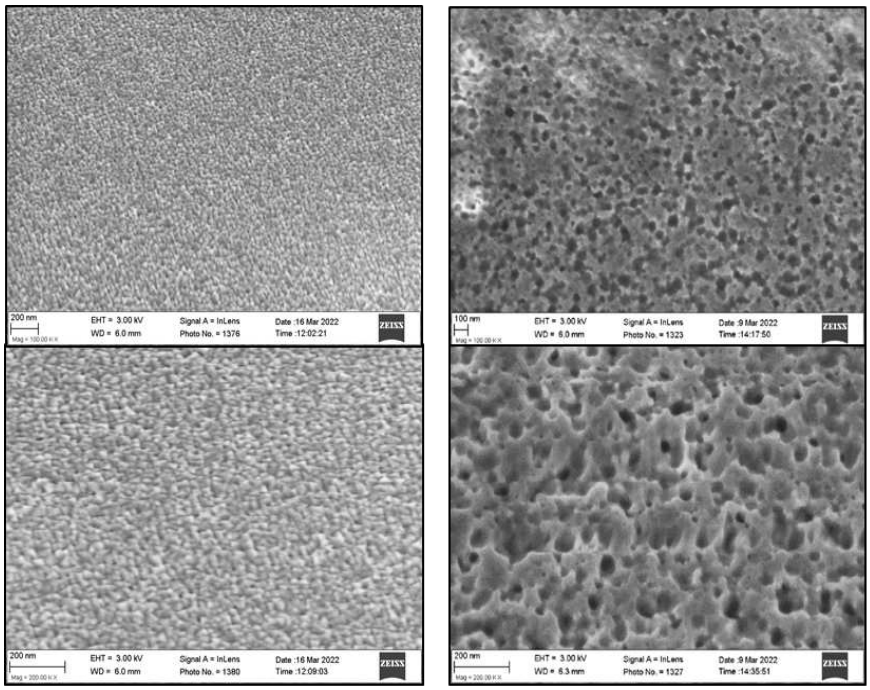

Figure 2-36 SEM images of a) flat TiN, b) 6-minute etched TiN at 100 KX (top) and 200 KX (bottom) magnification.

Images of the flat TiN and porous TiN electrodes are also illustrated in Figure 2-37. A darker color of the porous TiN surface can be easily recognized under a simple microscope.

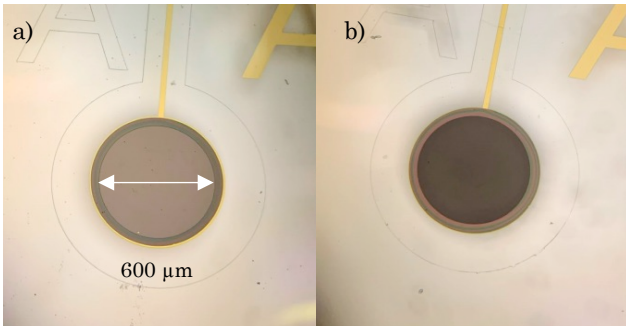

Figure 2-37 Images of a) TiN flat electrode and b) porous TiN (6-minute etched).

Electrochemical Property Improvements

Impedance of the two electrodes etched in 4 and 6 minutes were measured and compared to that of flat electrodes. In our application, the impedance at low frequencies is concerned rather than at high frequencies. Indeed, the OCV is measured at a very low current condition. Figure 2-38 shows a 6.3 time decrease in impedance (2.089 kΩ at 100 Hz) on the 6-minute etched electrode compared to the flat electrode (13.183 kΩ at 100 Hz). This demonstrates that the working effective surface area was significantly increased with our wet etching technique. To clarify the optimized etching time, the impedance in module and phase at 4-minute etching time are plotted, showing a slightly higher impedance module of 4-minute

etched TiN compared to that of 6-minute etched TiN. The visible change in the capacitive behaviour at low frequency confirms the surface porosity has been increased.

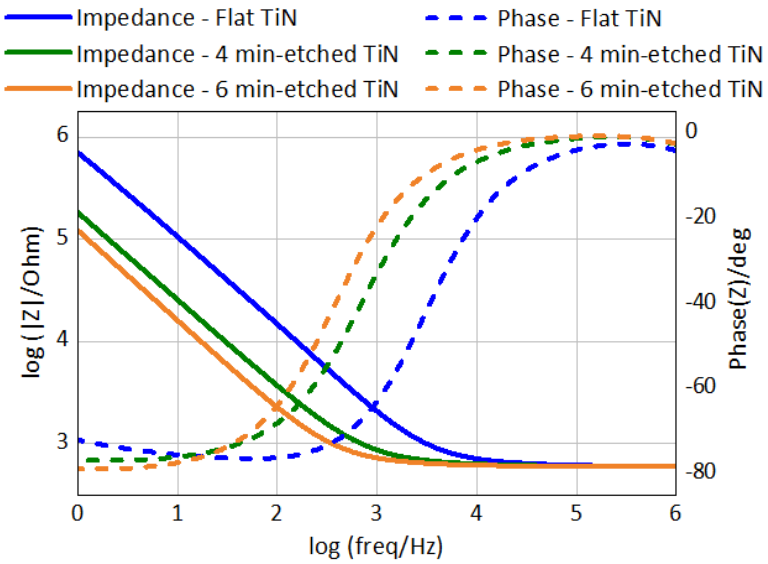

Figure 2-38 Impedance module/phase of flat TiN, 4-minute etched TiN and 6- minute etched TiN in PBS 0.01 M. Electrode diameter is 600 µm.

CV curve of the flat TiN electrode was compared to the 6 - minutes etched TiN electrode at 0.1 V/s scan rate in Figure 2-39. We observed a quasi-rectangular shape of CV curve on flat and porous TiN which is in coherence with literature [50], [51], [52], and indicates capacitive charge transfer behaviour by charging and discharging the TiN electrolyte double layer. Porous TiN is indicative of a higher capacitance compared to flat TiN. Furthermore, this shape of CV curve of the porous TiN electrode remained unchanged while experiment was performed at different scan rates from 50 to 500 mV/s (Figure 2-40). This signifies our porous TiN could be for instance a good candidate for supercapacitor electrode materials.

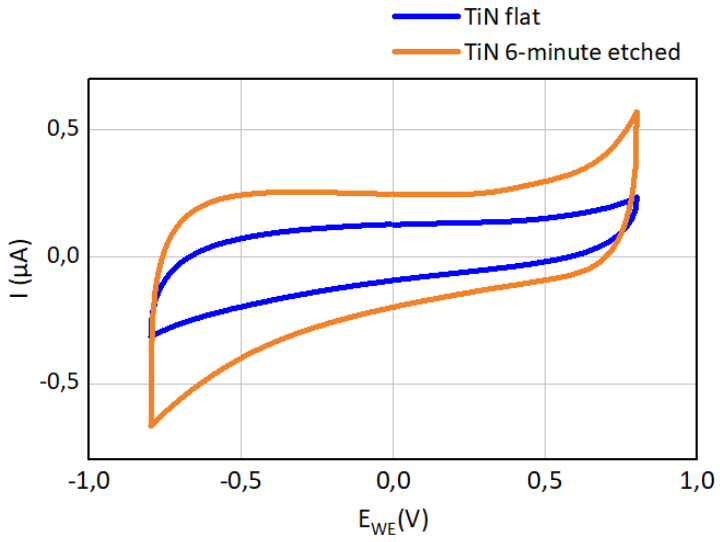

Figure 2-39 CV of flat TiN electrode and porous TiN (6-minute etched) electrode in LiClO4 0.1 M, scan rate 0.1 V/s and potential window from - 0.8 V to 0.8 V.

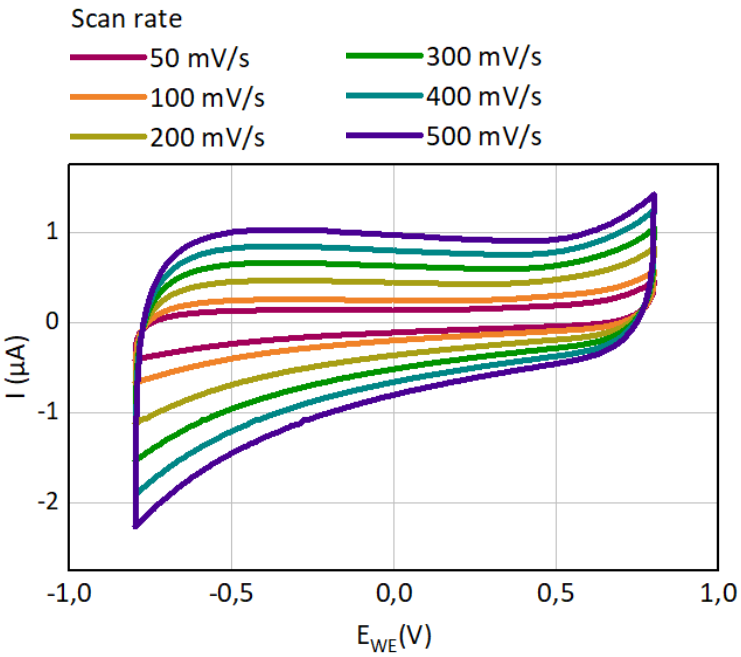

Figure 2-40 CV of porous TiN (6-minute etched) electrode in LiClO4 0.1 M, scan rate 0.1 V/s and potential window from - 0.8 V to 0.8 V.

Figure 2-41 plots the current ΔI/2 (positive value at 0V) measured at each scan rate and its value. Slope of the linear fit curve (0.001844 µAs/mV = 0.001844 mF) corresponds to the capacity in µF of the electrode. By dividing by the surface (diameter of 600µm, surface area is 0.002827 cm²), the capacity of the material TiN porous was found to 652 µF/cm².

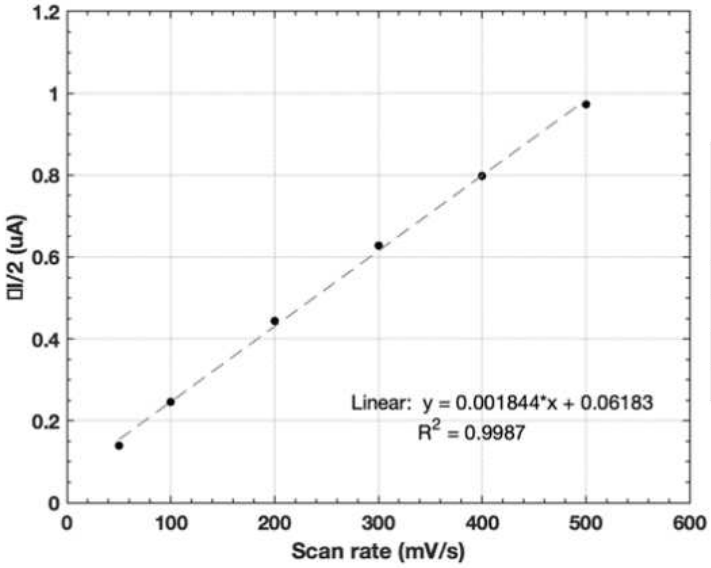

Scan rate mV/s	ΔI/2 µA
50	0,13904
100	0,24698
200	0,44343
300	0,62846
400	0,79795
500	0,97285

Figure 2-41 Plot of current ΔI/2 vs scan rate and the values.

pH Sensing Performance

OCV measurements were conducted in PBS solution at different pH levels ranging from 6 to 8. Data from 50 s to 100 s were averaged to determine sensitivity of the porous TiN. Sensitivity of the porous TiN electrodes was determined to be slightly higher than our reported flat electrode (67.06 mV/pH of porous TiN electrode compared to 61.8 mV/pH of flat electrode [53], Figure 2-42). This sensitivity is higher than the other reported TiN pH sensor (Table 2-6).

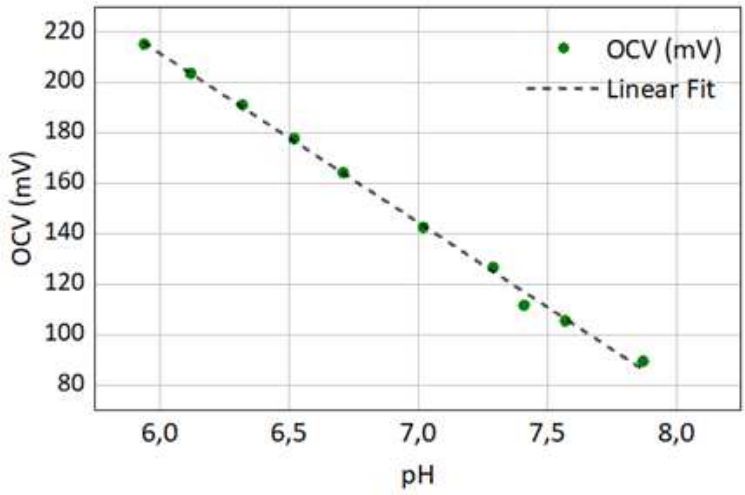

Figure 2-42 Sensitivity of porous TiN electrode (6-minute etched).

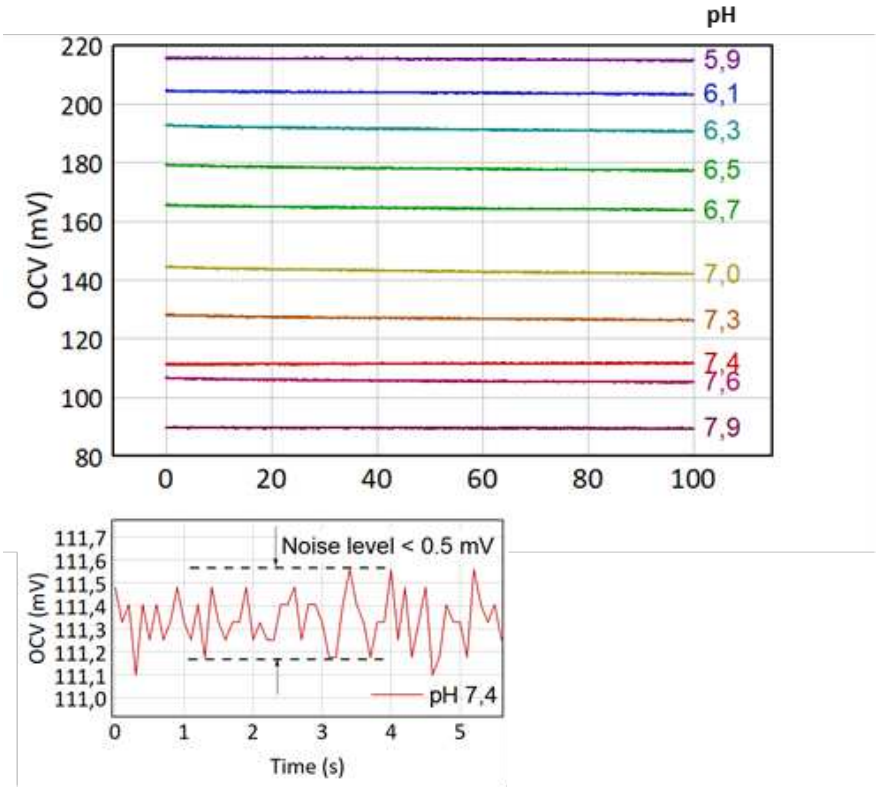

Figure 2-43 Stability of porous TiN electrode (6-minute etched) different pH levels (top) and noise level (bottom).

Figure 2-43 shows a stable OCV signal (a small drift of 2 mV on average) at each pH level during 100 s of experiment. Noise level of the OCV signal is recorded quite small at less than 0.5 mV.

Repeatability of the etched electrode while changing pH levels of test solution from 7.0, 7.3, 7.4 and reverted is presented in Figure 2-44. During six measurement cycles, a drift of 2.3 mV/cycle at pH level 7.3 was observed (Figure 2-45). This drift can be corrected by integrating a data post-processing in a microcontroller unit, which corresponds to calibration.

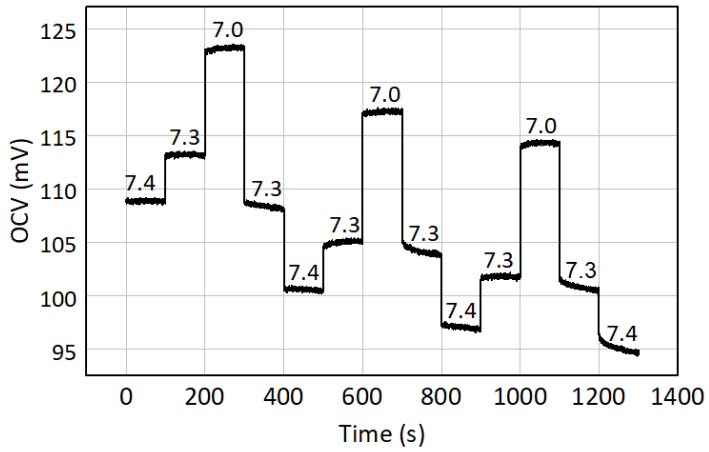

Figure 2-44 Reproducibility of porous TiN electrode (6-minute etched) at three pH levels (7.0, 7.3, 7.4).

After subtracting the drift, the maximum hysteresis of the etched electrode at pH level of 7.3 was determined to be 1.75 mV/pH (Figure 2-45).

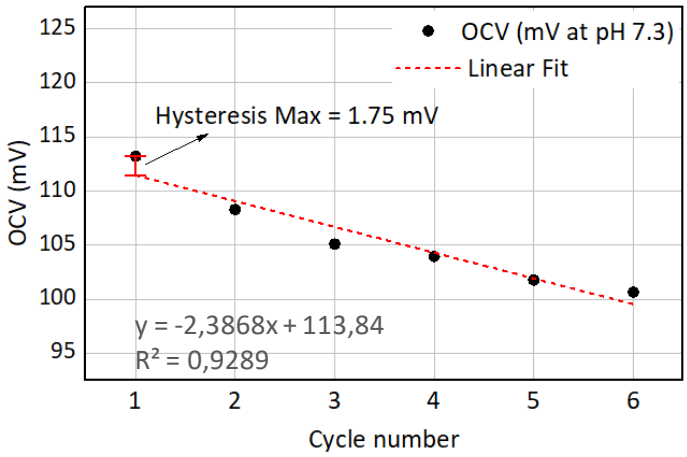

Figure 2-45 Drift at pH 7.3 over six cycles and hysteresis maximum regarding the drift slope of of porous TiN electrode (6-minute etched).

The precision of the developed pH sensor was calculated to be 0.03 in pH, by the hysteresis (1.75 mV/pH) divided by sensitivity (67.06 mV/pH). This result validates an improvement of factor 4.7 in precision of our pH sensor (precision on flat Tin electrodes was 0.14 [53]), better targeting fetal health monitoring constraints.

We tested the sensitivity and calculated the precision one several electrodes by the similar method. Results shows in Table 2-7 demonstrate the precision be could achive down to 0.02 in pH.

Table 2-7. Sensitivity and precision calculation on several electrodes.

Electrode	Impedance (kΩ)	Slope Sensitivity (mV/pH) (X)	R^2 (mV/pH)	Slope drift over 6 cycles (mV/cycle)	R^2 drift over 6 cycles (mV/cycle)	Hysteresis MAX vs. Fit curve (mV) (Y)	Precision (pH) (Y)/(X)
400µm Full/etched 6'– A	1,62	63	0,9916	-4,6 ± 0,3	0,9795	1,84256	±0,029
400µm Full/etched 6'– B	1,74	58	0,9949	-4,8 ± 0,4	0,97959	- 1,39039	±0,024
400µm Full/etched 6' – C	1,77	-	-	-6,5 ± 0,2	0,99634	- 1,39654	-
600µm Donut/etched 8' – A	1,15	60	0,9878	-0,9 ± 0,3	0,75665	1,21135	±0,020
600µm Donut/etched 8' – B	1,11	65	0,9957	-2,7 ± 0,2	0,97599	1,37266	±0,021
600µm Donut/etched 8'– B*	1,11	65	0,9957	-3,0 ± 0,1*	0,99161*	- 0,66066*	±0,010*

(*) tested again the next day/ same conditions

2.3.2.3. Conclusion on model 2

Model 2 of pH sensor based on porous TiN was developed and exhibits a good pH sensing performance. Characterisation results of pH sensor fabricated with porous TiN present a remarkable improvement in precision compared to flat TiN, from 0.14 to 0.03 in pH, showing a promising possibility to achieve the medical requirement (precision at 0.01 for fetal health monitoring to reach the decision threshold). The sensitivity slightly increased to 67.06 mV/pH and a drift of 2.3 mV/cycle appeared during six experiment cycles. This study is an intermediate step to understand the behaviour of the porous TiN in pH sensing within the same conditions as on flat TiN. Transferring the current structure onto a Polyimide

substrate is the next process, preparing for in vivo test on mice and later aiming for the fetal health monitoring application.

2.3.3. Model 3 – Miniaturized and flexible polyimide substrate/ Flat TiN

2.3.3.1. Fabrication process of model 3-a

The masks used in the photolithography process to fabricate different layers on the pH sensor were designed by Coventor software. There are seven materials in our flexible pH sensor design, as illustrated in Figure 2-46.

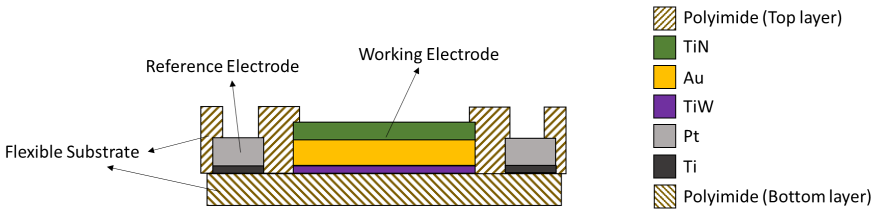

Figure 2-46 Stack of layers of flexible pH sensor combined of polyimide (top and bottom substrate), Ti/Pt (RE) and TiW/Au/TiN (WE).

Polyimide was used as flexible substrate and deposited at the top and the bottom layers due to its biocompatible properties and ease for sterilization procedure [36]. Gold (Au) was used as material for the track lines, contact pads and the layer underneath working electrode (WE) to maintain a high conductivity. A thin layer of Titanium Tungsten (TiW) was used as adhesion layer and followed by gold deposition. Working electrode was done by TiN on top of Au and Platinum (Pt) was used as a pseudo reference electrode (RE). The polymer top layer protects the full sensor including the track lines with openings on the WE, RE and the contact pads to the external connectors.

We designed several sizes of the flexible pH sensor probes, Figure 2-47, to test the performance of each design, in order to optimize the structure and to evaluate the feasibility of the small animal in vivo tests.

There are three single-probe designs and one triple-probe design. The single-probe designs are structurally similar but the sizes of the WE vary (300 µm x 600 µm, 400 µm x 800 µm and 600 µm x 1200 µm), as seen in Figure 2-47. Geometric structure and dimensions of a single-electrode probe are illustrated on Fig 2-48 and detailed in Table 2-8. To better compare the performance of the WE with different sizes, the surface area of RE were maintained the same by modifying the width of the RE. The triple-electrode design contains three electrodes of the intermediate size 400 µm x 800 µm. Multi-electrode sensor allows averaging and better reliability during the test.

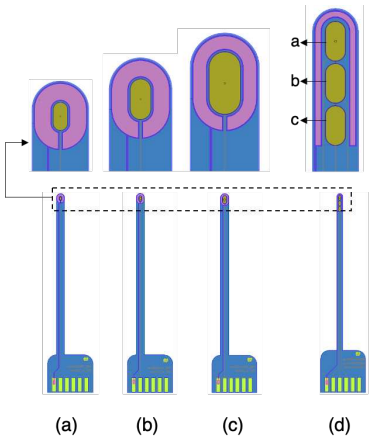

Figure 2-47 Design of the flexible pH sensor. Single-probe electrode designs: (a) 300 µm x 600 µm, (b) 400 µm x 800 µm and (c) 600 µm x 1200 µm. Triple-probe electrode design: (d) 400 µm x 800 µm for each electrode.

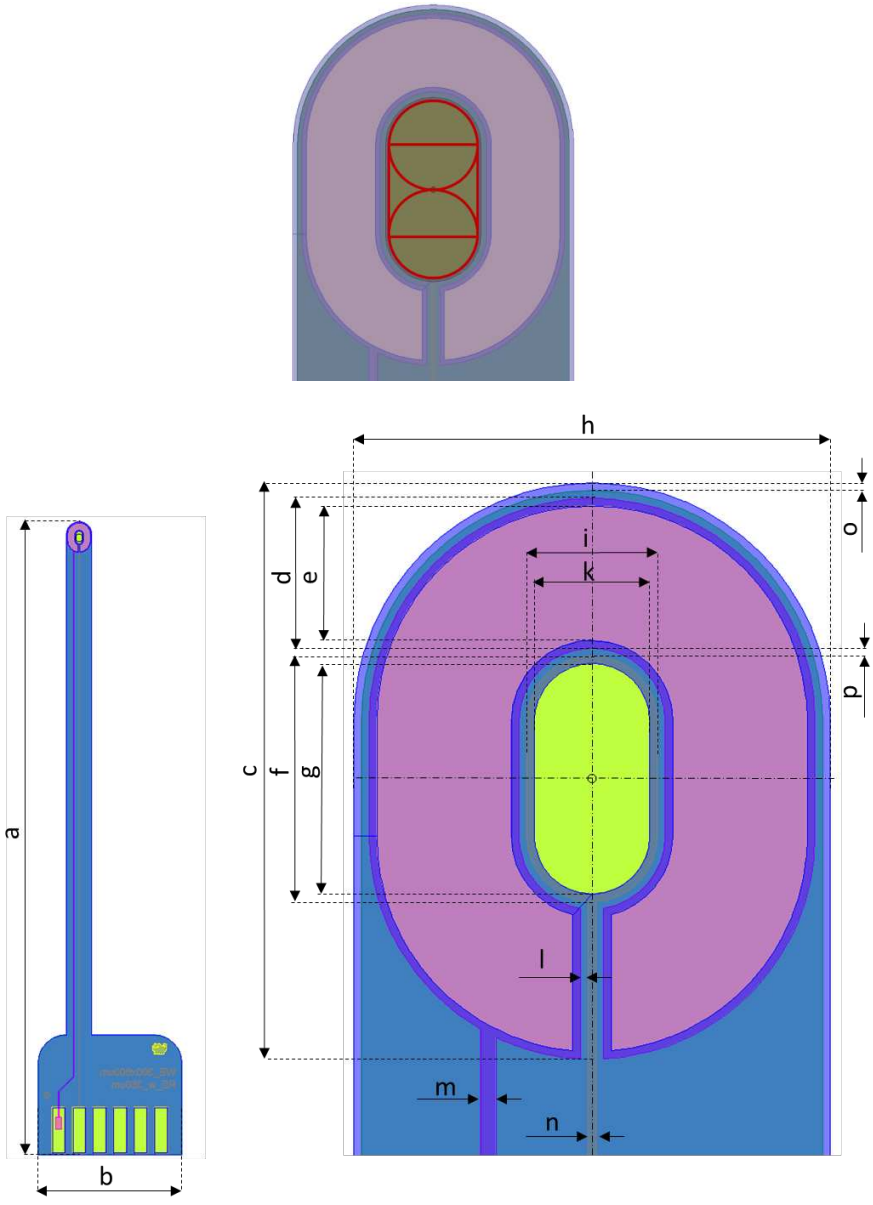

Figure 2-48 Geometric structure and Dimentions of a single-electrode probe.

Table 2-8 Dimensions (in µm) of a single-electrode probe.

Design	S1 300 µm x 600 µm	S2 400 µm x 800	S3 600 µm x 1200 µm
a	3000	30	30
b	7000	7000	7000
c	1500	1620	1900
d	390	350	290
e	350	310	250
f	640	840	1240
g	600	800	1200
h	1240	1260	1340
i	340	440	640
k	300	400	600
l	20	20	20
m	40	40	40
n	20	20	20
o	20	20	20
p	20	20	20

In order to successfully combine the six layers, the fabrication process was conducted from the bottom layer to the top layer on a silicon wafer as in Figure 2-49. The detailed description of the process is given in the next sections. Figure 2-50 illustrates some images under microscope from fabrication process step by step, for better idea about the actual colors and appearances of each layer once applied.

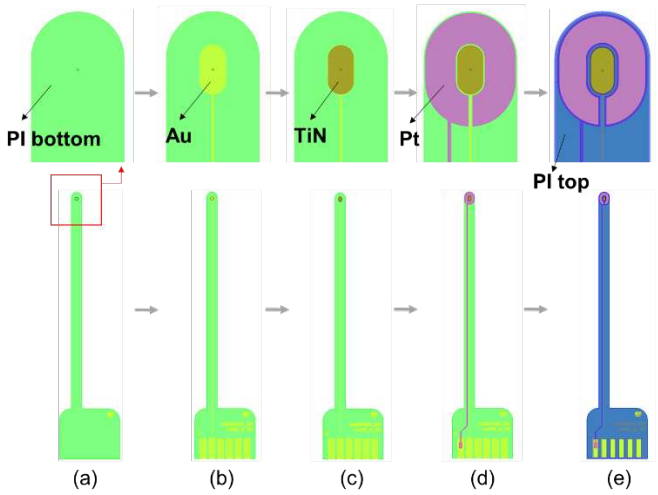

Figure 2-49 Fabrication steps. a) PolyImide (PI) bottom layer; b) TiW/Au deposition and lift-off; c) TiN deposition and wet etching (WE); d) Ti/Pt deposition and lift-off (RE); e) PolyImide top layer.

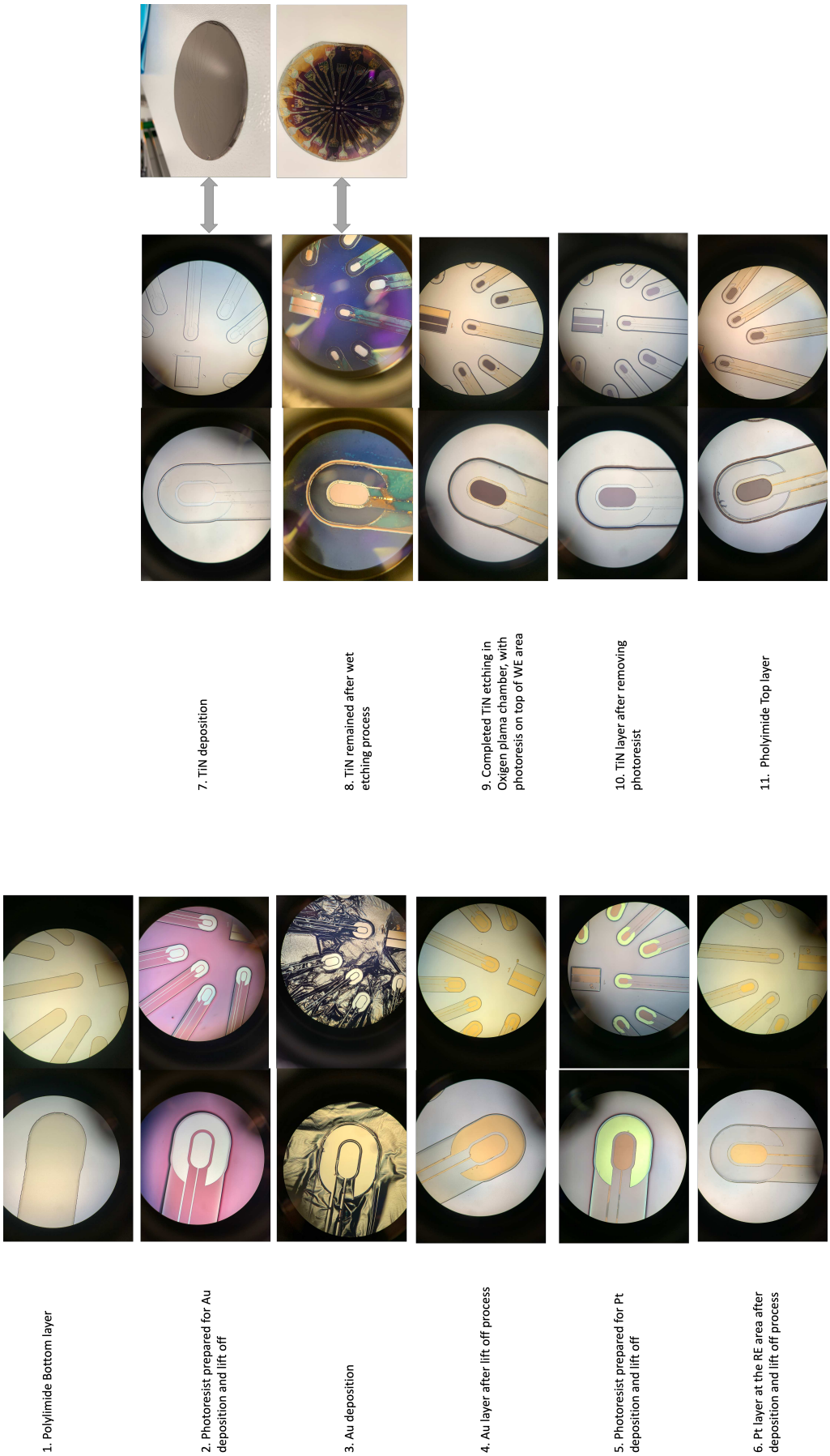

Figure 2-50 Photo under microscope of fabrication process step by step.

1) Layer 1: Polymer Bottom

A silicon wafer was prepared with an Aluminum layer of 500 nm thick deposited on one side, which plays the role of a sacrificial layer for the final releasing process. Before depositing bottom polymer layer, the wafer was placed on a hot plate at 110°C for 10 minutes to remove humidity. A positive photosensitive polyimide LTC 9320 was poured and spin-coated on top of the dried silicon wafer. A soft-baking was done at 110°C during 5 minutes. Photolithography was conducted on BSA K&W MA 1006 machine during 70 seconds exposure time. After the post-exposure bake, development was done in HTR solution and rinsed with RE 600 solutions. Finally, the wafer was left in an oven set at 230°C during 3 hours for polymer curing process (step a of Figure 2-49).

2) Layers 2 and 3: TiW/Au for metallization

The TiW/Au conductive layers were patterned using lift-off procedure with TI xLift X (Clariant) photoresist of approximate 5 µm to 7 µm thickness. A soft baking at 95°C was required before exposure during 15 seconds. The photoresist was then developed in a mixture of AZ400K/ Deionized water. The wafer was finally cleaned by Oxygen plasma using NEXTRAL RIE machine at 90 Watts. Alcatel plasma sputtering machine was used to deposit 20 nm TiW and then 500 nm Au layers at 200 Watts. To create the patterns of electrodes and tracks, lift-off process was performed using acetone in ultrasonic bath for 10 minutes. Finally, wafer was cleaned in isopropyl alcohol (IPA) and then in deionized water (DI) in 3 minutes. At this stage, the metal tracks, pads and electrode shapes were defined (step b of Figure 2-49).

3) Layer 4: TiN as sensitive material of the working electrode

Plassys plasma sputtering machine was used to deposit the TiN layer at 200 Watts. The same TI xLift X photoresist was used again with a negative mask. A specific baking step was required to revert the polarization of this photoresist. Next step was TiN etching in solution mixture of TechniEtch TBR19 (Technic) and DI with a mass ratio of 6:100. Finally, acetone was used to remove the photoresist before final rinsing (step c of Figure 2-49).

4) Layers 5 and 6: Ti/Pt for the reference electrode

Similar to TiW/Au layers, TI X Lift X was used as photoresist for the lift off process of Ti/Pt layers with a negative mask. The same Plassys plasma sputtering machine was used to deposit Ti/Pt at 200 W. Lift-off Ti/Pt was done in an ultrasonic acetone bath for around 4 minutes, before cleaning and rinsing (step d of Figure 2-49).

5) Layer 7: Polymer Top and release

A top polyimide layer was added with the same process described in step one but with a different mask which has openings on the WE, RE surfaces and on the contact pads. This

second layer is important to protect the whole sensor for better manipulation and to avoid electrical shortcuts.

The last step was to release the flexible sensors out of the silicon wafer by electro-chemical erosion of the Al sacrificial layer. Figure 2-51 shows the sample of pH sensors fabricated with the above-described process with their dimensions and Figure 2-52 gives a zoom on the electrodes under microscope.

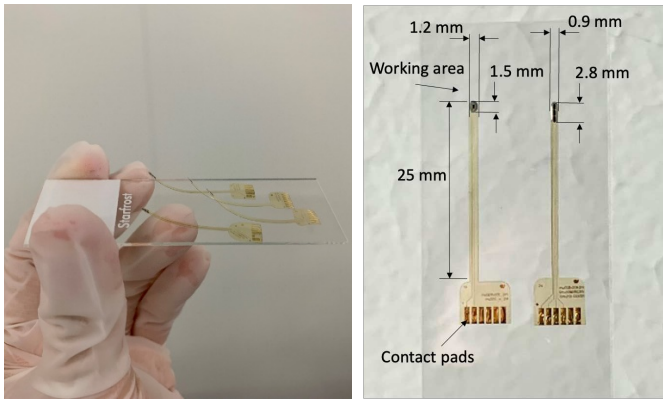

Figure 2-51 Sample of two flexible pH sensors model 3a.

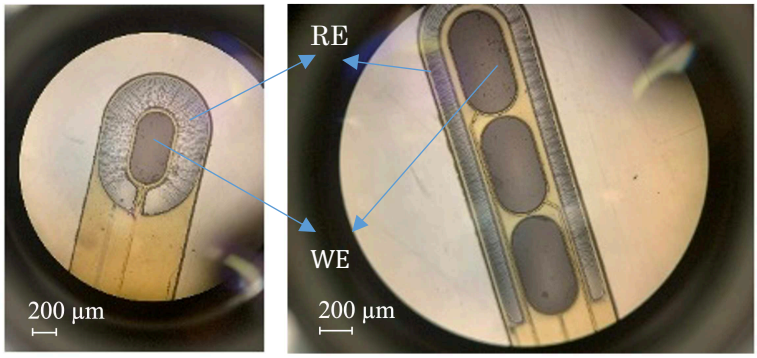

Figure 2-52 The final flexible pH sensor samples. Microscope images focused on the electrodes.

We must give some additional remarks on the process. The above mentioned technique was applied in the second run of fabrication in July 2022, which has succesfully manufacted 32 implants with full structure. A first run was held on May 2022, with the same mask levels and structure of materials but different fabrication process in term of layering order. The fabrication layer was done in a different order: Polymer bottom, Platinum, Titanium Tungsten/ Gold, Titanium Nitride and Polmer Top. This fabrication process failed because of the fracture of Platinum patterns, which meant to be the RE. This failure happened after TiN etching process in chemical solution, which caused the peal off of Pt patterns. Another failure happened to be the short cuts between the WE made of TiW/Au and TiN, and RE made of Pt. These errors were due to the TiN etching process which could not remove completely the TiN residue at the narrow gap between the WE and RE. This error was fixed

in the second run of fabrication in July 2022, when an oxygen plasma technique was applied in complement to wet etching during the TiN etching process.

2.3.3.2. In vitro - Results and discussion on model 3-a

a) Evaluation of sensor size vs sensitivity

We tested the functionalization of fabricated TiN on 10 single-electrode probes at 3 sizes (300 µm x 600 µm, 400 µm x 800 µm and 600 µm x 1200 µm) and 1 triple- electrode probe which contains 3 electrodes of 400 µm x 800 µm in size.

The sensitivity of the TiN electrodes fabricated with the above-described clean room process was determined by measuring the OCV values at different pH levels of the test solutions during 100 s. Results show that seven electrodes work with a good sensitivity (53-67 mV/pH, Table 2-10) and six electrodes are not functional or present lower sensitivity. These results are based on the very first probes fabricated with the described process which was also under development in parallel.

TABLE 2-9 SENSITIVITY OF FLEXIBLE PH SENSORS IN CASE USING EXTERNAL AG/AGCL REFERENCE ELECTRODE

Electrode	Size (µm x µm)	Sensitivity (mV/pH)	E_0 (mV)	R^2
Single 01	300x600	-67.6	655.6	0.9535
Single 04	400x800	-53.7	525.5	0.9978
Single 05	600x1200	-54.9	226.1	0.9481
Single 07	600x1200	-62.5	507.9	0.9997
Single 08	600x1200	-57.7	479.4	0.9982
Triple 01a	400x800	-53.3	482.5	0.9848
Triple 01c	400x800	-65.5	531.1	0.9909

(R^2 is correlation coefficient and E_0 is standard reduction potential)

Figure 2-53 illustrates the sensitivity of the seven functional electrodes after normalizing the OCV at pH 7 to zero. The absolute value of sensitivity of these electrodes are shown in Table 2-10. It is noticeable that the fabricated flexible sensor exhibits less uniform performance as fabricated on glass [54]. The sensitivity curve of the electrode with smaller size of 300 µm x 600 µm is less linear (Figure 2-54) than the larger electrode size of 400 µm x 800 µm and 600 µm x 1200 µm (Figure 2-55 and Figure 2-56). Since the size of these large electrodes

are still compatible with the practical insertion to the mice for in vivo tests, 400 µm x 800 µm and 600 µm x 1200 µm could be chosen as an appropriate design of the flexible pH sensor.

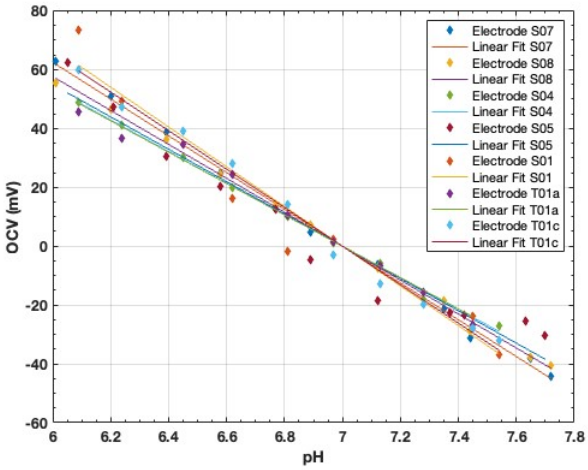

Figure 2-53 Sensitivity of flexible pH sensors tested in PBS solutions at different pH levels.

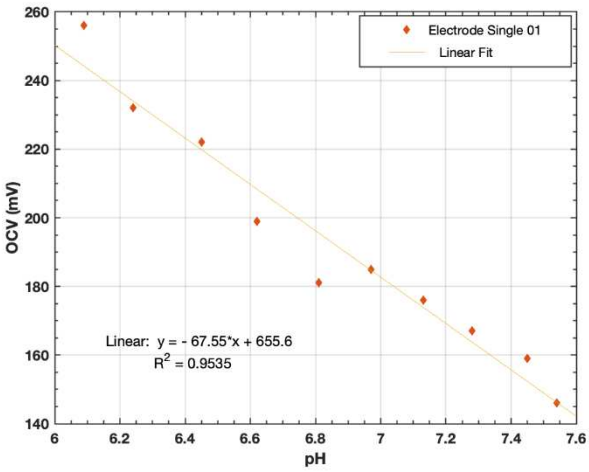

Figure 2-54 Sensitivity of flexible pH sensor tested in PBS solutions at different pH levels. Working electrode is 300 µm x 600 µm in size and Reference electrode is Ag/AgCl.

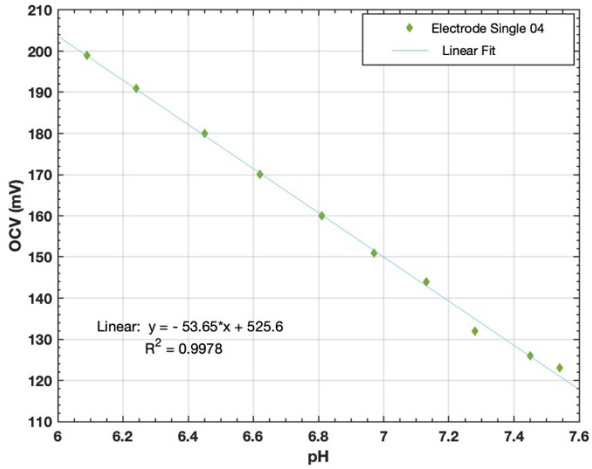

Figure 2-55 Sensitivity of flexible pH sensor tested in PBS solutions at different pH levels. Working electrode is 400 µm x 800 µm in size and Reference electrode is Ag/AgCl.

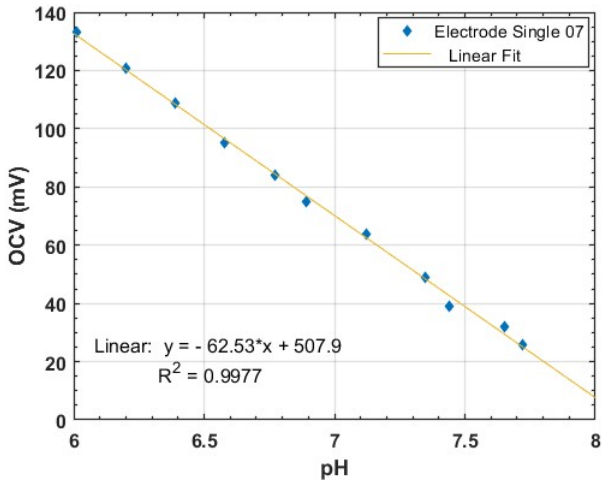

Figure 2-56 Sensitivity of flexible pH sensor tested in PBS solutions at different pH levels. Working electrode is 600 µm x 1200 µm in size and Reference electrode is Ag/AgCl.

a) Characterization of pH sensor performance at room temperature

Figure 2-56 shows the OCV curve of the best-performance single electrode with 600x1200µm in size, which has sensitivity of 62.5 mV/pH. The correlation coefficient was calculated to be 0.9977 and the standard reduction potential E_0 (tendency for a given chemical species to be reduced) is 507.9 mV, corresponding to the intercept of the curve. This result is in agreement with our previous work on TiN pH sensor on glass substrate [54]. Compared to literature results, this sensitivity is higher than for thin film TiN of same thickness (57.5 mV/pH, $R^2 = 0.9999$) [16], TiN nanotube array (55.33 mV/pH, $R^2 = 0.995$) and TiN nano powder (46.48 mV/pH, $R^2 = 0.992$) [35].

In addition, we achieve a better sensitivity than most of the other materials. Notably, we obtained a comparable sensitivity to IrO_2, which has been developed for in vivo and in vitro applications (69.9 ± 2.2 mV/pH [41]) and 51 mV/pH [46]). However, comparing to conductive polymer-based sensors such as polyaniline and polypyrrole blends (310 ± 40 mV/pH and 1300 ± 100 mV/pH, respectively [27]), our material has smaller sensitivity. Yet, because of the tendency to become unstable over time, conductive polymers are still limited in application.

Figure 2-57 shows the stability of the OCV of the same electrode in different pH levels during 200 s. A potential drift of less than 3 mV was observed during the first 50 s but stabilized after that. This drift might have been caused by the hydrogen ion trapping and diffusion phenomena into the lattice of the material.

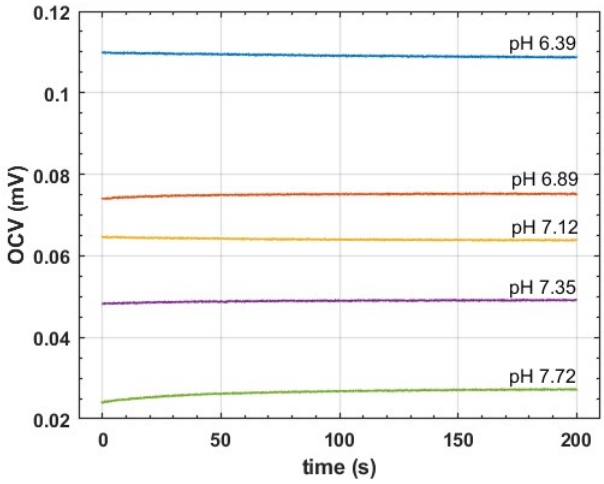

Figure 2-57 The stability of one TiN electrode at different pH levels of PBS solutions during 200 s.

A hysteresis of 6 mV maximum was observed with the pH range from 6.8 to 7.4 during 6 cycles, as shown in Figure 2-58. The hysteresis could be caused by the cross- contamination and possibly also by condition differences in the testing process, such as the stability of the pH test solutions, or temperature and connection problems. This hysteresis will be later used to calculate the precision of our pH sensor.

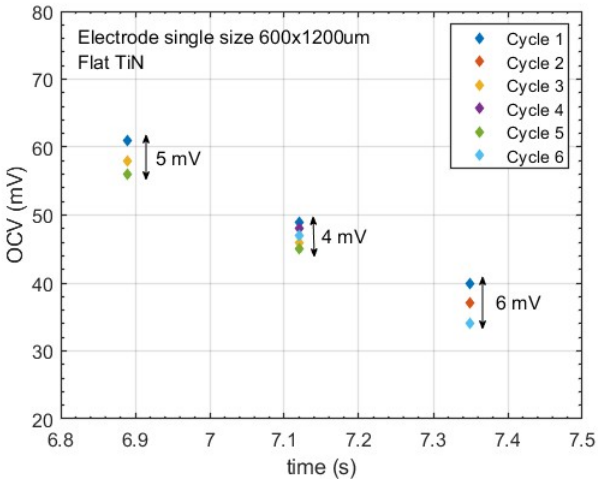

Figure 2-58 The hysteresys of one TiN electrode at different pH levels (6.89, 7.12 and 7.35) during 6 cycles of OCV measurements. Working electrode is 600 µm x 1200 µm in size and Reference electrode is Ag/AgCl.

Reproducibility during 3 loops of measurements on the same electrode is presented in Figure 2-59. The precision of pH measurement was calculated to be slightly below 0.1 (by hysteresis over sensitivity). It is not yet sufficient for the fetal tissue pH monitoring application but already interesting for other applications.

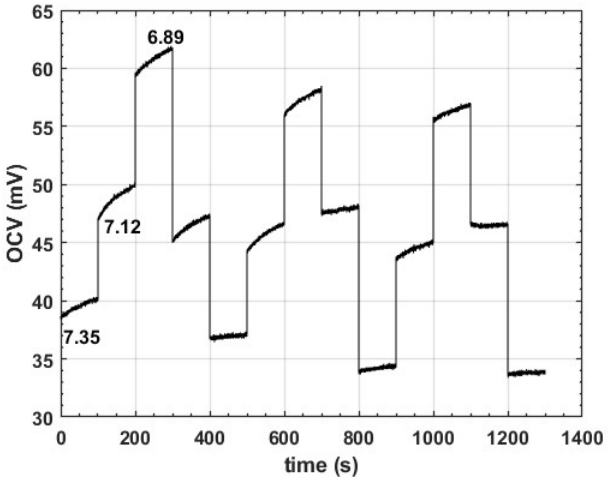

Figure 2-59 The reproducibility of one TiN electrode during 3 loops measurements in 3 pH levels: 6.89, 7.12, 7.35. Working electrode is 600 µm x 1200 µm in size and Reference electrode is Ag/AgCl

We also tested the performance of our TiN working electrode with the integrated Platinum reference electrode to compare with the external Ag/AgCl. Before starting the experiment, the fabricated electrodes were stabilized in PBS solution during 300 s to obtain a stable potential. The experiment results show that in case Platinum was used as RE material, the sensor recorded a higher drift at each pH level (Figure 2-60). Minimum drift was 1 mV over

100 s, recorded at pH 7.6 and 7.8. Maximum drift was 7 mV at pH 7.2, which could be caused by the instability of Platinum potential or the instability of the pH solution itself.

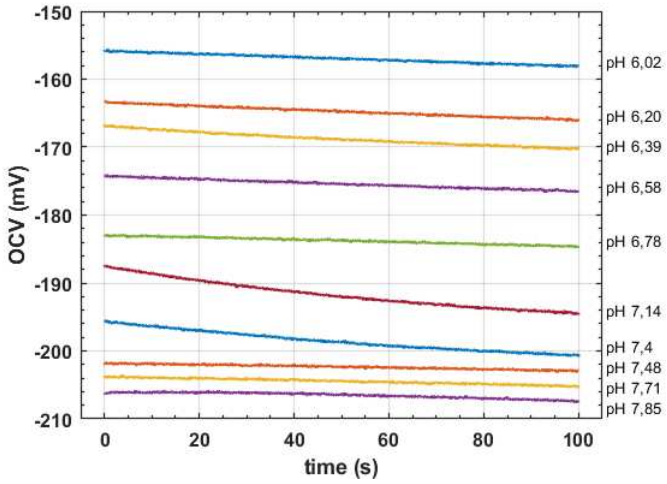

Figure 2-60 OCV measurements of single electrode size 600 µm x 1200 µm at different pH levels, in case of using integrated Platinum reference electrode.

TABLE 2-10 SENSITIVITY OF FLEXIBLE PH SENSORS IN CASE USING INTEGRATED PLATINUM REFERENCE ELECTRODE

Electrode	Size (um)	Sensitivity (mV/pH)	E_0	R^2
Single 07	600x1200	-27.2	4.2	0.9859
Triple 01a	400x800	-16.7	33.7	0.9576
Triple 01b	400x800	-23.4	10.8	0.9824
Triple 01c	400x800	-18.6	15.7	0.8390
Triple 02b	400x800	-22.8	166.5	0.9895
Triple 02c	400x800	-18.3	144.4	0.9936

The sensitivity of the sensor when using its integrated Pt electrode was determined to be 16.7 mV/pH – 23.4 mV/pH over 6 electrodes of size 400 µm x 800 µm and the result obtained from the above-described single electrode size 600 µm x1200 µm is 27.2 mV/pH (as shown in Figure 2-61 and table 2-11), which is lower than in case of using external Ag/AgCl as RE. This could be explained by the less stability in term of potentials of Pt, compared to Ag/AgCl. However, for applications which require an integrated and minimized pH sensor without an extremely high accuracy, this sensor could also be valid.

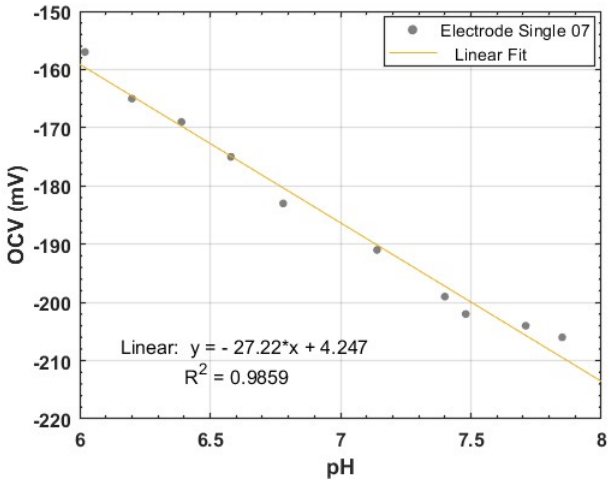

Figure 2-61 Sensitivity of flexible pH sensor size 600 µm x 1200 µm, tested in PBS solutions at different pH levels, in case of using integrated Platinum reference electrode.

A similar study was conducted with WE of 400 µm x 800 µm in size. A sensitivity of 53.7 mV/pH was determined as in Figure 2-55. With a hysteresis of 5 mV maximum, the precision was calculated to be 0.09 in pH. Similarly, in case of using Pt as RE, the sensitivity is lowered down to 21.3 mV/pH.

b) Long-term storage evaluation

We stored new electrodes at room temperature in 2 months and tested their sensitivity with an external Ag/AgCl RE. Those electrodes were cleaned by DI water and kept at room temperature in 6 more months from the first tests and we measured the sensitivity again. It appears that after 2 months being stored at room temperatures, the electrodes still well functioned with a normal sensitivity (-54.93 mV/pH and - 53.65 mV/pH in case electrode 'size are 600 µm x 1200 µm and 400 µm x 800 µm, respectively). However, after the first tests in PBS solutions and cleaned by DI water, six months later, one electrode shows a slight decrease in sensitivity (-53.07 mV/pH, in case electrode 'size is 600 µm x 1200 µm, Figure 2-62) while the other shows a bad sensitivity as seen in Figure 2-63.

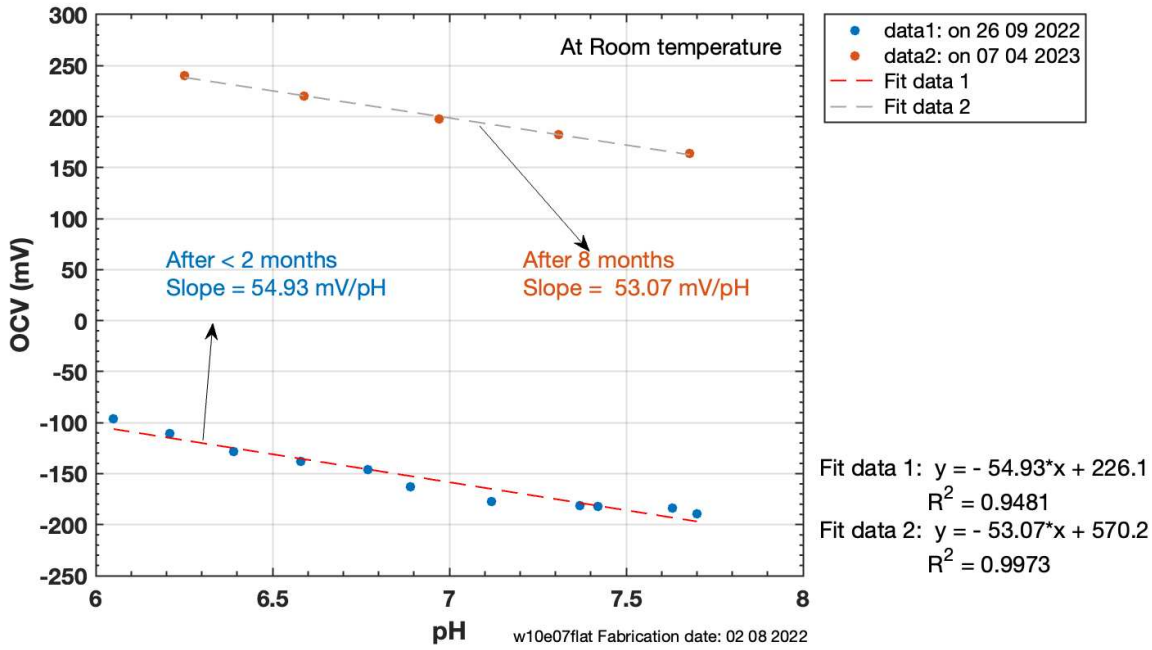

Figure 2-62 Sensitivity of electrode 600 µm x 1200 µm in size after approximately 2 months and 8 months from fabrication date. Reference electrode is Ag/AgCl.

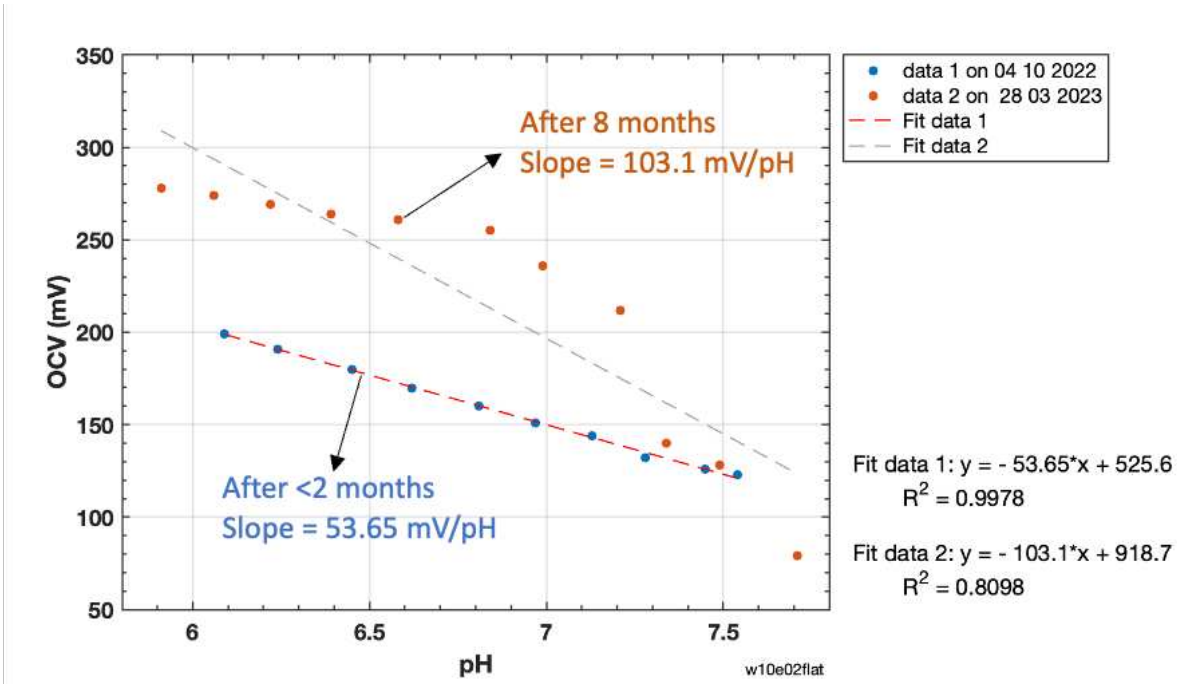

Figure 2-63 Sensitivity of electrode 400 µm x 800 µm after approximately 2 months and 8 months from fabrication date. Reference electrode is Ag/AgCl.

c) Characterization at 37°C (body's temperature)

By using the experimental setup described in Figure 2-25, section 2.2.3, OCV measurements were conducted at 37°C to evaluate the sensitivity of the TiN flat electrode under body temperature. Result in Figure 2-64 indicates a slightly higher sensitivity slope (56.12 mV/pH) at 37°C, compared to that of 27°C (53.07 mV/pH).

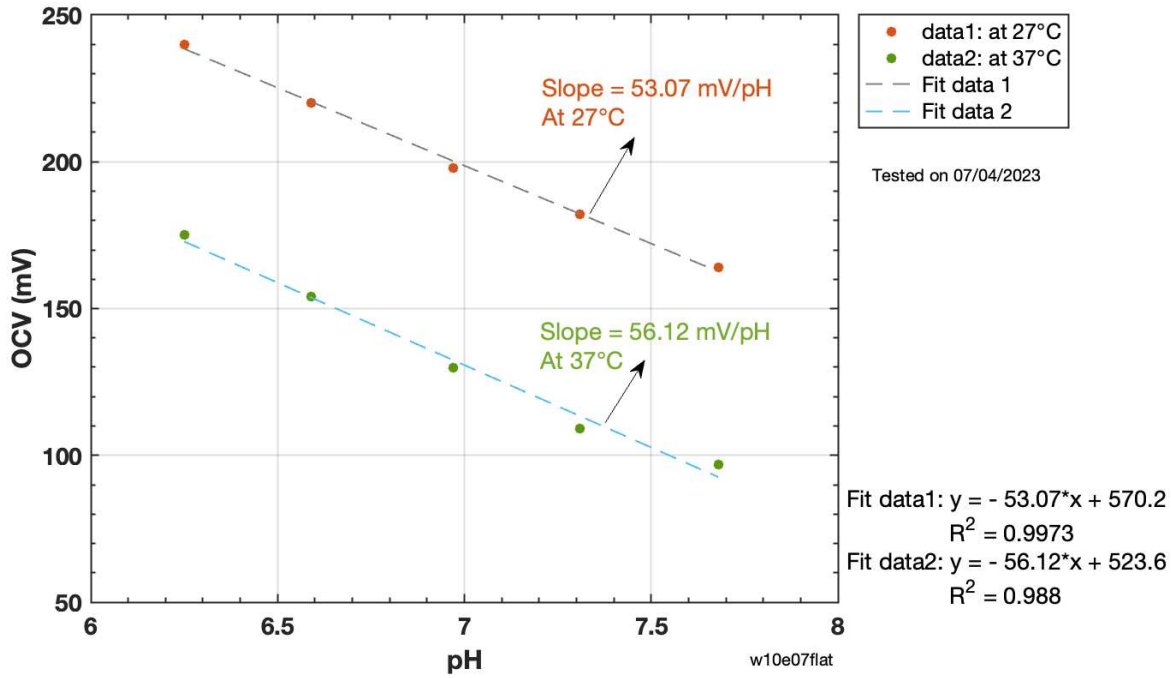

Figure 2-64 Comparison of sensitivity measured at 27°C and 37°C of the same electrode (600 µm x 1200 µm). Reference electrode is Ag/AgCl.

Reproducibility of the OCV measurements at different pH levels is presented in Figure 2-65. Five loops of measurements in PBS solutions pH 6.25, 6.59, 6.97, 7.31, 7.68 were conducted continuously, showing a hysteresis maximum of 10 mV as plotted on Figure 2-66. Thus, the precision of OCV measurement by electrode TiN flat (600 µm x 1200 µm) at 37°C, using Ag/AgCl as RE, is calculated to be 0.18 in pH.

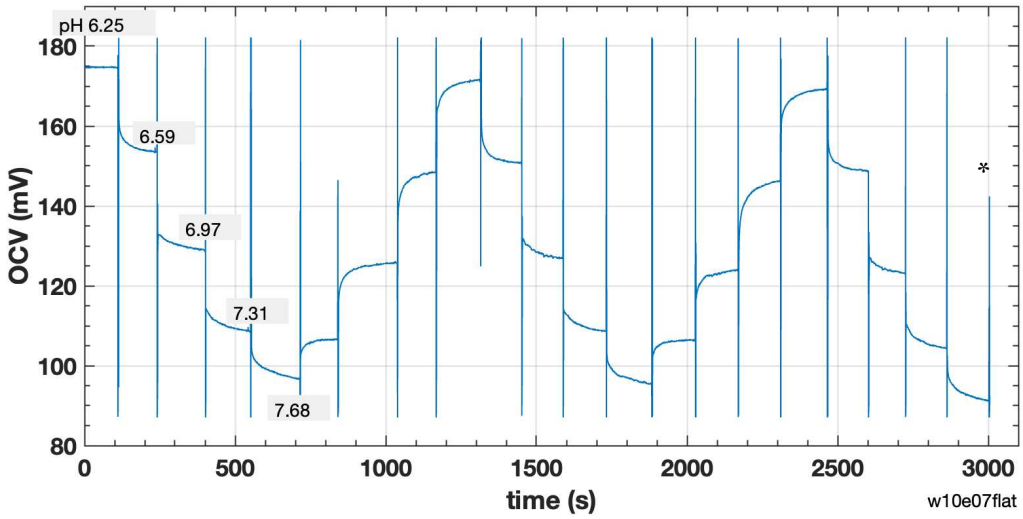

Figure 2-65 Reproducibility of electrode TiN flat (600 µm x 1200 µm) at 37°C, in PBS solutions at pH 6.25, 6.59, 6.97, 7.31, 7.68 and reverted. Reference electrode is Ag/AgCl. (*) is parasite signal due to manipulation.

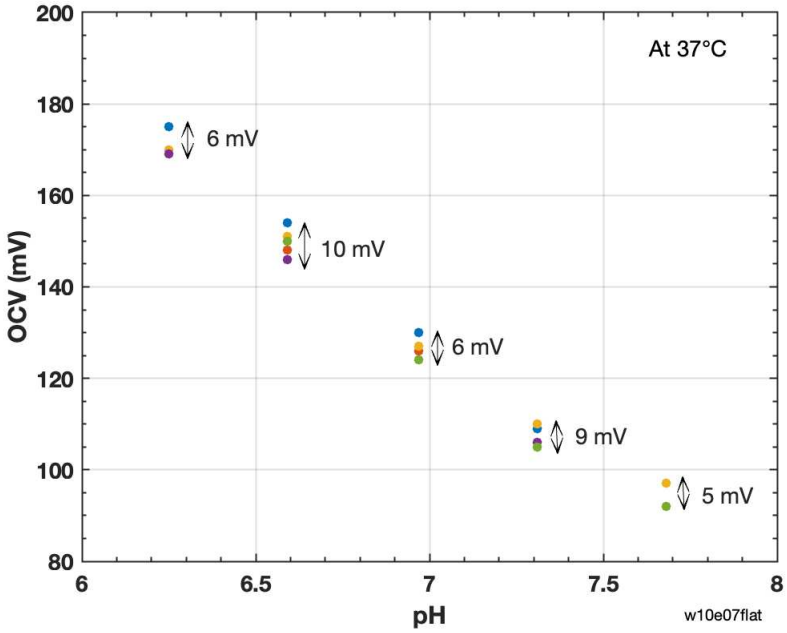

Figure 2-66 Hysteresis over 5 cycles of OCV measurement on electrode TiN flat (600 µm x 1200 µm) at 37°C, in PBS solutions at pH 6.25, 6.59, 6.97, 7.31, 7.68 and reverted. Reference electrode is Ag/AgCl.

Stability of an electrode TiN flat was tested in pH 6.25, at 37°C during 1.5 hours, using an Ag/AgCl electrode as the RE. Result in Figure 2-67 only shows a drift of 4 mV, which is smaller than ZnO-based pH sensor on polyimide substrate [55].

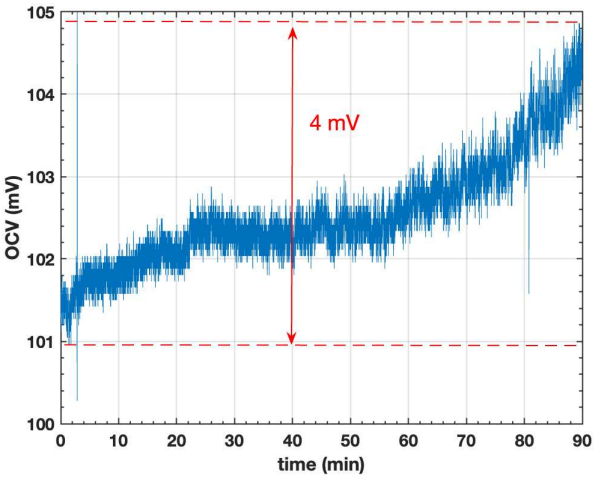

Figure 2-67 Stability over time of a flat-TiN working electrode of 600 µm x 1200 µm in size. Reference electrode is Ag/AgCl.

Response time of this electrode is demonstrated to be 29 s (Figure 2-68), which is longer than in case of model 1-glass substrate/Flat TiN (10s, see section 2.3.1.2).

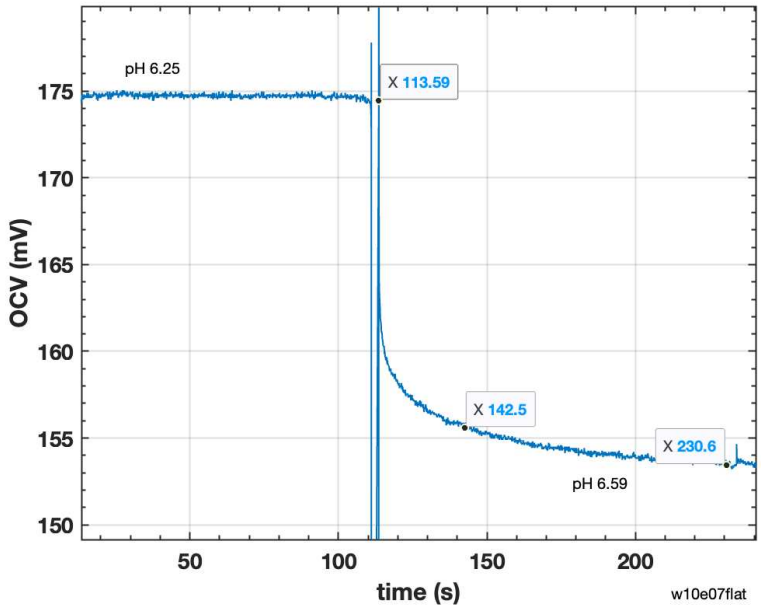

Figure 2-68 Response time of a flat-TiN working electrode of 600 µm x 1200 µm in size. Reference electrode is Ag/AgCl.

We tried to conduct OCV measurement while changing the temperature from room temperature to 37°C to evaluate the change of OCV level due to effect of temperature. Experimental protocol still had a limitation on method to control the temperature to be stable and accurate during each measurement. As described in section 2.2.3, we used a basic hot plate and had to adjust manually the temperature to be increased step by step and measure the actual temperature by the thermometer after every 200s approximately. Results shown

below in Figure 2-69 illustrate the trend of OCV variation and its value is plotted on Figure 2-70.

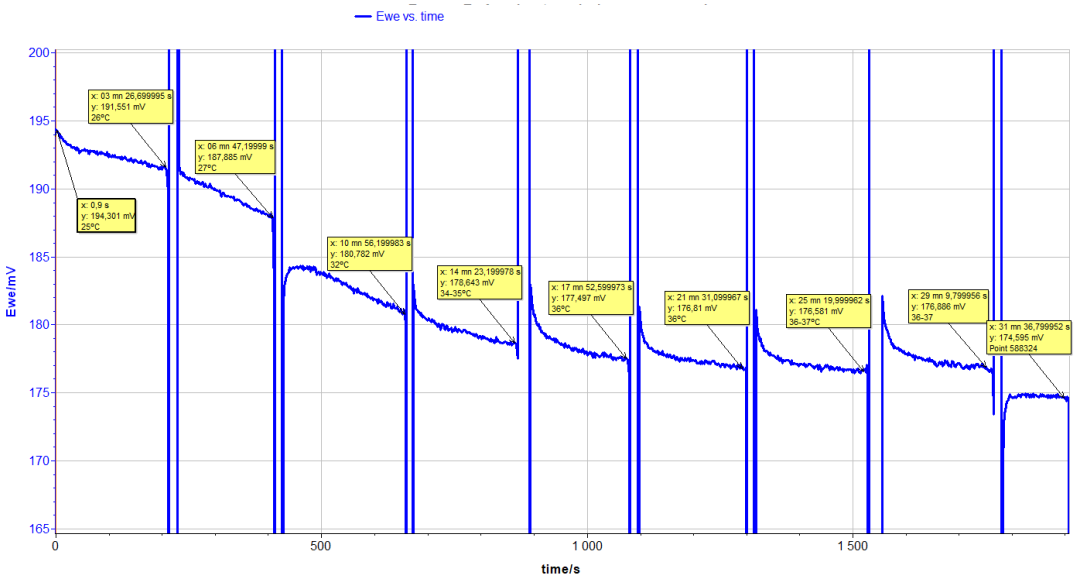

Figure 2-69 Variation of OCV following the change in temperature from room temperature to 37°C.

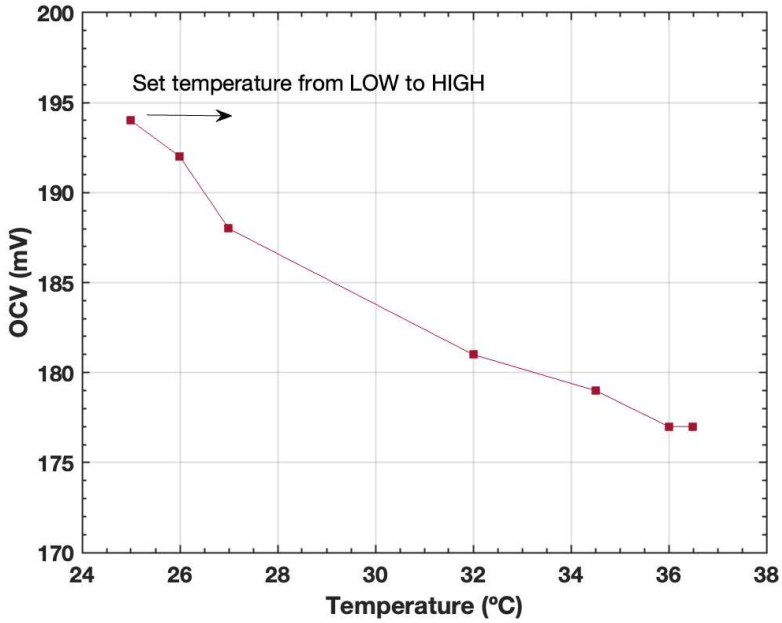

Figure 2-70 OCV measurement while changing the temperature from room temperature to 37°C.

In our opinion, it is necessary to improve the experimental set up in order to control and follow up with the temperature in a more stable way.

2.3.3.3. In vivo - Demonstration on mice of model 3-a

Experimental setup

An in vivo test was conducted on mice with the probe implanted under the skin, at IMRB animal facility, under #35095-2022013116589573 v11 authorization. Figure 2-71 illustrates the experimental setup on mice. A small incision was performed to implement our sensor under the skin at the tail or the leg positions, after the mouse was anesthetized. pH sensors were stabilized in PBS solution at pH 7 during 5 minutes before performing any experiment on the mouse. We recorded a stable OCV signal under anesthesia conditions in real time. The compact measurement system was designed with a customized LCD screen for signal visualization, an EZO™ ORP Circuit for data acquisition and an integrated SD card for data storage.

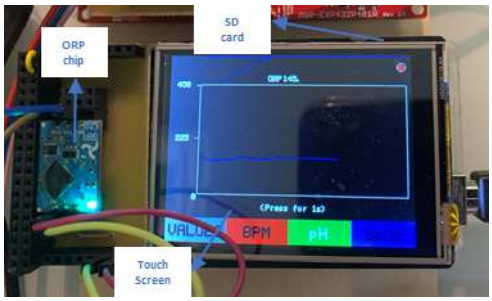

(a)

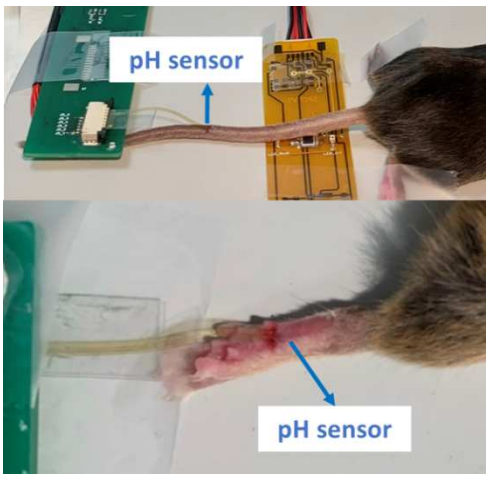

(b)

Figure 2-71 Experimental in vivo set up for the demonstration of pH sensors on mice. (a) Compact measurement system with a customized LCD screen, an EZO™ ORP Circuit for data acquisition and an integrated SD. (b) Incision to implement our sensor under the skin at the leg positions.

The results tested on mice

Some data from the trials were extracted and will be presented. It was not possible to test all our fabricated pH probes due to limited access to the animal facilities. There are two

electrodes that showed pH level at a very stable state (7.6 and 6.7) at leg position; the other tests were not good enough due to calibration issue. Figure 2-72 shows the recorded data of a flat TiN electrode of 400 µm x 800 µm in size in a triple-electrode design, which has sensitivity of 65 mV/pH – Table 2-9 - on a female mouse. After the insertion, during the first 4 minutes and 25 seconds, the system recorded a stable signal at 246 mV, corresponding to pH 6.7. At around 5 minutes, the pH sensor was removed and re-inserted back to the mouse at the same position. The signal was then back to the same level as before, confirming the good stability. Other tests conducted at the tail of the mouse also recorded stable signals, however not appropriated pH levels. This could be explained by the difference in contact environment of the skin, regarding the contact force and volume of extracellular fluids and blood that requires an improvement in our calibration methods.

We also tested once our sensor in extracted blood sample from the heart of the mouse, Figure 2-73. One blood sample is extracted before the mouse was dead and the other was extracted after the death, showing a change of 0.6 pH (decreased pH value after death), which is reasonalble in term of pH variation reported in literature [56], [57].

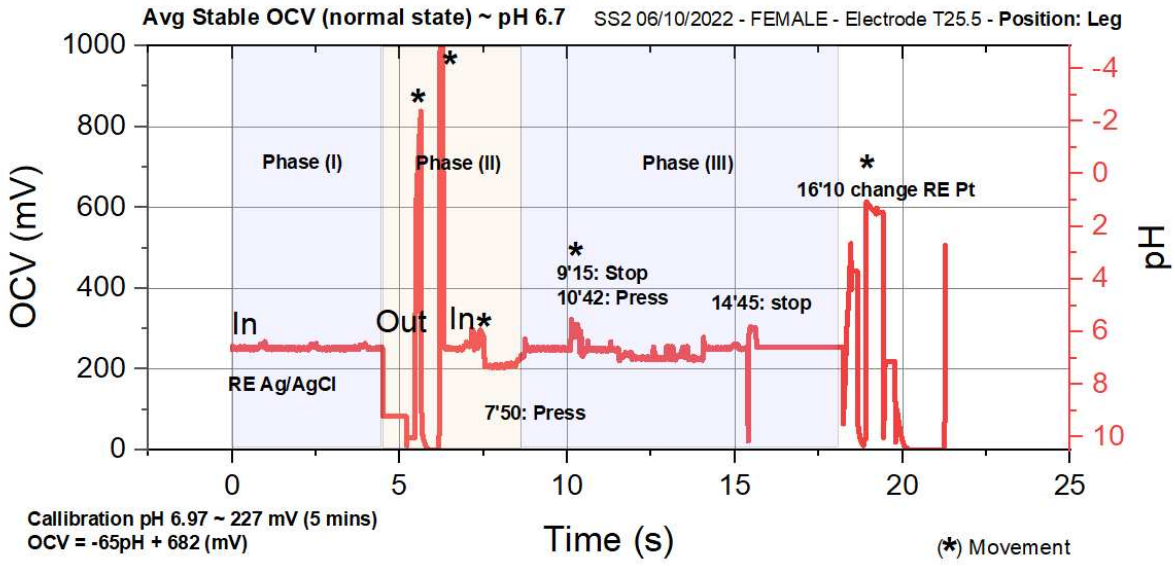

Figure 2-72 OCV measurement of pH sensors on mouse's leg under anesthesia condition. Phase (I): stable signal recorded, phase (II): noise due to plug in – plug out the sensor and phase (III): stable signal restored. (*) indicates parasite caused by external movement.

Figure 2-73 OCV signal recorded by flexible pH probe in mouse's blood. Average level of variation is obtained by subtracting the parasitic noise due to manipulation.

2.3.3.4. Conclusion on model 3-a

This session introduced the micromanufacturing process to fabricate flexible and miniaturized pH sensor, targeting to replace capillary sampling technique to measure blood pH on the fetal scalp during labor. TiN was employed as pH sensitive material, integrated on polyimide substrate in a potentiometric design, at a probe head size of 1.2 mm x 1.5 mm (width x length) on single-probe design and 0.9 mm x 2.8 mm (width x length) on triple-probe design. In vitro results demonstrated a compatible sensitivity on several functional electrodes, ranging from 53.3 to 67.6 mV/pH in case of flat TiN, with a good reproducibility upon 3 loops of measurement. A preliminary in vivo test was conducted on mice, recorded a stable OCV signal under anesthesia conditions. We introduced a compact measurement system for signal visualization, data acquisition and data storage.

A wireless system can be added if required and the implementation can be further extrapolated to other biological application (sweet, saliva, wound, blood monitoring). Indeed, in human beings, each part of the body operates optimally at a specific pH level. Most tissues has physiological pH around 7 to 7.4 with some exceptions [58]. Meanwhile, pH level in different position of healthy organs or tissues could be found ranging from 6 to 8, for example: pH 6.0 – 7.0 in saliva, pH 6.2-8.0 in urinary tract or 7.3-7.7 in healthy tear [5]. In diagnostic of abnormal conditions and disease, an acidic pH level was discovered in extracellular tumor (6.5-7.2), inflamed tissue (4.5) or cardiac ischemia (5.7) [59]. Thus, the need of employing an accurate and miniaturized pH sensor is commonly motivated by daily medical practice and our results open the way to many applications.

2.3.3.5. Supplementary study on model 3-b

As previously mentioned in section 2.2.2, on this sub-model, the geometric shape of the pH probe is improved and the thickness of TiN layer is varied to evaluate the performance of the sensor. In addition, we attempted to integrate a reference electrode (RE) from various materials such as Platinum, Gold and Ag/AgCl to compare with external classical RE. Figure 2-74 illustrates the three probe designs fabricated with our improved masks. Actual shape and size of the probe is presented in Figure 2-75. The following section will first describe the work on different RE, then the characterization of the uniformity of the process, and finally the influence on TiN thickness.

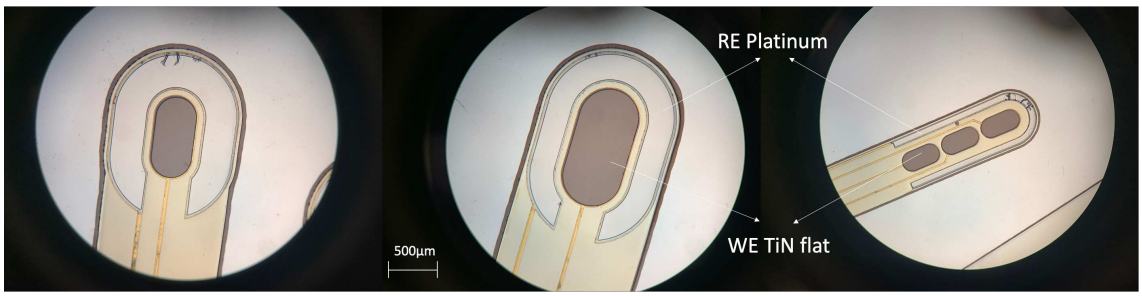

Figure 2-74 Three probe designs of model 3-b – Flexible/Flat TiN.

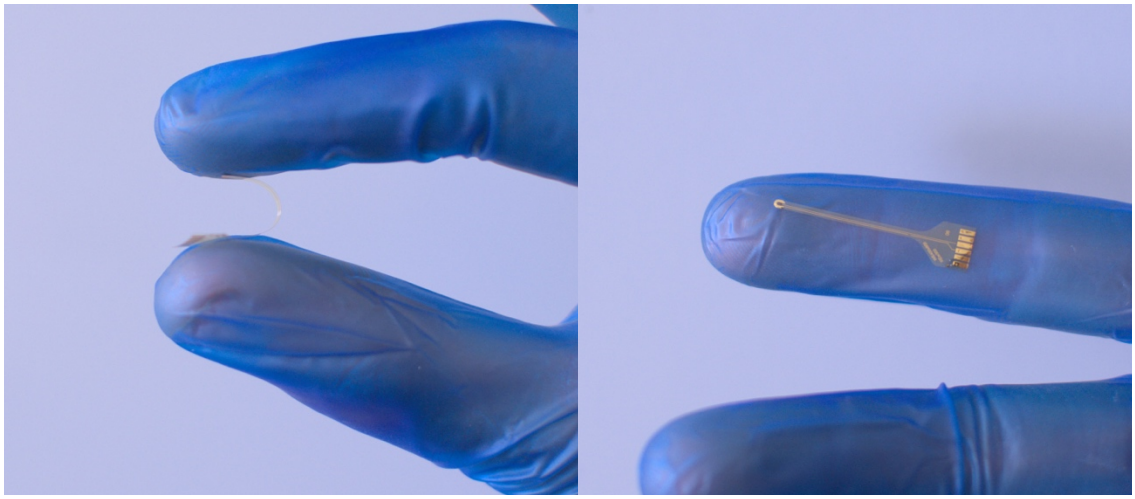

Figure 2-75 Sample of fabricated flexible electrode model 3-b.

a) Comparision of the integrated Pt electrode to an external Pt wire as a counter electrode

To evaluate the quality of our fabricated Platinum electrode in our integrated design, we compared by impedance spectroscopy the same TiN working electrode (numbered S06) used with the same external Ag/AgCl reference electrode, and using either our internal Pt electrode or an external Pt wire as couter electrode (CE). Result on Figure 2-76 shows the same impedence modulus and phase, which proves our fabrication technique of integrated Pt is correct.

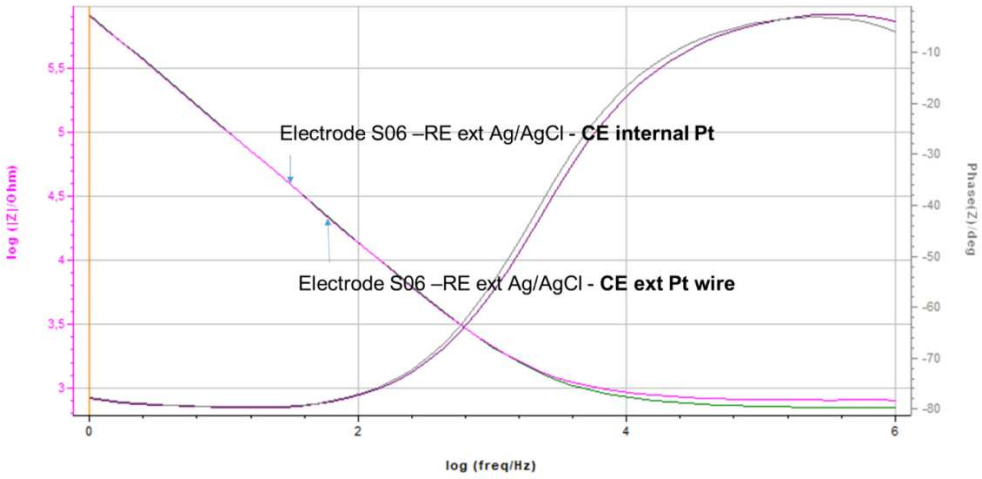

Figure 2-76 PEIS measurement to compare fabricated internal Pt with external Pt wire as CE.

b) Comparision of using integrated Au electrode versus external Pt wire as a counter electrode

We also attemped to use Au as a peusdo electrode instead of Pt (because it could simplify the fabrication process if positive results). The comparision on Figure 2-77 shows that when using Au as a couter electrode, the impedance is a bit higher than using Pt.

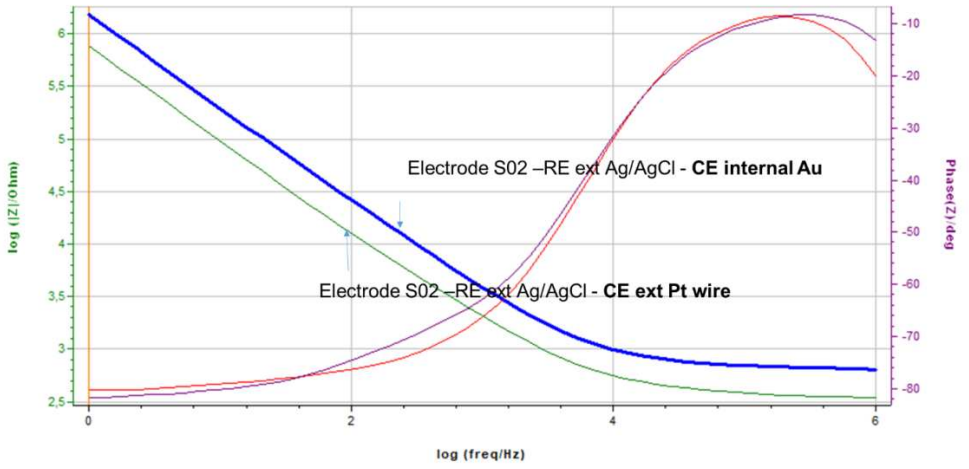

Figure 2-77 PEIS measurement to compare fabricated internal Au with external Pt wire.

c) Reproducibility of the fabrication process

We decided to test the sensitivity of two electrodes with the same size, same design and fabricated with the same process (but from different wafers). Figure 2-78 shows a similar sensitivity (size 400 µm x 800 µm, sensitivity -51.7 mV/pH, E_0 = 470.5 mV, R^2 = 0.9887) compared to the results presented in section 2.3.3.2 on electrode single 04 (size 400 µm x 800 µm, sensitivity -53.7 mV/pH, E_0 = 525.5 mV, R^2 = 0.9978).

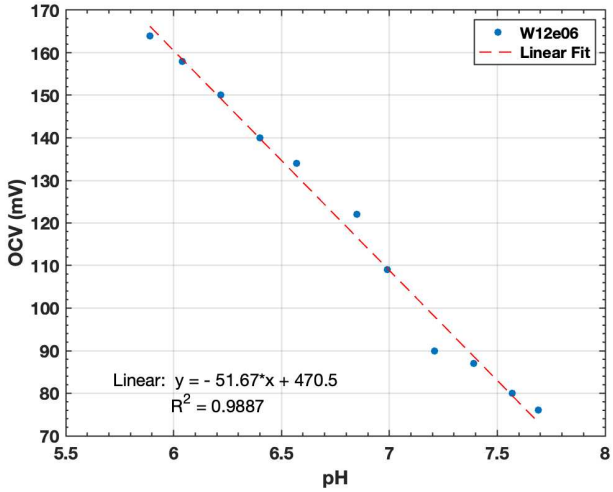

Figure 2-78 Sensitivity of flat TiN electrode fabricated on another wafer, with the same process as in session 2.3.3.2 and same dimensions.

We also test the sensitivity of several electrodes TiN flat fabricated on one wafer, 37°C, using Ag/AgCl as RE. Figure 2-79 illustrates the sensitivity of the five electrodes after normalizing the OCV at pH 7 to zero. The absolute value of sensitivity of these electrodes are shown in table 2-11. Compare to Table 2-10, section 2.3.3.2a, it is noticeable that the fabricated flexible electrodes model 3b exhibits more uniform performance (sensitivity is in the range of 51-60mV/pH, no non-functional electrodes, standard potential is close between 427-469 mV), as the very first fabrication of model 3a.

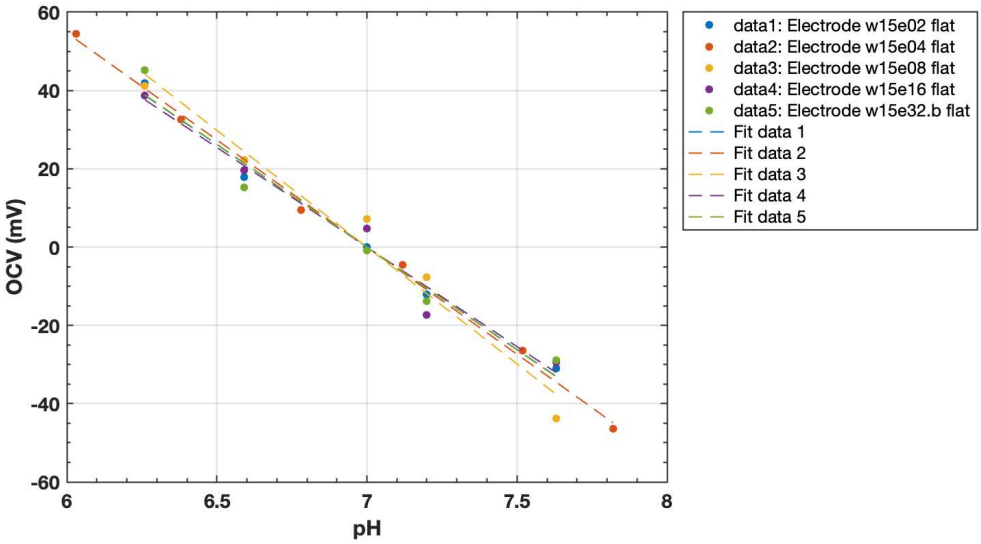

Figure 2-79. Sensitivity of electrodes TiN flat fabricated on the same wafer.

TABLE 2-11 SENSITIVITY OF FLEXIBLE PH SENSORS – MODEL 3B (TIN THICKNESS = 200 NM) IN CASE USING EXTERNAL AG/AGCL REFERENCE ELECTRODE

Electrode FLAT	Size (µm x µm)	Sensitivity (mV/pH)	E_0 (mV)	R^2
W15e02	400x800	-52.38	449.72	0.9908
W15e04	400x800	-54.72	466.57	0.9969
W15e08	400x800	-59.65	449.31	0.9708
W15e32b	400x800	-52.55	426.71	0.9660
W15e16	600x1200	-50.866	469.36	0.9725

To explain the variation of sensitivity slope on those experiments, we investigated the interference of the RE. In fact, we used one RE Ag/AgCl to run experiments on several fabricated WEs. Among those experiment, sometimes in the later experiments, it resulting a lower slope of sensitivity. By checking the sensitivity of the same WE TiN flat, measured in the similar condition, in case using a new and dry Ag/AgCl RE and in case using an Ag/AgCl RE which used just before in measurements on several electrodes. Results on Figure 2-80 shows that the older the Ag/AgCl RE, the lower the slope of sensitivity (45.94 mV/pH and 52.55 mV/pH with old and new Ag/AgCl RE, respectively).

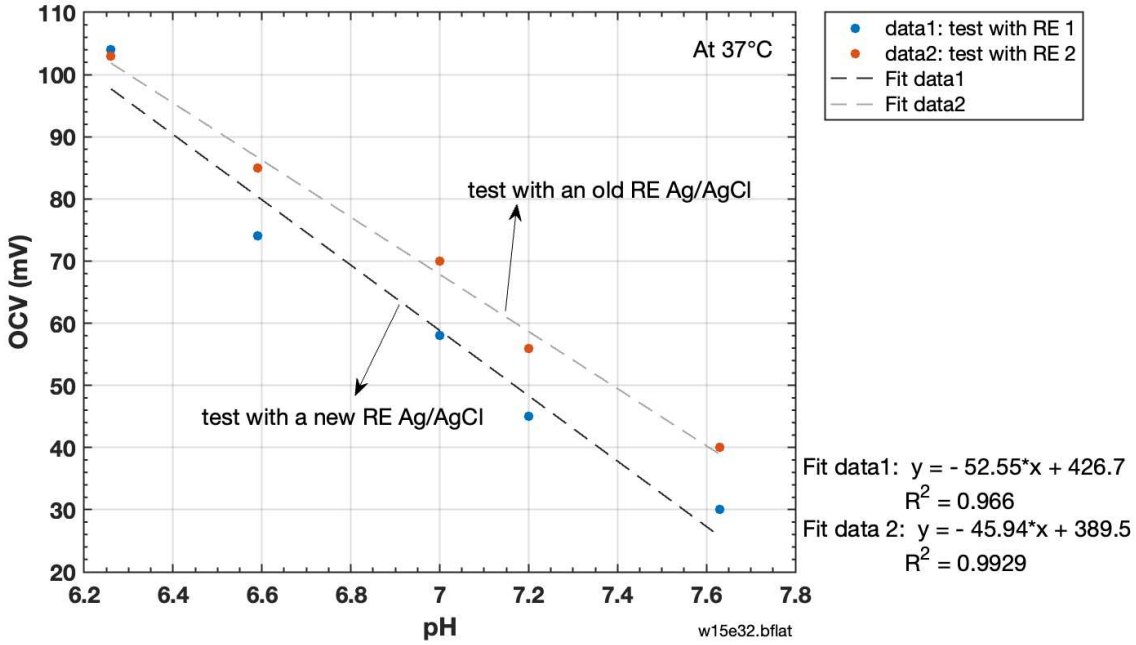

Figure 2-80 Interreference of RE quality to the measurements.

Generally, it is recommended to fill an Ag/AgCl RE with filling solution (e.g., potassium chloride KCl 3.5 M) before using to ensure accurate potential measurements. The filling

solution helps to maintain a stable potential by providing a consistent and known concentration of chloride ions around the reference electrode. It also prevents air bubbles from forming, which can interfere with accurate potential measurements. In some case, Ag/AgCl REs are designed with a gel filling that does not require additional filling solution. These gel-filled reference electrodes have a small volume of electrolyte embedded in a gel matrix, which provides a stable and reproducible reference potential.

d) Characterization of the uniformity of the fabrication process

Below are also given the PEIS characterization results in vitro in case TiN layer has thickness of 300 nm (Figure 2-81). On our wafer, we have in total 13 electrodes of the same size 400 µm x 800 µm. We tested randomly 6 electrodes among them and results of the PEIS show almost similar characterizations for all. This proves the reproducibility of the fabrication process with a uniform quality.

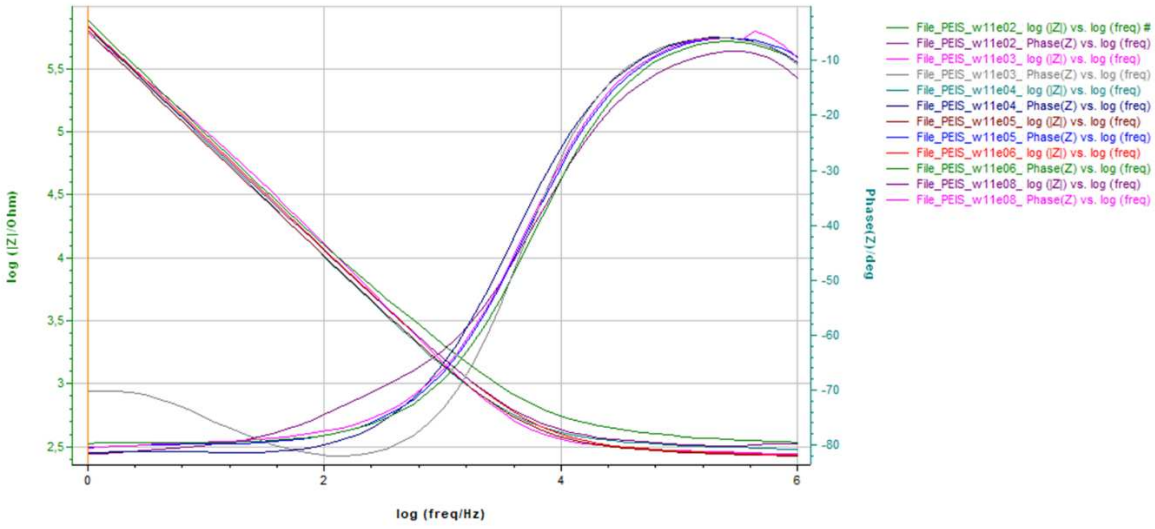

Figure 2-81 Impedence of 6 pH probes fabricated on one wafer. Thichness of TiN is 300nm.

e) Sensitivity in case thickness of TiN is 300nm

We tested the sensitivity of several electrodes which have 300 nm thickness of TiN instead of 200nm as in model 3-a. Results (Table 2-12) show that we obtain a lower sensitivity (mostly around 40-45 mV/pH) at 16 °C (due to the fact that the temperature was very low in the lab during this time of experiment). This result is compliant with what we found in the case with higher temperature (results presented on Fig. 2-64, previous session 2.3.3.2c) and TiN thickness optimization could be done around the 200 nm range, with 10nm accuracy required, which is difficult to achieve with our available facilities.

Figure 2-82 illustrates the best-performance electrode which has a sensitivity of 53.6mV/pH for a 300nm TiN thickness (first line of Table 2-12).

TABLE 2-12 SENSITIVITY OF FLEXIBLE PH SENSORS – MODEL 3B (TIN THICKNESS = 300 NM) IN CASE USING EXTERNAL AG/AGCL REFERENCE ELECTRODE

NEW MASK-Flat TiN thickness 300nm	Electrode number	Sensitivity (mV/pH)
400x800um	S02	53.6
	S03	40.0
	S04	42.2
	S06	44
600x1200um	S18	41.7
	S20	37
	S25	51
	S26	38.5

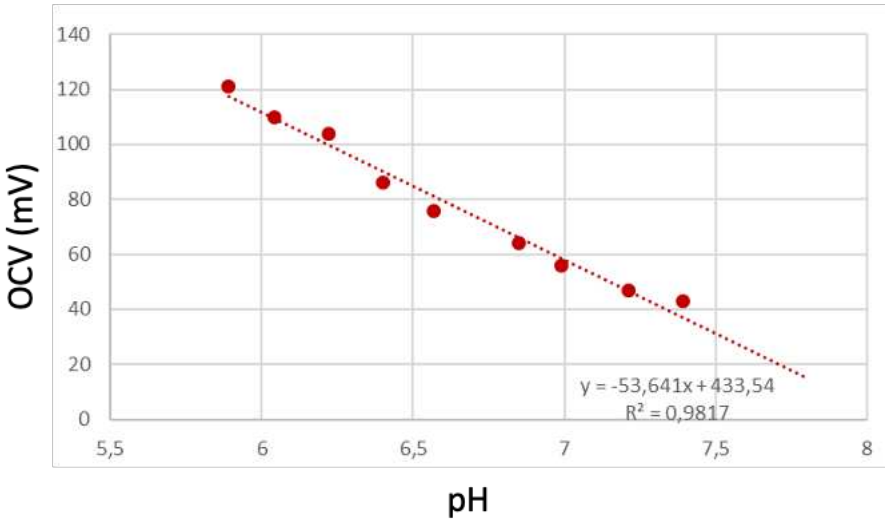

Figure 2-82 Sensitivity of the best-performance electrode which has thickness of TiN at300nm.

2.3.4. Model 4 – Miniaturized and flexible polyimide substrate/ Porous TiN

2.3.4.1. Fabrication process of model 4-a

To improve the precision of our pH sensors, a porous profile was created on the surface of working electrodes to increase the effective working area, as it was tested on the glass substrate samples initially. Porosity of the TiN surface has been obtained by a wet etching process in a mixture solution of TechniEtch TBR19 (Technic) and hydrogen peroxide (H_2O_2) 30%. A complete study on the improvements of porous TiN compared to flat TiN was reported in our previous work [60], which indicates a lower impedance and a higher conductivity of

this material. The fabrication process was kept the same except this additional etching step of TiN.

2.3.4.2. In vitro - Results and discussion on model 4-a

Similarly, performances of this porous TiN pH sensor were demonstrated with the same methods as for its flat TiN counterpart. Figure 2-83 shows a linear sensitivity OCV curve of the flexible porous TiN sensor, which indicates that the porous TiN has maintained the sensitivity of 53.2 mV/pH compared to the flat TiN. Stability is better in the first 50s as shown in Figure 2-84a, with a maximum drift of 3 mV detected at pH 7.13 and 7.28. OCV measurement performed a small noise level of less than 0.5mV as shown in Figure 2-84b, which means the porous TiN WE has no defects and keeps a good quality after the above-mentioned post-fabrication technique. Hysteresis, Figure 2-85, was found small at 3mV maximum after 6 cycles of OCV measurement at 3 pH levels with approximately 0.15 pH steps (7.13, 7.28 and 7.45). Finally, in case of porous TiN, a precision of 0.056 was determined which is better compared to flat TiN (with a precision just below 0.1). The sensitivity of this porous TiN was then re-tested after the in vivo experiment on mice, showing a slight decrease of sensitivity down to 50 mV/pH. This proves that the sensor could withstand the skin contact during implementation in the in vivo experiment and was not degraded by mechanical stress, keeping the material porosity and integrity.

Reproducibility of porous TiN electrode is also presented in Figure 2-86. In case of using Pt reference electrode instead of external Ag/AgCl, the sensitivity (Figure 2-87) was reduced to 23.6 mV/pH, in agreement with our flat TiN study presented above. The main advantage of porous TiN is to combine a good sensitivity with a higher stability and better accuracy.

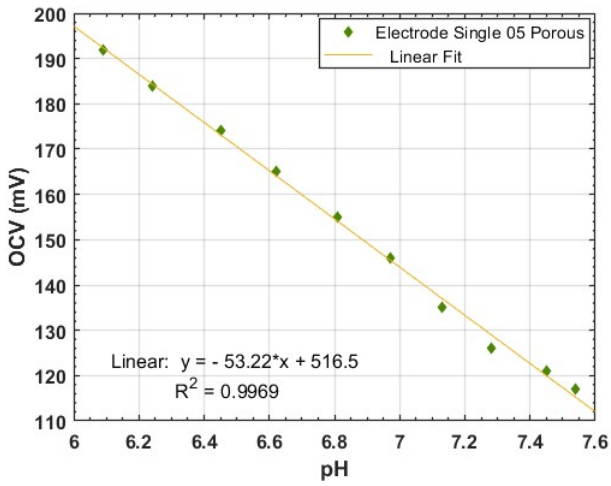

Figure 2-83 Sensitivity of flexible pH sensor with porous TiN tested in PBS solutions at different pH levels. Working electrode is 400 µm x 800 µm in size and Reference electrode is Ag/AgCl.

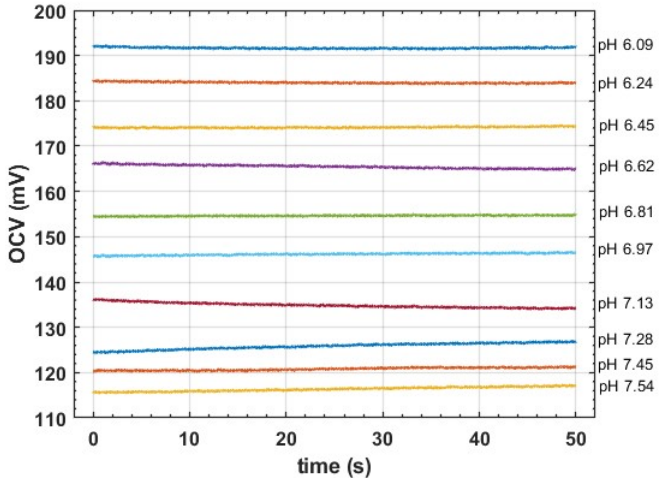

(a)

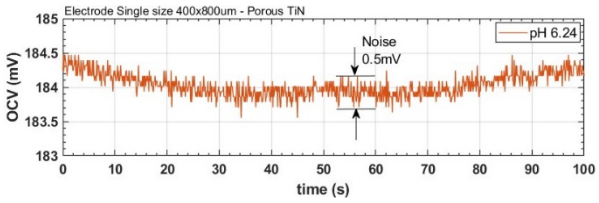

(b)

Figure 2-84 a) The stability of one porous TiN electrode at different pH levels of PBS solutions during 200 s. Working electrode is 400 µm x 800 µm in size and Reference electrode is Ag/AgCl. (b) Corresponding noise level of OCV measurement.

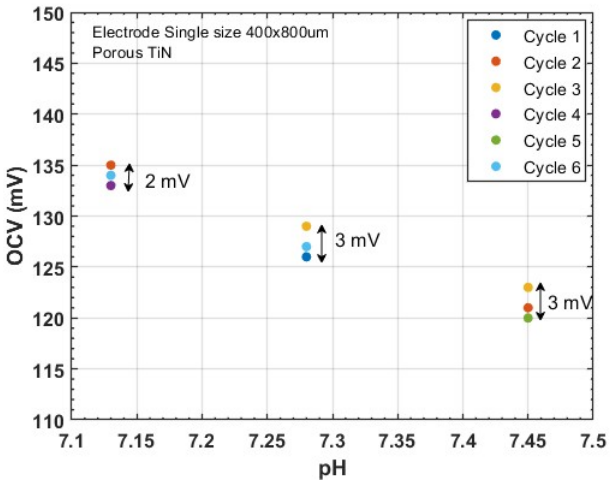

Figure 2-85 The hysteresis of one porous TiN electrode at different pH levels (7.13, 7.28, 7.45) during 6 cycles of OCV measurements. Working electrode is 400 µm x 800 µm in size and Reference electrode is Ag/AgCl.

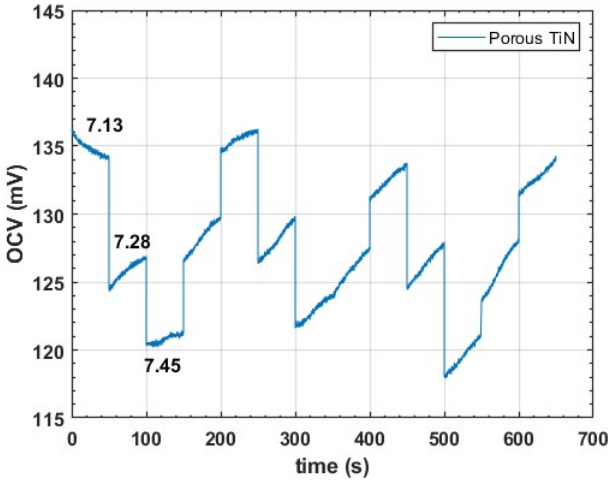

Figure 2-86 The reproducibility of one porous TiN electrode during 3 loops of measurement in 3 pH levels: 7.13, 7.28, 7.45. Working electrode is 400 µm x 800 µm in size and Reference electrode is Ag/AgCl.

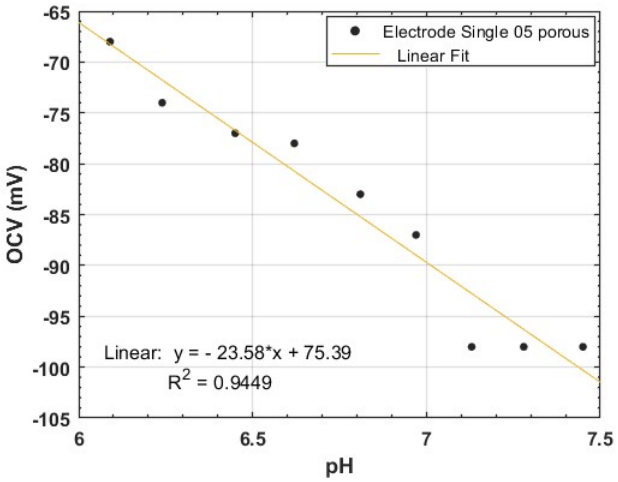

Figure 2-87 Sensitivity of flexible porous TiN pH sensor with size 400 µm x 800 µm, tested in PBS solutions at different pH levels, in case of using integrated Platinum reference electrode instead of external Ag/AgCl.

2.3.4.3. In vitro - Results and discussion on model 4-b

We chose 3 electrodes model 4-b fabricated from one wafer to test the sensitivity at 37°C. Table 2-14 shows 2 electrodes among them have sensitivity in the appropriate range (- 54.09 mV/pH and - 51.28 mV/pH) compare to sensitivity of electrode Porous TiN model 3a in Figure 2-88, section 2.3.4.2 above.

We reincluded results on sensitivity of the corresponding electrode flat TiN (from Table 2-11) in table III below for a better comparison.

TABLE 2-13 SENSITIVITY OF FLEXIBLE PH SENSORS – MODEL 4B (TIN THICKNESS = 200 NM) IN CASE USING EXTERNAL AG/AGCL REFERENCE ELECTRODE

Electrode POROUS	Size (µm x µm)	Sensitivity (mV/pH)	E_0 (mV)	R^2	Electrode FLAT	Sensitivity (mV/pH)	E_0 (mV)	R^2
W15e02	400x800	-43.06	466.01	0.9943	W15e02	-52.38	449.72	0.9908
W15e08	400x800	-54.09	522.76	0.994	W15e08	-59.65	449.31	0.9708
W15e16	600x1200	-51.28	513.20	0.9975	W15e16	-50.866	469.36	0.9725

One electrode has lower sensitivity of 43.06 mV/pH. This electrode has a higher impedance compared to the good electrode (Figure 2-88), which could be relevant to the performance of pH sensing.

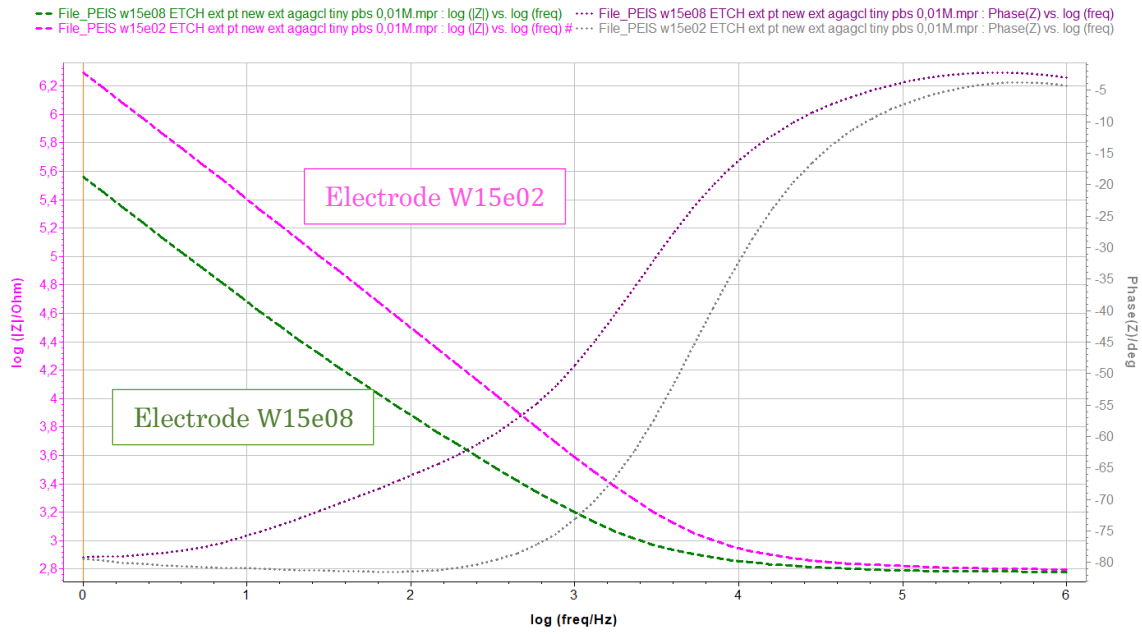

Figure 2-88 Comparison of PEIS between a normal electrode (W15e08)with a poor sensitivity electrode (W15e02).

Overall, the sensitivity tests on model 4a and 4b demonstrates the reproductivity of our technique to fabricate porous TiN electrodes.

We tested the stability of one electrode with porous TiN by measuring the OCV for 1.5 hours at 37°C. After 1.5 hours, a drift of 13 mV was observed (Figure 2-89a, which is higher compared to the case of the flexible flat TiN electrode. During the first 10 minutes, the drift was minimal at 1 mV and started to increase at a faster rate after 10 minutes (Figure 2-89b). We have noticed this drifting issue with porous TiN since the prototype on the glass substrate. However, it is noteworthy to mention that on the newly fabricated and clean electrode, we observed a lesser drift effect in our OCV measurements.

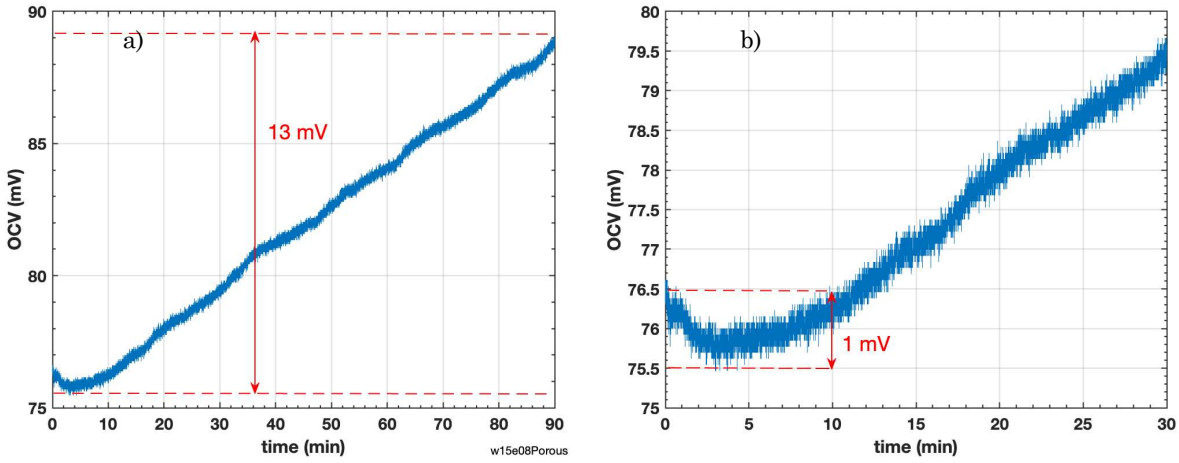

Figure 2-89 Stability of electrode TiN Porous plotted in 90 minutes (a) and zoom in the first 30 minutes (b).

The flexible electrode size 400 µm x 800 µm with porous TiN was also tested in extended pH range from 4 to 10, as showed on Figure 2-90. It is observable that there is a slower response of OCV at high pH (>8). This also means in very base solution, our TiN electrode needs longer time to be stabilized. There is a similar phenomenon with glass electrode for pH sensing, so called acid error or alkaline error. While acid error starts approximately at pH = 2 for most pH glasses, the alkaline error starts at pH = 8 to 11 depending on the sources and composition of the glass membrane [2].

Response time of flexible electrode size 400 µm x 800 µm with porous TiN was found to be 12.8 s from pH 6.04 to pH 7.02 (Figure 2-91). This is better than the flexible flat TiN (29 s, model 3a, see section 2.3.3.2d) and in the same range as prototype on glass substrate (10 s, model 1, see section 2.3.1.2).

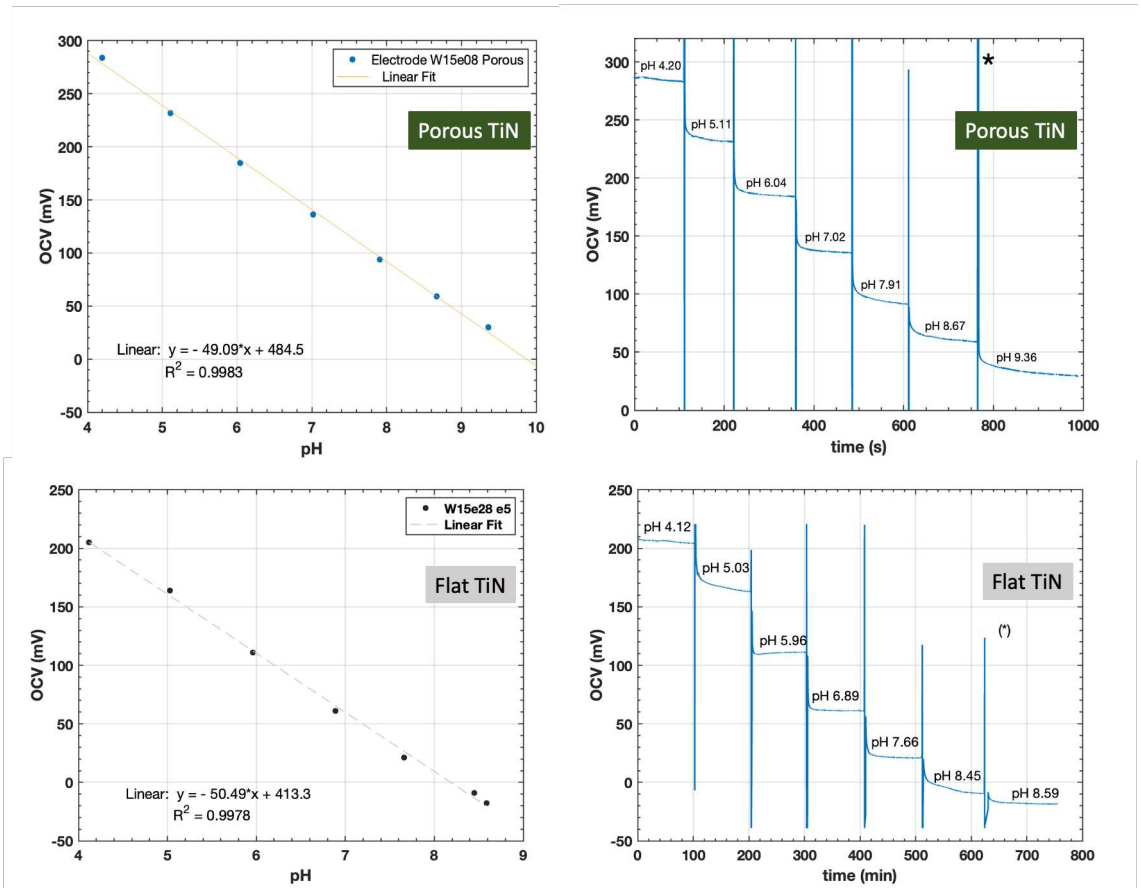

Figure 2-90 Sensitivity of the flexible electrode size 400 µm x 800 µm with flat TiN(top) and porous TiN (bottom) tested in extended pH range from 4 to 10. (*) is parasite signal due to manipulation.

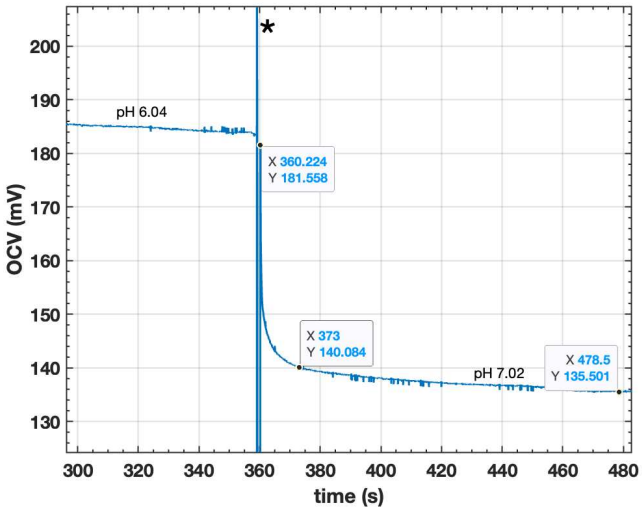

Figure 2-91. Response time Sensitivity of the flexible electrode size 400 µm x 800 µm with porous TiN. (*) is parasite signal due to manipulation.

2.3.3.4. Conclusion on model 4- Flexible Polyimide substrate/Porous TiN

A specific treatment was applied to obtain nanoporous profile of TiN at the working electrode, instead of flat surface, to improve the precision of the sensor from 0.1 to 0.05 in pH. The sensitivity of TiN porous was slightly reduced on the polyimide flexible substrate compared to that of glass substrate (down to 0.02 in pH, see section 2.3.1) but still very low. In vitro results demonstrated a sensitivity of 53.2 mV/pH on the porous TiN flexible sensor with accuracy below 0.06 in pH (which is close to the initial target). A slight decrease in sensitivity of the porous TiN sensor after the in vivo test was observed, from 53.2 mV/pH down to 50 mV/pH, which however validates the consistency under insertion conditions. The reproducibility of the fabrication process was also evaluated. Reproducibility of the process to obtain porous TiN was evaluated, showing the variation of sensitivity in the range of 51-54mV/pH).

2.4 Conclusion on chapter 2 and perspectives

This chapter presented our study on designing and developing a flexible and micro pH sensor with a very high accuracy, targeting fetal health monitoring during labor and other biological application related to human and animal health. Herein we summarize the main results that were accomplished, including:

1. A microfabrication process developed and optimized on flexible polyimide;
2. A new WE material tested (TiN flat and porous);
3. Several mask levels designed and implemented, successfully produced a down to 300µm x 600µm in size TiN working electrode;
4. A full in vitro characterization protocol developed and used for all the probes (SEM, OCV, CV, PEIS, influence of the Temperature);
5. Some in vivo preliminary test done on mice showing the POC;
6. pH sensitivity and accuracy achieved close to the expected target for the fetal application taking in consideration the miniaturization and material constraints.

As perspectives, in the final form of the device, the flexible pH electrodes could be considered to be attached into a specific needle, which is adaptable for clinical skin insertion. This pH sensing needle will be fixed with the SpO_2 sensing board (later introduced in chapter 3) using a flexible polyimide substrate in a customized design package.

The important challenges to be considered for this work in the future are:

1) to find the best mechanical design to be easily used by the medical staffs and prevent any damage for the fetus and the mother;

2) to guarantee the sensitivity and accuracy in real use-case;

3) to establish a protocol for temperature correction, sterilization and storage of the pH sensing electrodes.

In addition, new applications are under evaluation, for cardiac ischemia detection for instance. New tests are undergoing in animal facilities on different animal models at the Ecole Vétérinaire d'Alfort to complete the work in the near future.

Chapter 3

SPO_2 SENSORS

Abstract

In this chapter, we present a prototype which is our first attempt to get continuous measurement of SpO_2 and provides a clear photoplethysmogram (PPG) in real time, considered as a complementary second line measurement on the foetus during labor. This work targets to make a SpO_2 sensor which can register raw pulse oximetry signals for biological research purpose. In addition, SpO_2 measurement is helpful to evaluate our pH measurement as correlation exists between low tissue oxygenation and lower pH. A reflectance SpO_2 sensor was designed, employing two LEDs at 630 nm and 940 nm wavelengths with one wideband photodiode and being monitored by a MSP432 microcontroller. Several versions of the SpO_2 sensor were fabricated. Result recorded of the first prototype of the classical hard-type PCB shows close behavior to a commercial device. We optimized the analog front end (AFE) circuit and transferred it to a flexible PCB, fabricating a second prototype. Further developments to improve the accuracy of the sensor can be investigated in the future, based on this preliminary study.

Content of chapter 3

3.1. Bibliography study/ State of Art of SpO_2 sensor

3.1.1. State of Art and literature reviews

An overview on the history of pulse oximeter development

As explained in chapter 1, session 1.2, SpO_2 indicates the blood oxygen saturation measured by pulse oximetry technique using a non-invasive sensor attached to a patient's finger, earlobe, wrist-worn, forehead, nose, foot, or toes. or other body part. Blood oxygen saturation refers to the percentage of hemoglobin molecules in the blood that are bound with oxygen.

The concept of blood oxygen saturation has been known for many decades. SpO_2 sensors have become an essential tool in medical settings, personal health and fitness supporting for monitoring respiratory function and overall health. Technology behind a SpO_2 sensor continues to evolve to meet the demands of the market, especially wearables.

In 1935, Karl Matthes developed the original ear O_2 saturation meter with red and green wavelengths [61]. In 1940, J.R. Squire discovered the red and infrared light transmission difference for calculating oxygen saturation, and in 1942, Glen Millikan developed the first portable pulse oximeter for pilot training during WWII. While their device was obstructed by the noise generated by the pulse of blood, in 1972, Dr. Takuo Aoyagi presented a solution to eliminate the noise from the measurement, resulting in the first conventional pulse oximeter, which used SpO_2 sensors to measure oxygen saturation levels in the blood [62], [63].

The device was first commercialized in 1981, and the use of pulse oximetry for continuous oxygen monitoring in newborns was first described in 1986, and later is used widely in the delivery room during resuscitation [64]. It is also utilized to screen for congenital heart disease [18].

In the early 2000s, SpO_2 sensors began to be used in home healthcare settings, allowing patients to monitor their own oxygen saturation levels and alerting them to potential health problems. More recently, SpO_2 sensors have been incorporated into wearable fitness trackers and other consumer health devices, making them more widely accessible to the general public. The increasing of chronic respiratory diseases, such as chronic obstructive pulmonary disease (COPD) and sleep apnea, as well as the COVID-19 pandemic, has driven demand for SpO_2 sensors in both medical market (monitoring during surgery, intensive care, home healthcare, telemedicine, etc.) and consumer markets (wearable fitness trackers, smartwatches, etc.).

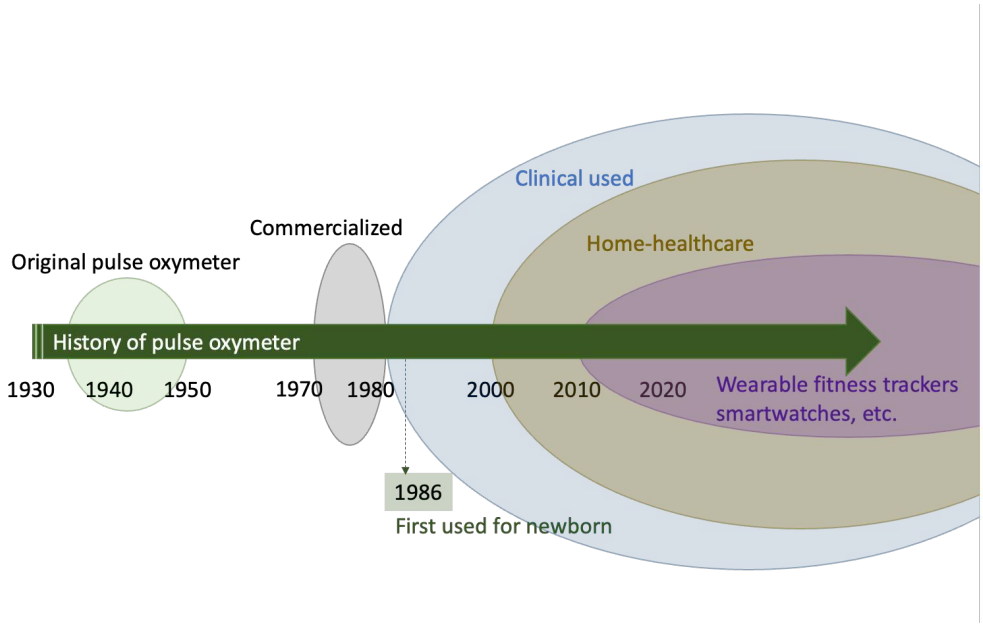

Figure 3-1 The overall development of Pulse Oximeter.

Evolution of pulse oximeter over time

The world's first pulse oximeter is ear oximeter OLV-5100 invented by Dr. Aoyagi in 1974 (Figure 3-2). It used an earpiece with incandescent light, filters, and photo transistors. Looking back into history, pulse oximetry may have been invented earlier than the development of semiconductor devices, such as light-emitting diodes (LEDs). Therefore, a small probe suitable for clinical use could not be developed.

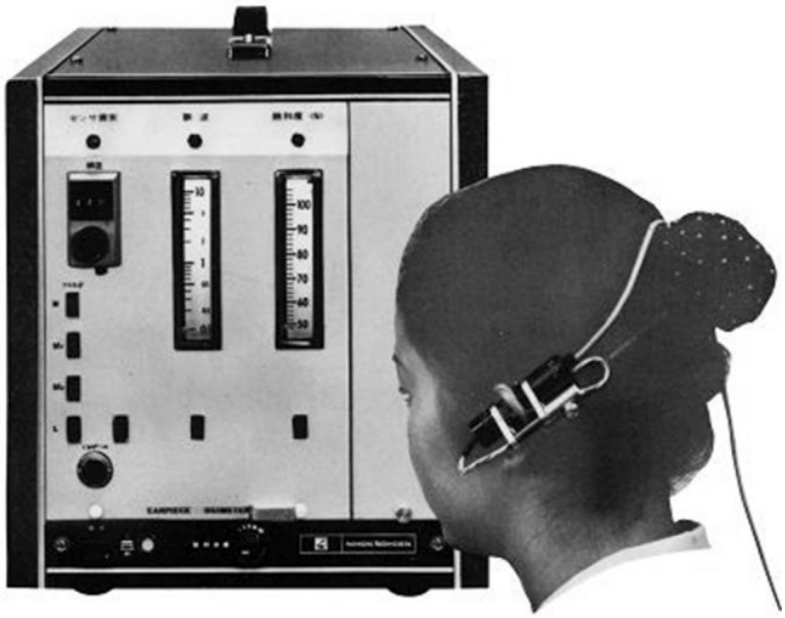

Figure 3-2 The world's first pulse oximeter is ear oximeter OLV-5100.

In 1977, the Minolta Company developed Yamanishi's oximeter concept using a fingertip probe to take advantage of the greater pulse amplitude. Minolta's device was marketed in 1977 as the Oximet MET-1471 (Figure 3-3) [62], [65]. The light emitted by a light emission diode travel to the finger probe and the transmitted light is analyzed by a silicon photodiode mounted in the chassis. The incident and transmitted light travel to and from the chassis through the fiberoptics, respectively.

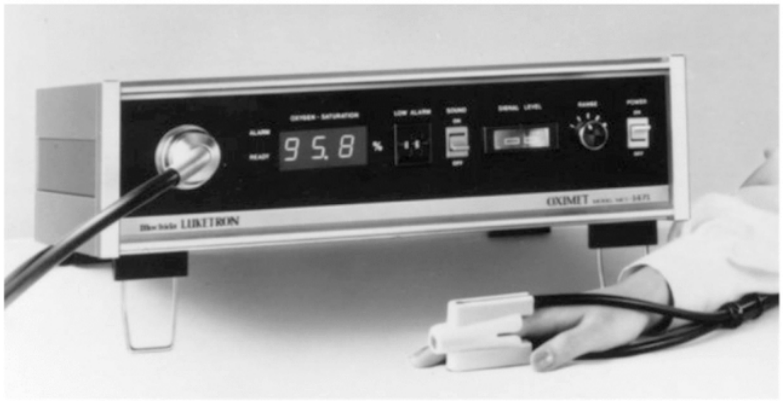

Figure 3-3 OXIMET Met 1471.

Nellcor introduced their device, the N-100 Pulse Oximeter (Nellcor) in 1983 with a great simplicity and considered more human factors design features (Figure 3-4), for example, changing sound of the pulse tone with decreasing saturation.

Figure 3-3 N-100 Pulse Oximeter (1983, Nellcor).

Nowadays, many SpO_2 sensors can be found in the market with competitive optimizations such as: small size, ease of use, wireless, integrated in watches, phones, and for use in clinic as specialized medical equipment for children and fetuses (Figure 3-5).

Figure 3-4 Examples of Commercial SpO_2 sensors on the market. a) Masimo MightySat b) Philips Respironics WristOx2 c) Philips Avalon Fetal Monitor d) Doppler fœtal Sonicaid SR2 e) NeoPulse Pulse Oximeter f) OxiFirstTM FS14 Sensor g) Nellcor OxiMax N-65 Handheld Pulse Oximeter h) iHealth Air Wireless i) Nonin Onyx Vantage 9590.

Despite the availability of SpO_2 device on the market, we found an essential need from the medical study point of view, to register the raw data of the PPG signal before any signal processing. Indeed, the PPG signal (to be further explained in Figure 3-7) can be useful to determine pulse wave characteristics, contains specific and critical information that of dicrotic notch, systolic and diastolic phases, etc.…This information could be useful in extreme state of the patient for specific emergency situation. Thus, developing our own device on which we could control the filtering of the signal is interesting for us and could be helpful to support biological study. In addition, we can design our own specific package adapted to our application.

Medical aspect of SpO_2 sensors

The normal range of SpO_2 on a healthy adult is between 97% to 100%. In practice, the SpO_2 range of 92–100% is generally acceptable for most people. Some experts have suggested that a SpO_2 level of at least 90% will prevent hypoxic tissue injury and ensure client safety [66].

In February 2021, the Food and Drug Administration warned that pulse oximeters may give inaccurate or inconsistent readings if a person has poor circulation, dark skin pigmentation, thick skin, cool skin temperature, or is wearing dark fingernail polish, artificial nails, or if their fingers are not clean [67]. This is remarkable issues to be noticed in the measurements of our home-made device (chapter 3, session 3.4).

There are two methods to calculate SpO_2: the detection of transmitted or reflected light (Figure 3 -6). In our study, due to the targeted application which needs to place the sensor on the head of the fetal scalp, we choose to develop a reflectance SpO_2 sensor.

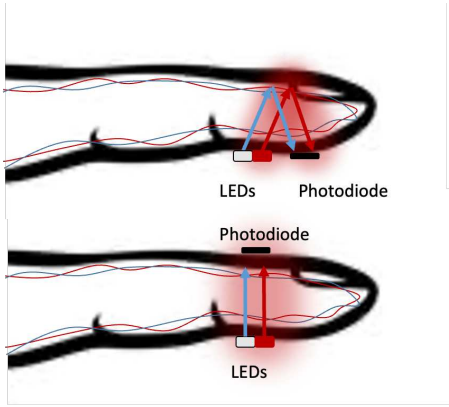

Figure 3-5 Reflectance and transmittance of SpO_2 sensor.

Literature review on the technique of reflection SpO_2 sensor

Pulse oximetry for the assessment of oxygen saturation (SaO_2) is based on photoplethysmography (PPG). During systole, light absorption increases leading to a decreased of reflected light intensity. The maximal and minimal values of the PPG pulse reflect this phenomenon (Figure 3-7). Hemoglobin is the main source for light absorption in tissue in the red and near-infrared regions, but other chromophores like melanin and myoglobin can also absorb light in these wavelength regions.

Figure 3-8 shows the extinction coefficients of oxygenated hemoglobin (HbO_2) and non-oxygenated hemoglobin (Hb) as a function of wavelength in the visible and near-infrared regions [68]. The extinction coefficient of each type of hemoglobin is defined as the absorption constant of the hemoglobin, divided by the hemoglobin concentration in the sample. The hemoglobin in blood includes HbO_2 of extinction coefficient εO and Hb of extinction coefficient εD.

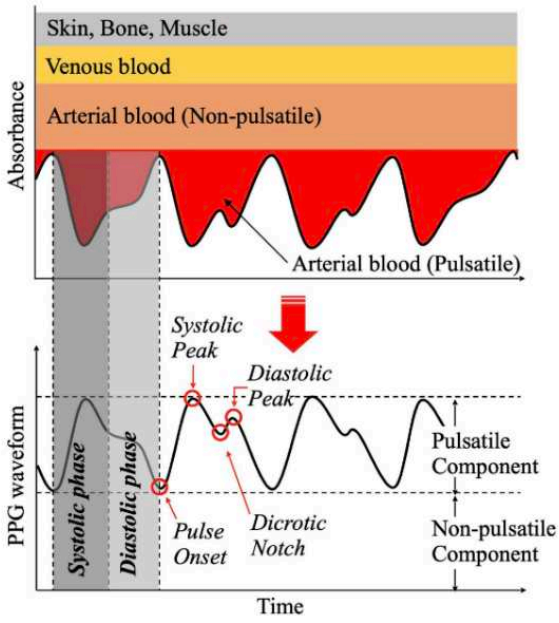

Figure 3-6 Principle of photoplethysmogram generation and waveform features [69].

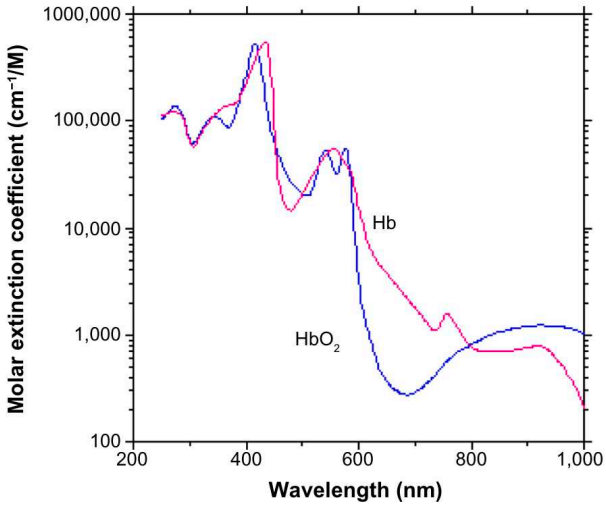

Figure 3-7 Explain on the technique of pulse oximetry [18].

Pulse oximetry exploits the light absorption difference between Hb and oxygenated hemoglobin (HbO2). HbO2 absorbs more infrared light (9400 nm wavelength) and less red light (660 nm wavelength) than Hb. Then, the reflected light is received by a photodiode on the same side. The recorded light signals consist of a direct current (DC) component and pulsatile alternating current (AC) component. Pulse oximetry calculates the modulation ratio R by using the DC and AC components of the red and infrared signals as follows:

$$R = \frac{AC^{red}/DC^{red}}{AC^{IR}/DC^{IR}} \quad (3\text{-}1)$$

An empirical calibration equation is established and could be different depending on the SpO2 measurement system. An example is shown on Figure 3-9.

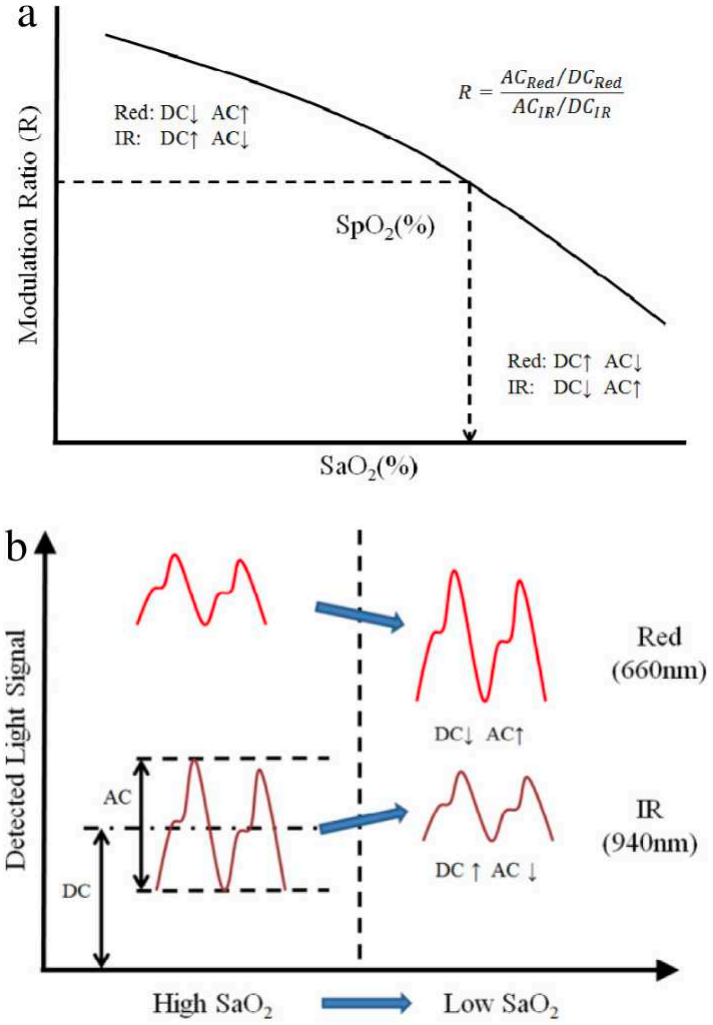

Figure 3-8 (a) Changes in ACR, ACIR, DCR, and DCIR with decreased SaO2. (b) Empirical relationship between modulation ratio R and SaO_2 [70] .

There have been many efforts of researchers for improving the accuracy of the SpO2 measurement. Niwayama et al introduced a non-contact measurement using spatially resolved near-infrared spectroscopy [71]. Hay et al reported their pulse oximetry with two infrared wavelengths without calibration in extracted arterial blood, based on the reduce of the difference in optical pathlength of the two wavelengths, compared to the case of one red and one infrared wavelength [72]. In another approach, a reflection SpO_2 sensor based on 3 LEDs (red 660 nm, green 535 nm and IR 940 nm) is introduced by Sun et al, employing a low-power microcontroller solution to integrate a subtraction to other blood component which can also absorb the light beside hemoglobin oxygenated and non-oxygenated [73].

Effect of distance between the LEDs and the photodiode (PD)

It is noteworthy to mention about the effect of distance between the LEDs for light emitter and the photodiode (PD) for light detector. Kanayama et al mentioned in their work of developing a finger-mounted fetal tissue oximetry using near-infrared spectroscopy, that the distance of 6-8 mm between the pair of source-detector is appropriate (Figure 3-10), considered the sensitivity and size of the probe [74]. As a smaller distance could lead to a lower sensitivity, we started to build our prototype with the distance of 6 mm between LEDs and PD (see session 3.3.3).

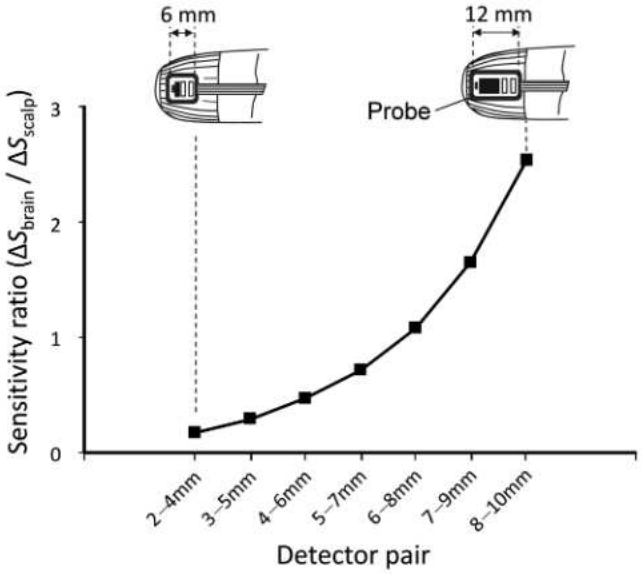

Figure 3-9 Relationship between the sensitivity and the pair of source-detector distances [74].

3.1.2. An overall summary

Overall, attempt to measure blood oxygen saturation has been established since many decades and the first fingertip-pulse oximeter was put on the market in 1977. Since then, SpO_2 sensors were broadly used in home healthcare and fitness support systems, making them more widely accessible to the general public and got a significant attention since the COVID-19 pandemia.

In our project, we attemp designing our own SpO_2 sensor for two purposes: i) to use SpO_2 as a supplemental measurement to confirm our pH measurement since both value decreases signify the oxygen level of the tissue or blood is changing, and ii) to provide a real time raw PPG signal as material for further data analysis for further biological study.

From the technical point of view, the state-of-the-art shows that it exists several methods to achieve an accurate SpO_2 sensor, such as using near infrared field or multiple wavelengths as light emitters. At this state of our project, we developed our device without targeting an

extremely high accuracy, with a basic principle using one RED and one IR LED and one photodiode (PD). The next sessions of this chapter will present our different prototypes and could be further developed in the future if necessary. The initial idea was also to embed the SpO_2 sensor with the pH probe on the same miniaturized package for easy manipulation in the fetal scalp application.

3.2. Methodology

The SpO_2 sensor was designed combining an optical probe to detect the light, an analog front end (AFE) circuit to provide an elementary filtered and amplified signal and a micro controller unit (MCU) to conduct signal processing, data display and storing (Figure 3-10).

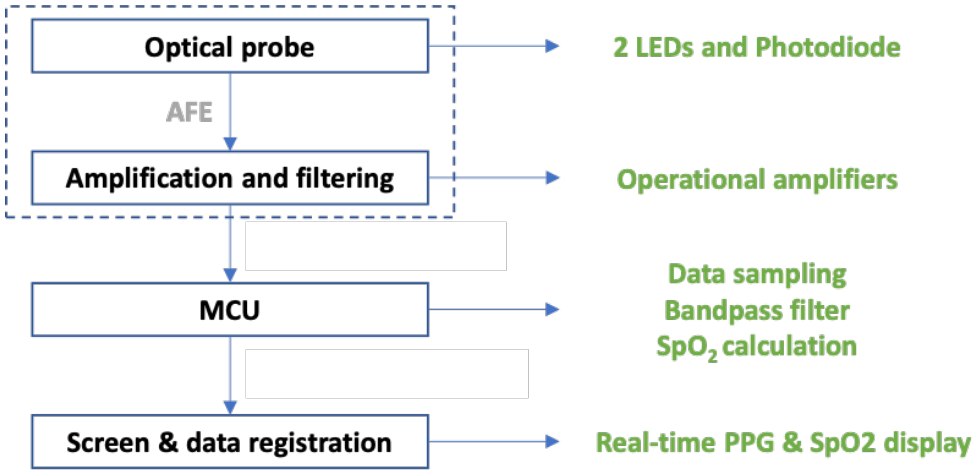

Figure 3-10 Scheme of SpO_2 sensor system.

All these different blocs will be described in the following sections.

Our method to develop the analog part of the sensor has been to work at the beginning with usual tools and material. And for that we have designed the first boards on a classical FR4 material. With this technology it is easy to fabricate the circuits in our laboratory to improve them and test different solutions. These different steps are not explained here but we present the scheme we obtained at the end of the first design sequence (see 3.3).

In parallel we have been working on the digital section of the system with a microcontroller unit for digital signal processing and a display of the results.

A comparison of results given by our sensing system to results given by a commercial pulse oximeter has also been performed.

A final step of our work has been an attempt to change the material of our PCB material for a flexible one that could be possible to implement on a non-flat surface like the head of a baby. It is an important technical change for us, and the PCB boards cannot be fabricated in

the laboratory. Anyway, different tests have been conducted and we arrived at a scheme giving rather good results and that will be presented in this manuscript.

3.3. Design and development of reflection SpO_2 sensor on hard-type PCB

3.3.1. Analog front end

In this section we present the global Analog Front End (AFE) which is designed with an optoelectronic probe and an amplifying section. The scheme is given in the following figure (3.11).

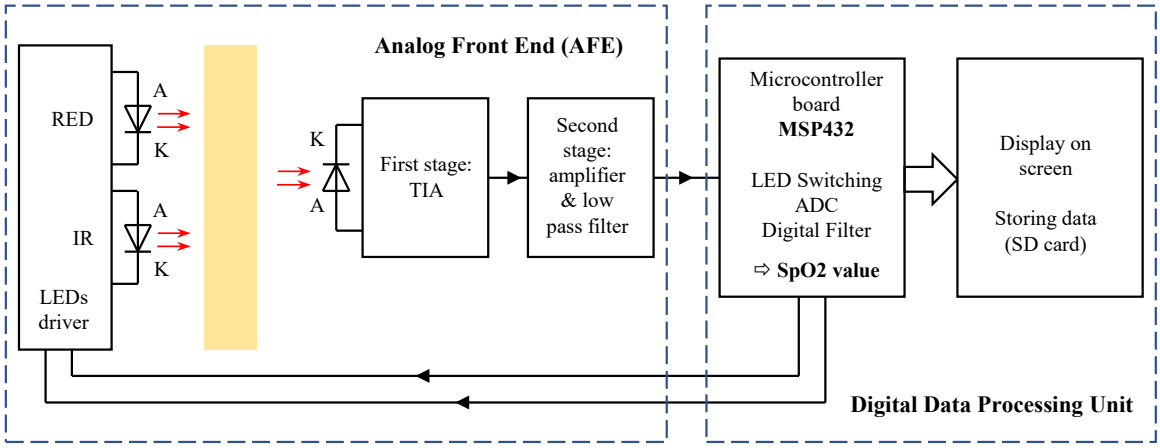

Figure 3-11 Global scheme of the optical reflectance SpO2 sensor. The power supply is not represented.

The optoelectronic probe is built around two LEDs for light emission and a photodiode for light detection. The two LEDs are: a Red one (ref. LS L29K from OSRAM) with a dominant wavelength of 630 nm and a peak at 643 nm; an Infra-Red one (ref. IKP 2012F3C from Kingbright), with a peak wavelength at 940 nm. The light is transmitted through the skin and is detected by a PIN photodiode (ref. BP104S from OSRAM) with a maximum sensitivity wavelength at 850 nm. The photodiode is connected to a first stage converting the current delivered by the photodiode into a voltage, and called transimpedance amplifier (TIA). This first stage acts also as a first order filter. A second stage achieves amplification and provides some more filtering. The AFE is supposed to be placed on the patient, and it is connected by a cable to the power supply and to the second part of the system, the Digital Data Processing Unit. Both sections are detailed below.

The optoelectronic emission circuit with the LEDs and the electronic driver circuit is shown in the Fig. 3.12.

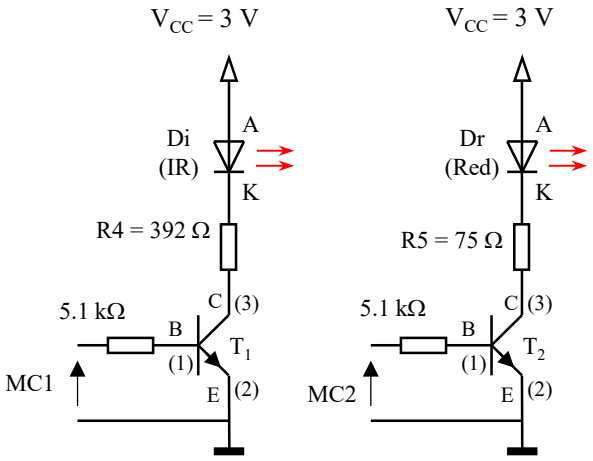

Figure 3-12 Optoelectronic light emission unit.

The LEDs (IR and Red) are switched on-off by two bipolar transistors NPN type, MMBT3904, noted T1 and T2. The command of the transistor is given by the microcontroller unit (input signals MC1 and MC2). The desired current intensities are tuned respectively by the resistors R4 and R5 in serial position with the LEDs, according to the datasheet characteristics. Measurement of the forward voltage of IR LED (Switch Red Off – Switch IR On) and red LED (Switch Red On – Switch IR Off) in continuous mode indicated 1.1V and 1.9V, respectively. Measurements also give the direct current into the LEDs when they are working alone: respectively 12 mA for the Red and 4.7 mA for the IR LED.

The activation time diagram of the two LEDs, driven by pulses is illustrated on Figure 3-13. The pulses are generated and controlled by the microcontroller MSP432, which will be further explained in the next session 3.3.2. The two diagrams are not symmetric. It has been chosen to work with the IR LED quite continuously (its current consumption is smaller) only switched off to turn on the RED one. The RED LED is turned on, the IR LED is turned off during 180 µs and the sampling of the RED signal is performed in the middle of this time interval of 180 µs. Then the IR is switched on again the sampling occurring 320 µs after the sampling of RED LED; the Red LED is turnd off. The global period of these signals is 5 ms, corresponding to 200 Hz for the sampling frequency.

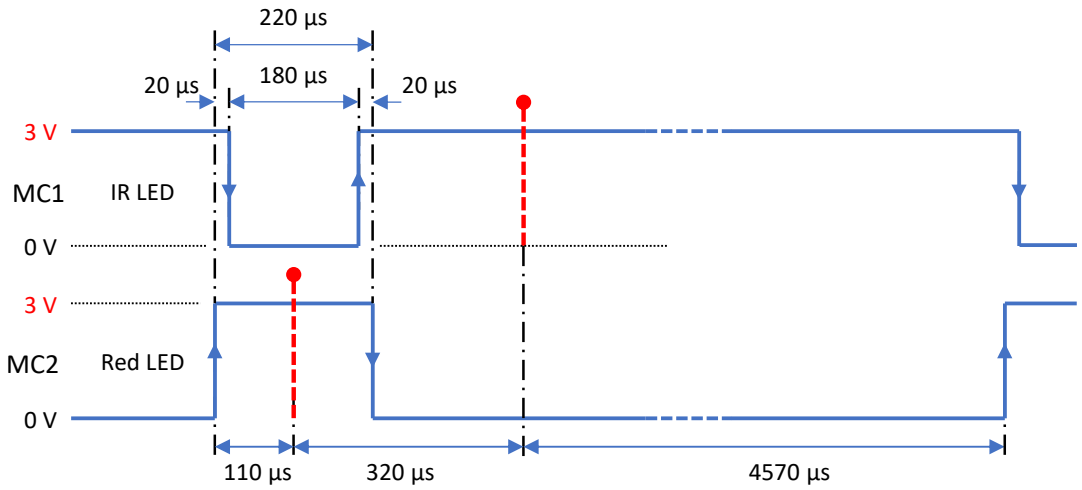

Figure 3-13 Switching time frame of the first prototype.

As the ADC used in the MCU is working with 14 bits it is logical to make the sampling at a time instant such as the transient of signal can be considered as finished with the same or a little better resolution. As $2^{14} = 16384$ and considering transient signals of first order, decreasing as $e^{-t/\tau}$, we should have $e^{-t/\tau} \leq 1/16384$ which leads to $t \leq 10\tau$ between the switching time and the sampling time. Therefore, for the signal going through the two low pass filters on the AFE board, and especially when turning off the IR LED the Red LED being already on, the time constant need to be less than $(180/2)/10 = 9$ µs.

On the sensing board a trans-impedance amplifier stage and a second operational amplifier stage, both based on operational amplifiers OPA376 (each in a SMT SOT23 case), are used for analog signal processing, providing amplification, and filtering and also driving the cable connected between the AFE and the microcontroller board. Calculation of each stage is detailed below.

This trans-impedance amplifier (TIA) converts the current signal provided by the photodiode into a voltage signal (Figure 3.14).

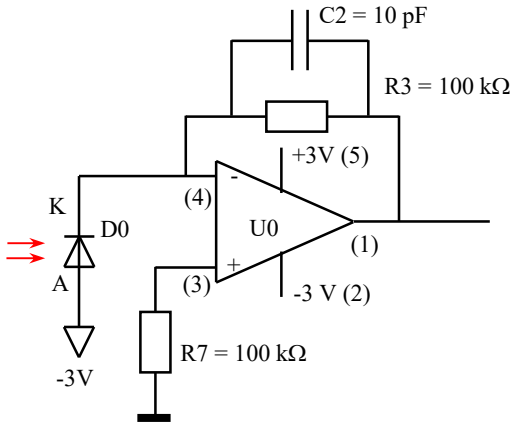

Figure 3-14 First stage: Trans-Impedance Amplifier (TIA) based on an OPA376.

The resistor R3 is chosen to convert the current signal to a significant voltage level. The capacitor C2 is used for two purposes. The first purpose is for stabilizing the structure of the TIA which is intrinsically oscillating without capacitor, and the second purpose is to achieve a low pass filtering taking advantage of the capacitor presence. The purpose of R7 is to reduce the offset at the output of the amplifier. The photodiode is connected to get a positive signal at the output of the TIA.

The transfer function of this stage is given ($\underline{I_{in}}$ being the current at the output of the photodiode) by: $\underline{H_1} = \frac{\underline{V_S}}{\underline{I_{in}}} = -\frac{R_3}{1+j\tau_1\omega}$.

This structure is a classical first order filter with a time constant $\tau_1 = R_3C_2$ and a cut-off frequency equal to $f_{c1} = \frac{1}{2\pi.R_3C_2} = 159$ kHz corresponding to $\tau_1 = 1$ µs.

The second amplifier stage (also based on an OPA376) has a non-inverting structure and provides a second filtering effect. The scheme is given in Figure 3.15.

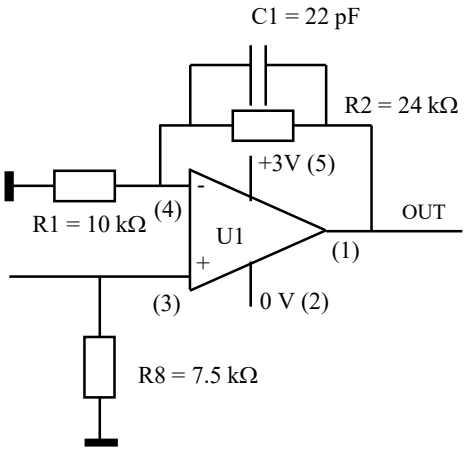

Figure 3-15 Second amplification stage: non inverter amplifier based on an OPA376.

The transfer function of this second stage is given by: $\underline{H_2} = A_2\frac{1+j\tau_3\omega}{1+j\tau_2\omega}$ where $A_2 = 1 + \frac{R_2}{R_1}$, $\tau_2 = R_2C_1$ and $\tau_3 = \frac{1}{A_2}R_2C_1 = \frac{\tau_2}{A_2}$.

The amplification at low frequency is given by A_2 ; the denominator shows the desired low pass behaviour with a cut-off frequency $f_{c2} = \frac{1}{2\pi.R_2C_1}$ and the numerator has a behaviour of a high pass filter but at a higher cut-off frequency than f_{c2}, it is $f_{c3} = \frac{1}{2\pi.\tau_3} = \frac{A_2}{2\pi.R_2C_1}$.

The global transfer function of the sensor is given by:

$$\underline{H} = \frac{\underline{V_{out}}}{\underline{I_{in}}} = -\frac{R_3A_2}{1+j\tau_1\omega} \times \frac{1+j\tau_3\omega}{1+j\tau_2\omega}$$

We can consider that the time constant at the denominator is $\tau_g = \tau_1 + \tau_2$ and at the numerator it unchanged equal to τ_3.

With the values seen in Figure 3-16 we get:

$A_2 = 3.4$; $f_{c2} = 301$ kHz ; $\tau_2 = 0.53$ µs , $f_{c3} = 1.025$ MHz ; $\tau_3 = 0.16$ µs and so $\tau_g = 1.53$ µs.

The voltage of the power supply is low ± 3 V for compatibility with microcontroller boards and for reducing the power consumption, keeping in mind a possible use of batteries. The gain A_2 should not be too high to avoid saturation of the second stage, considering that the first stage is already providing a significant signal. According to the condition determined previously we have a good margin of error, $\tau_g < 9$ µs.

Figure 3-16 shows experimentally, that the rise time and the fall time of the signal after passing by the two stages of amplifiers and filters are short enough to get a good sampling of the IR part of the output signal, in the middle of the pulse turning of the IR LED, the Red one being already activated.

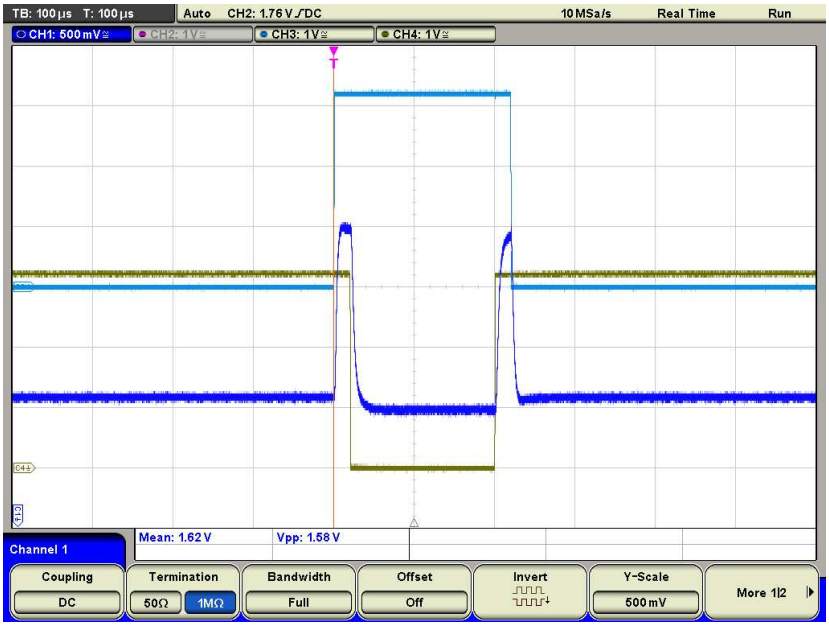

Figure 3-16 Signal going through the two amplifier stages shown in dark blue with both switching signals MC1 for the IR LED in green, and MC2 for the RED LED in light blue. The rise and fall times are easy to see.

One of the solutions to achieve better signal with less noise level, will be to implement a digital filter by the microcontroller unit as presented in a following section.

3.3.2. The first device on homemade hard PCB

The global scheme is given in Figure 3.17.

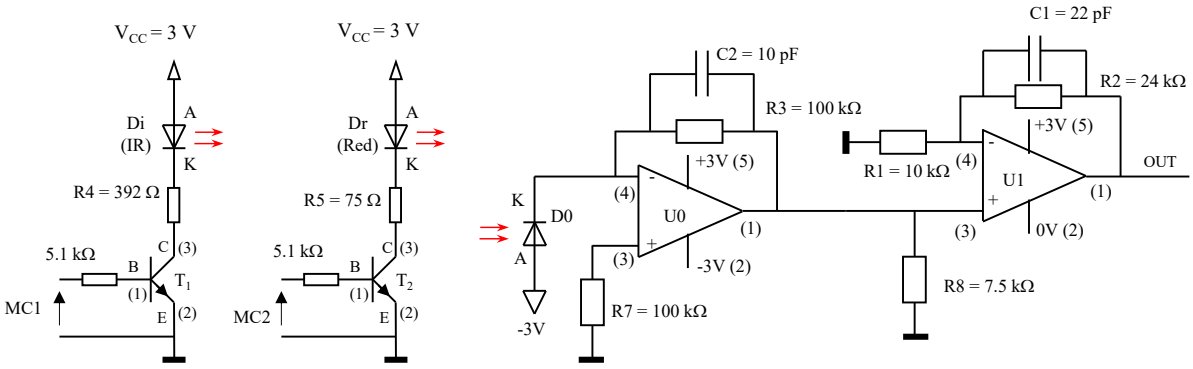

Figure 3-17 Global SpO_2 sensing board.

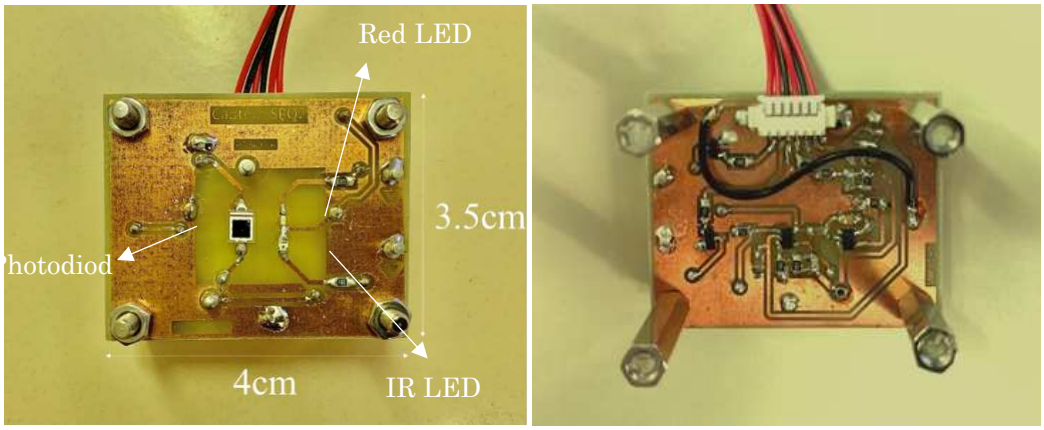

Figure 3-18 SpO_2 sensing board composed of a Red LED (630 nm), an IR LED (940 nm), a photodiode, a transimpedance amplifier and a second amplifier stage.

Figure 3-18 shows the hard-type PCB of the first SpO_2 sensor prototype with the above-mentioned scheme. This sensor is fabricated on a classical FR4 Printed Circuit Boards (PCB) and will be later implemented with some improvements on a flexible substrate (session 3.4).

3.3.3. MCU programed for switching control, sampling, filtering, and calculation.

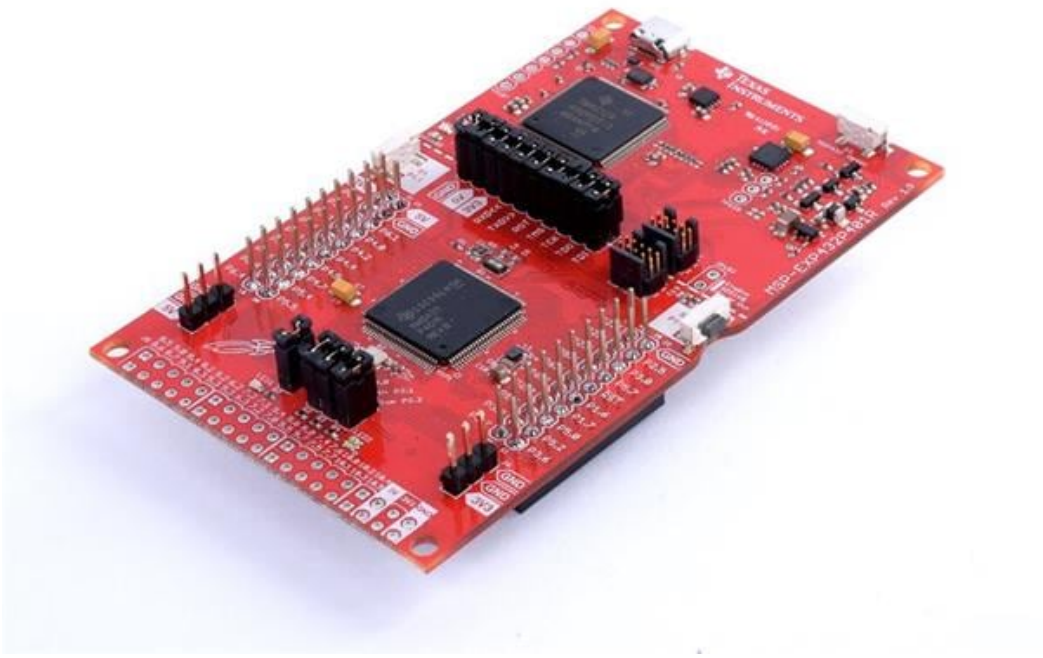

Figure 3-19 MSP432 microcontroller development from Texas Instrument Company.

The MSP432 board (ref MSP-EXP432P401R) is used to control the LEDs, to achieve the data sampling by a 14 bits Analog to Digital Converters (ADC) and to perform some signal processing. A band pass filter with 5 Hz high cutoff frequency and 1 Hz low cutoff frequency is implemented to obtain clear PPG signals. These frequencies have been chosen according to the heart rate of adults (for our own tests in the laboratory); they should be changed in case of measurement on a baby because of the higher heart rate. We see here a big advantage to work with digital filters easy to program. Programing of MSP432 was conducted by Quentin Rousset (M2 student, ENS Paris Saclay).

As explained in the previous section 3.3.1, the LEDs are activated sequentially from pulses delivered by the microcontroller and the sampling frequency can be adjusted depending on the circuit. The LEDs information is acquired and separated in the microcontroller leading to two digitized signals for each wavelength. The corresponding peak-to-peak amplitudes (AC for Alternating Current component) and mean values (DC for Direct Current component) are determined to calculate the ratio (R) value as given by equation 3-1. As until now we did not make the complete calibration, the SpO_2 is determined using the R value and an empirical formula (equation 3-2), based on application note AN1525 from Zhang Feng, Microchip Technology.

$$SpO_2 = 119 - 32.5R \tag{3-2}$$

3.3.4. SpO_2 measurement as control for fetal monitoring

The signal waveform also known as photoplethysmogram (PPG) can be useful to determine pulse wave characteristics, such as dicrotic notch, systolic and diastolic phases. The data acquired from sensors including pH, SpO_2, heart rate and PPG can be saved in a SD card or in computer and be displayed on a compact screen or customized interface on computer. We present here the characterization of our SpO_2 circuit shown in Figure 3-18.

Figure 3-20 shows a comparison between the raw data collected from the sensing board and the filtered data for display purpose and easy reading. The noise, including 50 Hz, is significantly reduced to obtain better waveforms and we can clearly see PPG signals.

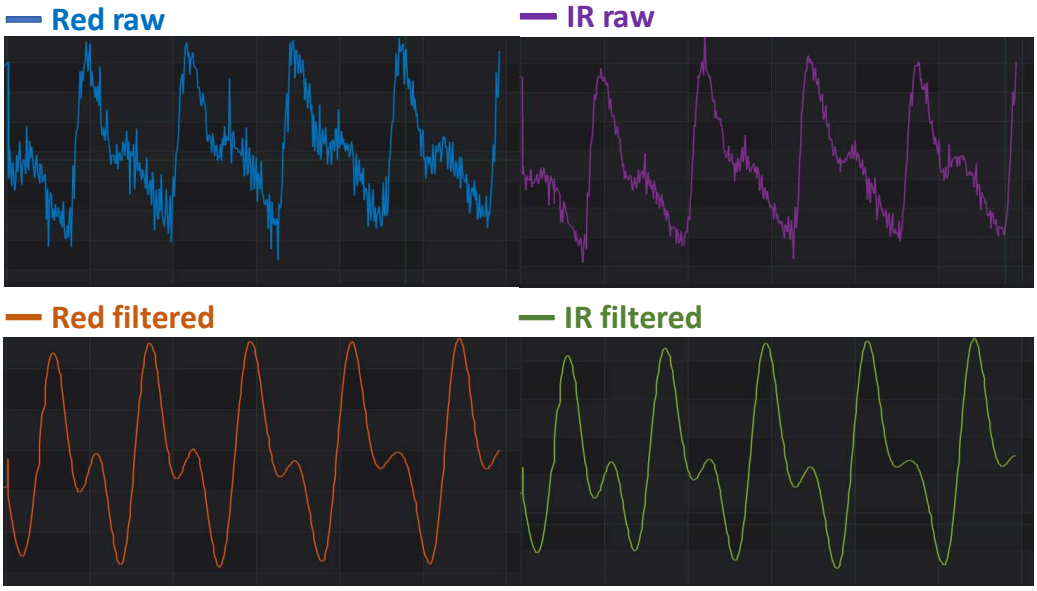

Figure 3-20 Comparison between raw signals sent from the sensing board and the filtered signals by a band-pass filter with 5 Hz high cutoff frequency and 1 Hz low cutoff frequency.

3.3.5. Method to calibrate and test the sensor.

We evaluated our SpO_2 sensor by measuring SpO_2 in parallel with a commercial device from Nellcor pulse oximeter as in Figure 3-21.

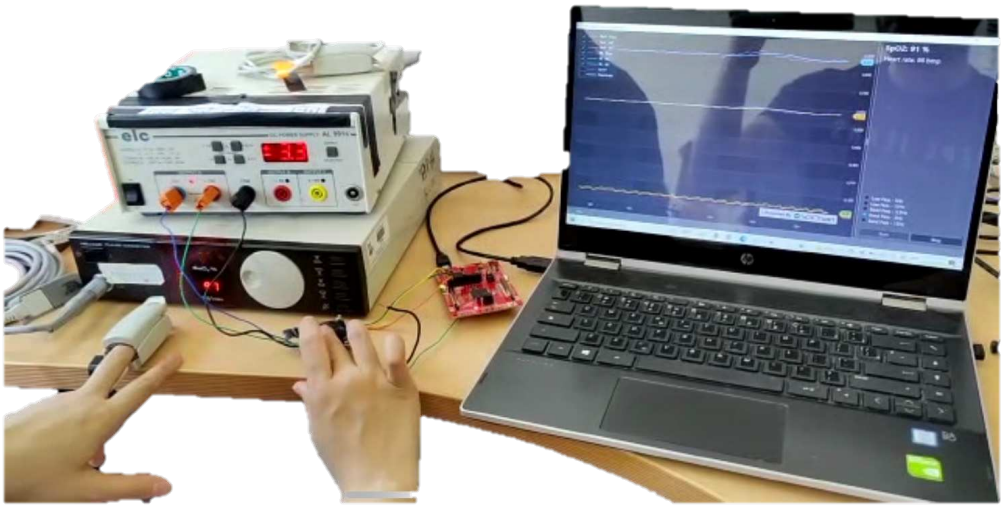

Figure 3-21 Protocol to calibrate the SpO2 sensor.

We have done measurements with both tools simultaneously on the middle finger of seven healthy individuals. In each measurement by the prototype, we waited at least one minute before recording data to be sure that the signal was stabilized. We accessed the results by comparing the average values in 2-minute intervals. The errors of measured signal by the prototype varied from 1 to 6% in absolute values, as seen on Figure 3.22.

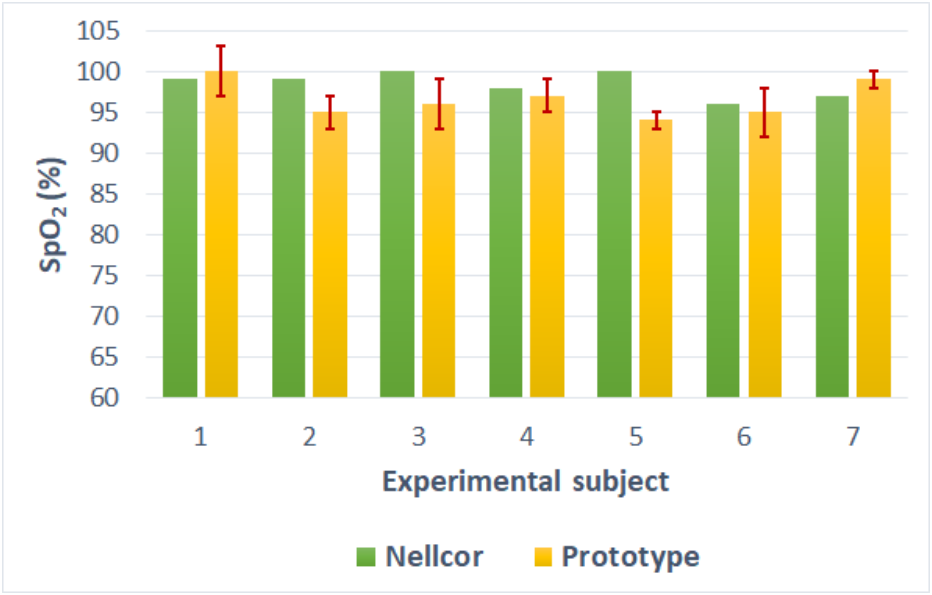

Figure 3-22 Comparison between the SpO2 measured by Nellcor device (green) and our prototype (yellow) on the middle finger of seven healthy individuals. The error bars are in absolute values.

The average relative error of the prototype compared to the Nellcor device is -1.9%. The difference between the two mean values comes from the use of equation 2 for a non-calibrated device. Some influencing factors have been observed, which are the pressure of the finger to the sensing board, the skin color, the perspiration, finger temperature and the difference in

thickness of epidermis. This should be overcome by improving the mechanical design and packaging of the sensor. An ambient light filter could be added to improve the signal. However, the behavior of the prototype is quite close to the reference system from Nellcor, which was our initial goal to get relevant PPG signals on a miniaturized circuit.

3.4. Optimization of a miniaturized SpO_2 sensor on flexible PCB

3.4.1. Optimization of AFE circuit and improvement of LED switching control

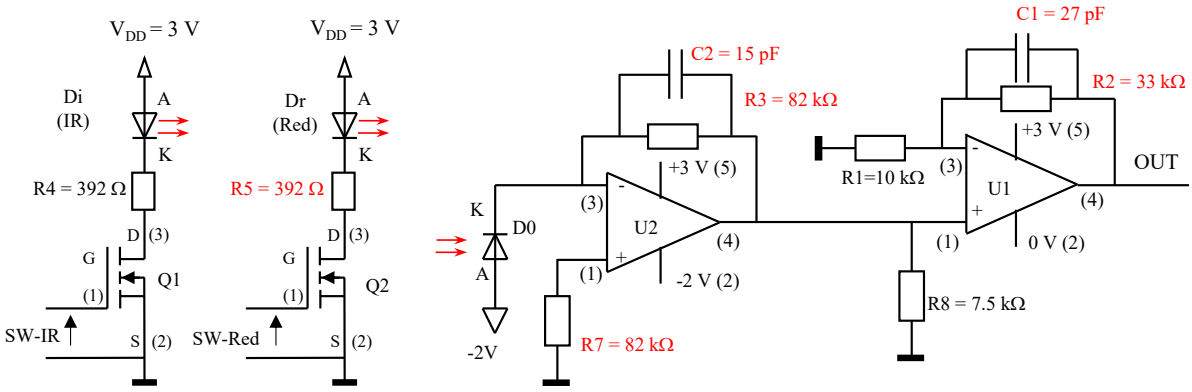

Figure 3-23 Optimized circuit of AFE, the changes for the passive components are written in red.

After the first development we decided to make some changes to the sensing part leading to a new version based on flexible material to be able to put it on a non-flat surface. We also decided, if possible, to reduce the size of the circuit

On the optimized AFE circuit (Figure 3-23), we made some change in the selection of components (LED, transistor, amplifier) to improve the efficiency of the light emitting and optimize the lowpass filters. We also changed passive components to a smaller size (from case 0805 to case 0603) and decreased power consumption:

The transistors have been changed from a bipolar NPN transistor to a N Channel Enhancement mode MOSFET transistor (ref Sil302DL from Vishay Company). First reason is to reduce the power consumption (here it concerns the base current which is canceled); for this kind of MOSFET the voltage command applied to the gate is positive, so it is compatible with the signals given by the MCU. Second reason is size reduction: with a voltage command it is possible to suppress base resistor (so there are two resistors less on the circuit) and this transistor is also available in a very small package (SC070-3 in place of SOT23 for the bipolar one). For these MOSFET transistor the typical $R_{DS(on)}$ is 0.6 Ω leading with drain current intensity of some mA to a very small voltage drop V_{DS}.

The red LED is changed into KS DELPS1.22 from OSRAM (with a peak wavelength of 637nm and a dominant wavelength of 628 nm); it presents a higher efficiency than the previous one.

For approximately the same output level for the sensor working with only the Red LED working and a finger on the sensor the current in the LED is approximately 3.6 mA, obtained with now R5 = 392 Ω. For the case of IR working alone the intensity is 3.8 mA.

The operational amplifier is changed from OPA 376 with a package SOT23 to TSV521 with a smaller package SC70-5. The maximum voltage supply difference being 5 V we use +3 V / -2 V.

The lowpass filters at the TIA and OPA have re-calculated with new values of capacitors and resistors. With the new values in Figure 3-23 we get now:

$$\tau_1 = R_3C_2 = 1.23\ \mu s\ ;\ f_{c1} = \frac{1}{2\pi.R_3C_2} = 129\ kHz\ ;$$

$A_2 = \frac{R_2}{R_1} = 4.3\ ;\ f_{c2} = \frac{1}{2\pi.R_2C_1} = 179\ kHz\ ;\ \tau_2 = 0.89\ \mu s\ ,\ f_{c3} = 1.025\ MHz\ ;\ \tau_3 = 0.16\ \mu s$ and so $\tau_g = 2.12\ \mu s$.

The switching of the two LEDs was changed to a new diagram as seen in Figure 3-24, along with the signal obtained with the oscilloscope. With this new switching principle, the LEDs are only activated for 220 µs each so it improves the power consumption without affecting the sampling.

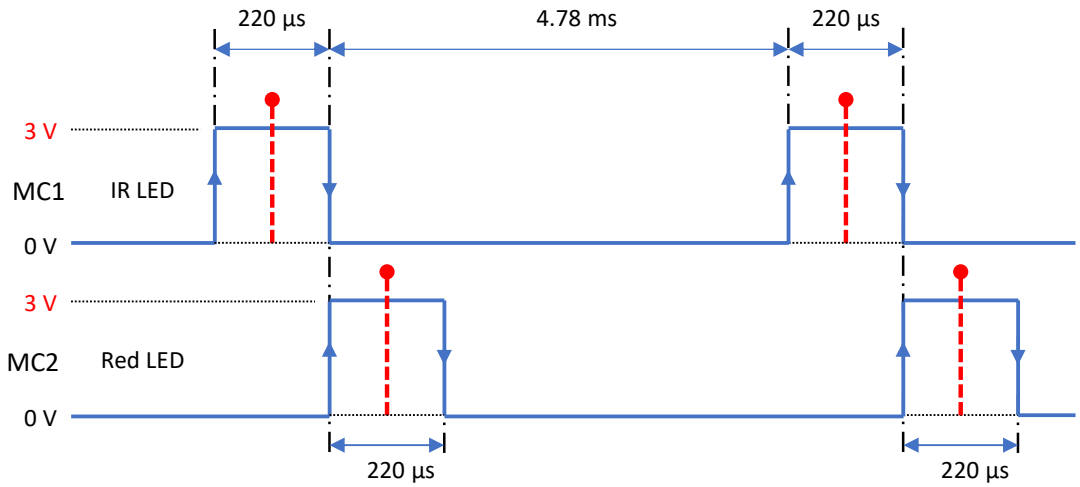

Figure 3-24 The second switching time frame of the two LEDs.

Now the sampling is done 110 µs after the switching, so the time constant need to be less than $(110)/10 = 10\ \mu s$ once again to have at least 14 bits resolution. We still have a good margin and for a future prototype we could be less careful.

In the next Figure we can see the signal obtained at the output of the sensor with this new switching technique.

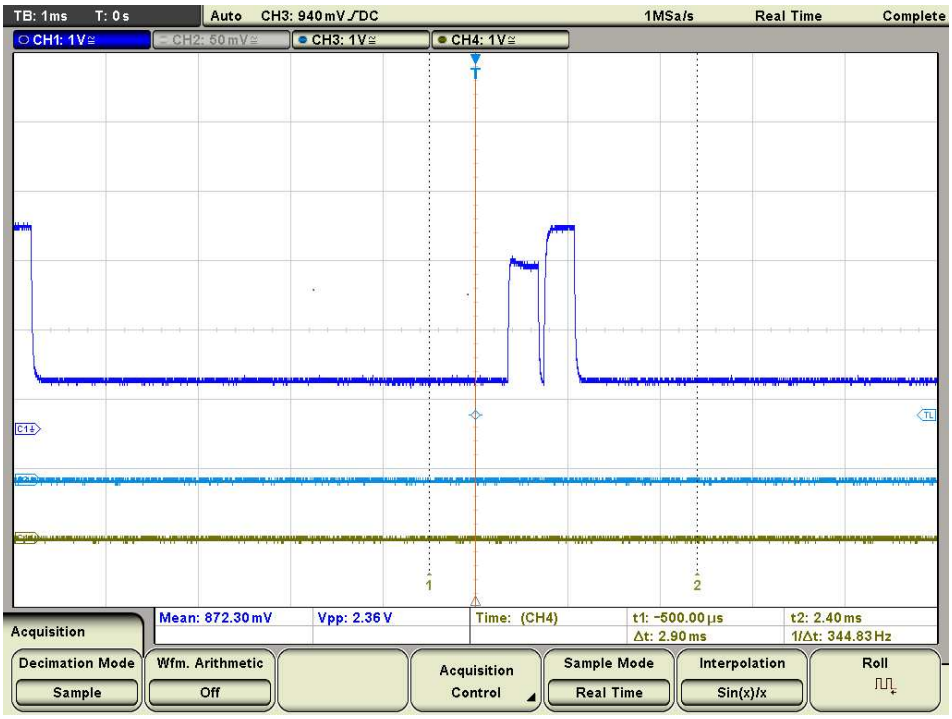

Figure 3-25 The experimental switching of the two LEDs on the output signal of the sensor.

3.4.2. PCB design

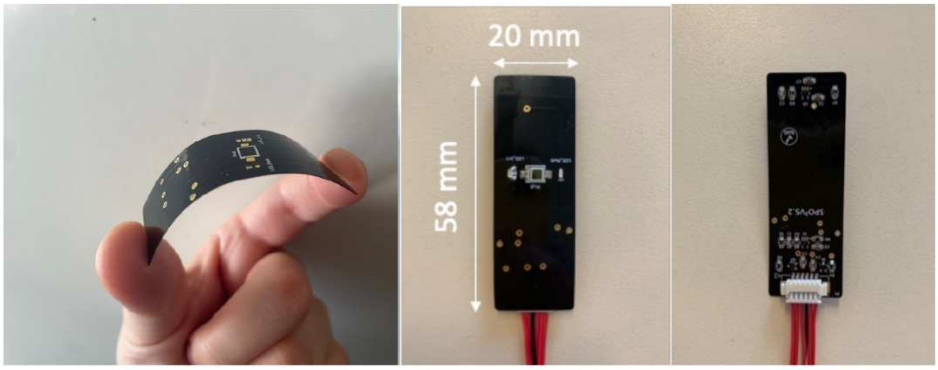

Figure 3-26 Flexible PCB of the optimized circuit.

Figure 3-26 shows our flexible PCB with the optimized circuit, designed by technician Simon Lhorset (ENS Paris Saclay). Material of the substrate is Polyimide Laminate from SHENGYI and components were soldered at clean room in ESSIE Paris.

The circuit shown in Figure 3-26 is the third board that we realized with flexible substrate. For the first one, there was an internal short circuit because of a multilayer structure. Back to a classical two layers material, it was finally too thin and bad contacts appeared. Material of the third one presented above is thicker, with a black coating to avoid light reflection.

3.4.3. SpO_2 measurement

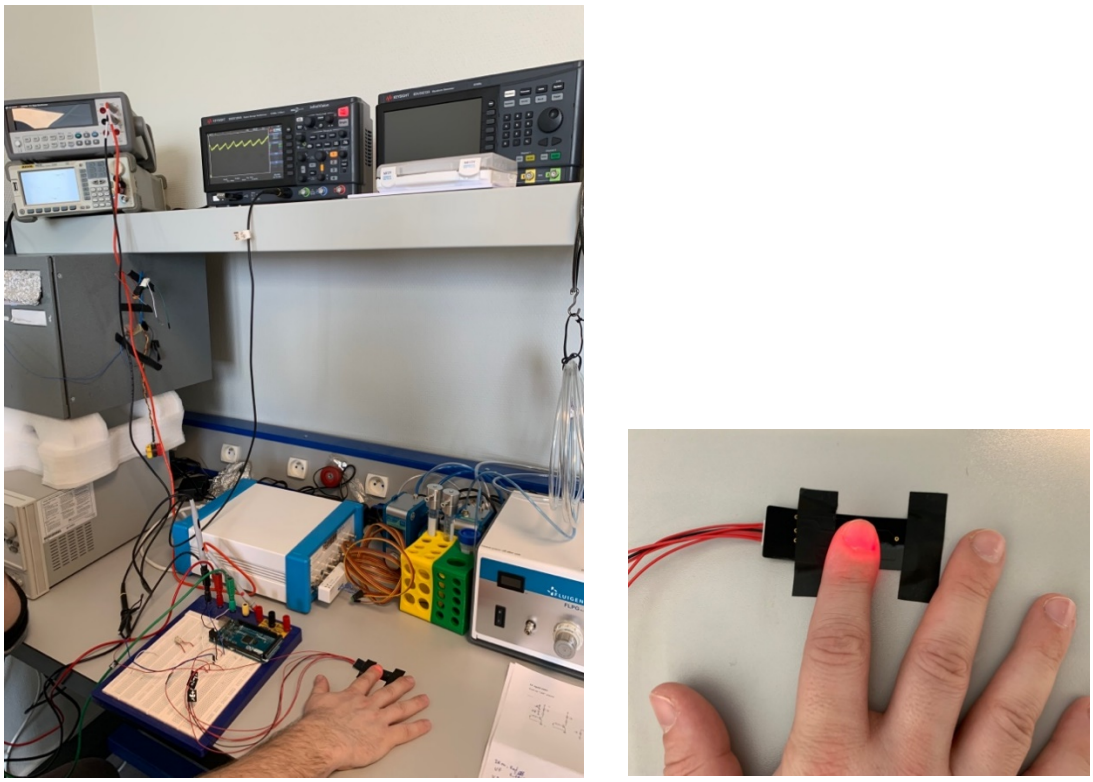

Figure 3-27 Measurement of the signal in continuous mode (case of the RED LED on).

We measured the signal at the output of the AFE board while turning on each LEDs in continuous mode by an oscilloscope as seen on Figure 3-27 for the Red LED, but for each LED separately.

Measurement results (Figure 3-28 and Figure 3-29) show a quite good signal at the output of the AFE unit, before being filtered and amplified later by the microcontroller. The average values for both signals are quite similar, that was one of our goals. This could be used to collect the raw data for further biological data analysis if necessary. Even without signal processing, it is possible to see dicrotic notch and diastolic peak.

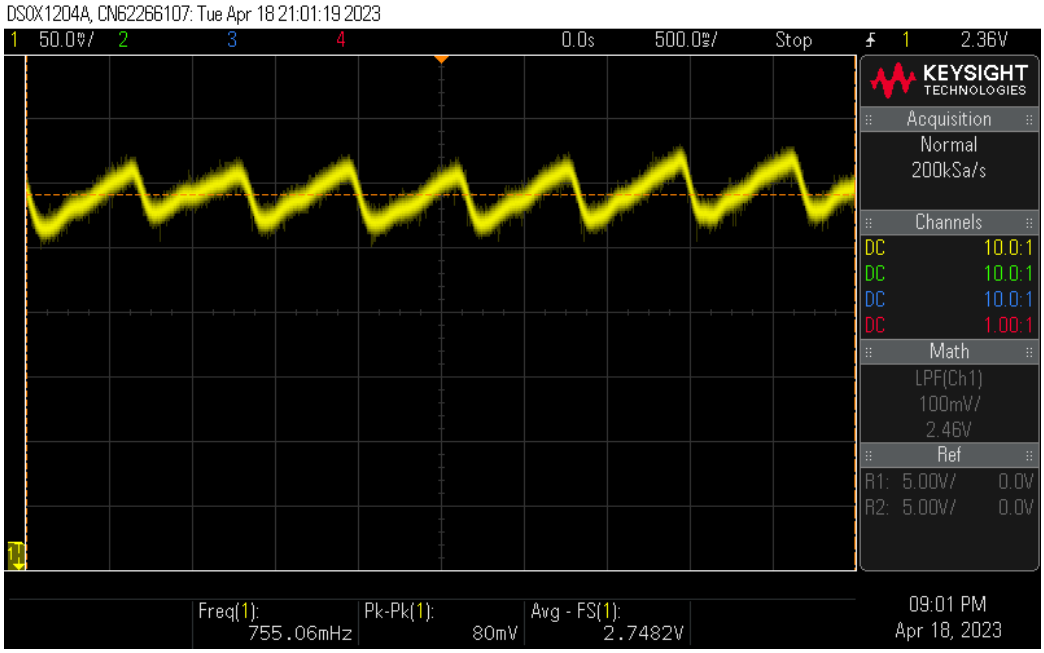

Figure 3-28 Output signal passing through AFE board in case IR off – Red on.

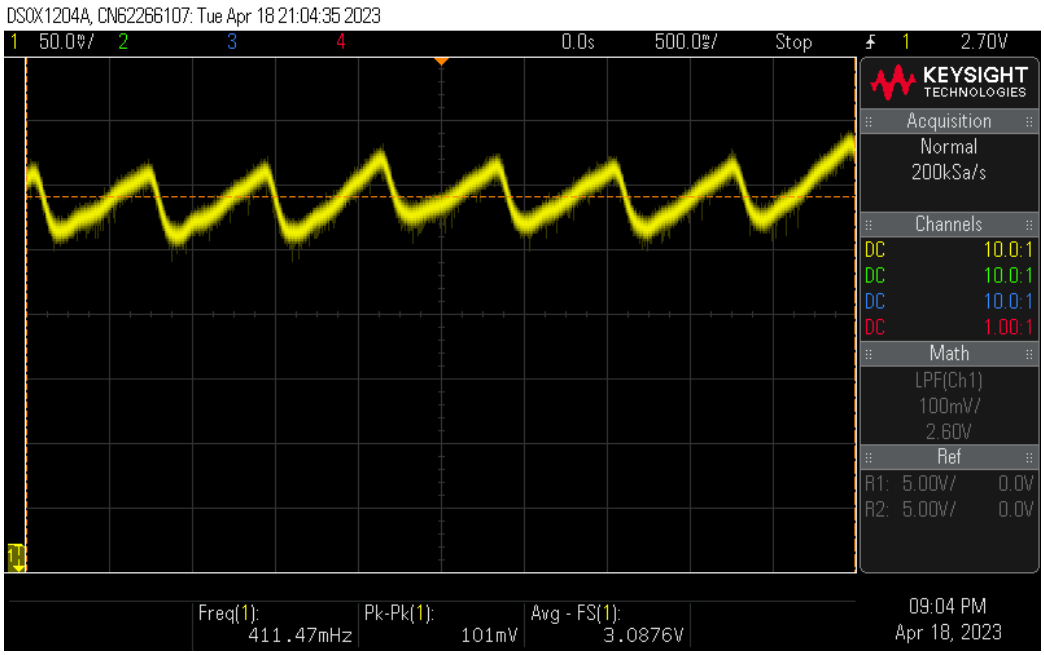

Figure 3-29 Output signal passing through AFE board in case IR on – Red off.

We also tested our system on a person. Signal was plotted real-time showing a clear PPG waveform after being filtered by the microcontroller, which also provided the calculated SpO_2 value and heart rate value (HR). Data were saved in the computer (Figure 3-30).

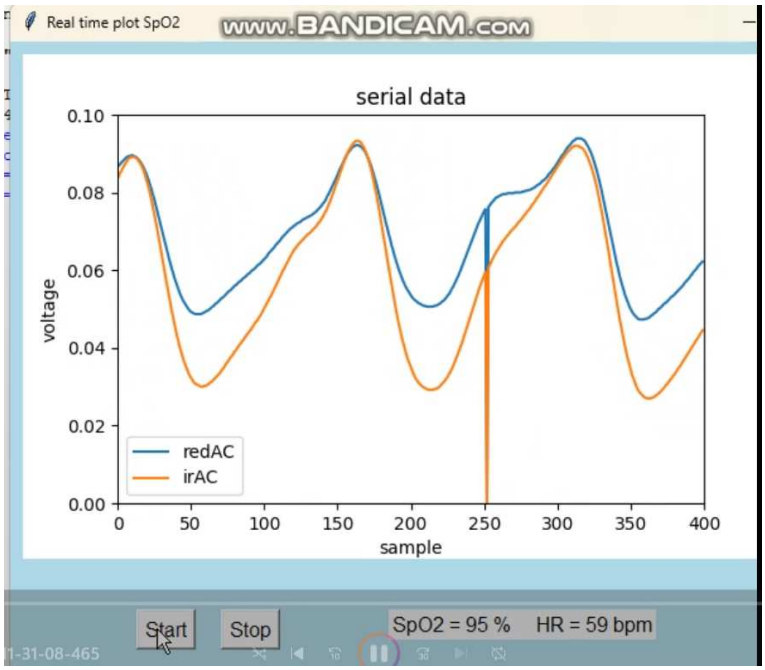

Figure 3-30 Signal plotted real time while testing the SpO_2 sensor on a person.

At the current stage, we are developing a more compact system with a mini screen (Wio-terminal) for data visualization and storage in an SD card (as seen on Figure 3-30), to avoid the use of a laptop during in vivo experiments. This work is under contribution of KHAZAAL Elio, BROCHEN Loïk, MERIEAU Lucas, ILIKOUD Maxime, NNA Alain Vaillant and ANTANINAS JOSEPH in R1 project. More proposals about possibility to a complete and appropriate system will be described in chapter 4.

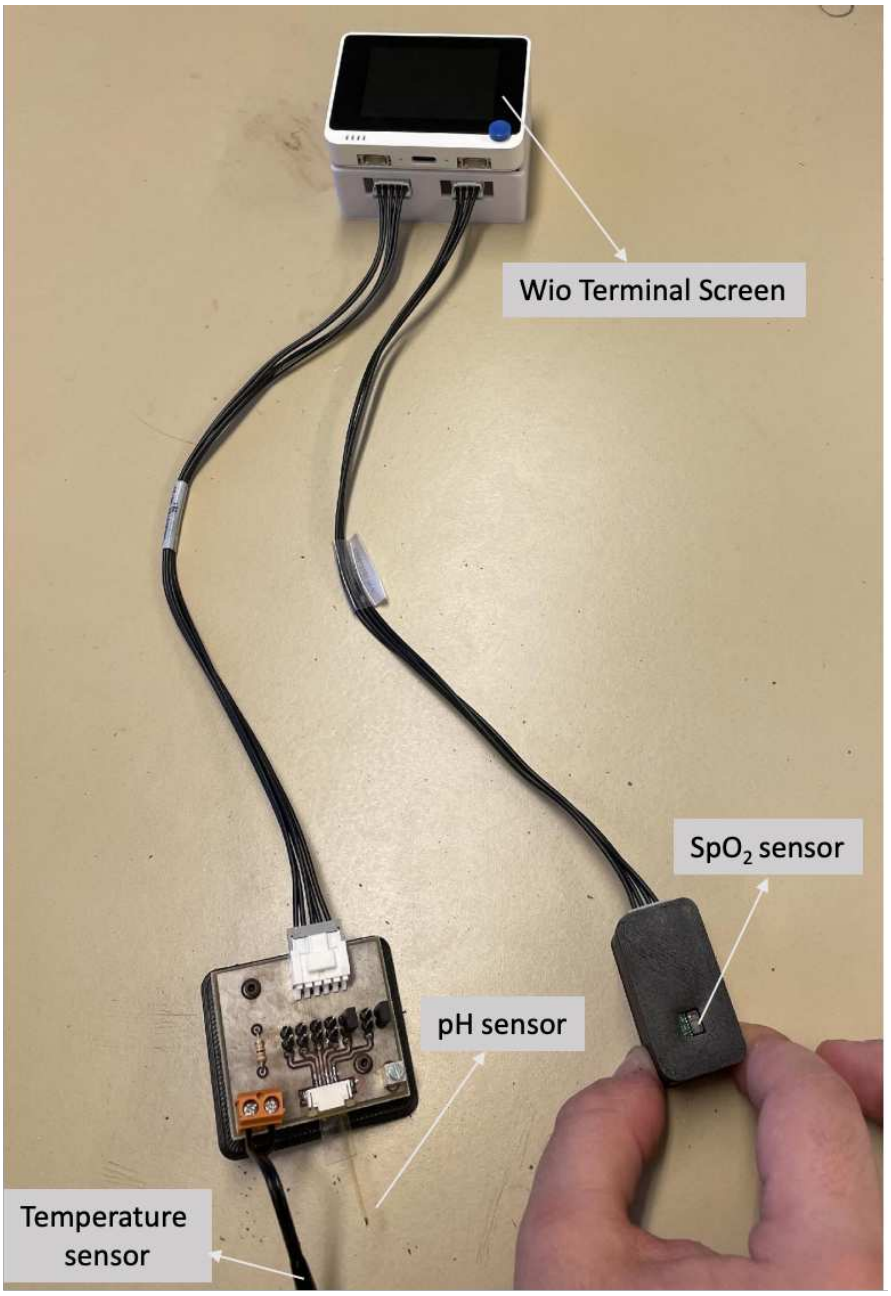

Figure 3-31. Compact system integrating pH and SpO2 probes, with a mini screen (WIO-terminal) for data visualization and storage in an SD card. Project R1.

3.5. Conclusion

This chapter introduced our work to develop a prototype of miniature SpO_2 sensor on a flexible substrate, which could register raw PPG signal and could be used as a supplementary measurement tool to validate our pH measurement.

Indeed, as stated in the introduction, capillary pH on fetal scalp is frequently monitored as a second-line examination beside fetal heart rate in delivery rooms, to reduce false positives rate for predicting the fetal acidosis. Our project is to integrate on a unique device both SpO_2 and pH sensors with a continuous monitoring.

A first prototype of optical reflectance SpO_2 sensor on a hard type PCB, capable of measuring SpO_2 and register a clear PPG signal has been developed showing promising initial performance. A microcontroller MSP432 was employed to control the light emission and data acquisition at 200 Hz sampling frequency. Our SpO_2 sensor produced a quite close behavior to commercial devices and a clear PPG signal available through a customized simple interface. A new optimized circuit on a flexible substrate was introduced and tested, showing a good output signal. However, we need to investigate more to find a more suitable flexible material for the final system, especially taking into account "medical requirements".

At this stage, the sensors are separated but an integrated package is considered for the next step using both a flexible electronic circuit for SpO_2 and a flexible substrate fabrication for the pH sensor. This integration work is expected to provide a device embedding all above-mentioned sensors into a flexible solution for later in vivo testing but compatible with medical constraints (material biocompatibility, sterilization, easy manipulation of the final device by the medical staff…).

Chapter 4

CONCLUSION AND PERSPECTIVES

4.1 Conclusion and summarize the results achieved in the thesis.

Monitoring fetal well-being during labor is a common practice of daily obstetrical activities. Ensuring the good oxygenation of the fetus is important to prevent the risk of asphyxiation and its most serious consequences: peripartum death and distant sequelae, in particular neurological disorders. In this work, we define the significance of pH and SpO_2 measurement to human health in general and fetal health monitoring in particular. Biological aspect of pH imbalance and the relevant to SpO_2 is explained, along with the need of real time measurement in order to get over the limitation of the current blood analyzing technique. A prototype, which is a first attempt to get continuous fetal health monitoring during labor, is designed and fabricated. This system is capable of simultaneously measuring pH, SpO_2 and provides a clear photoplethysmogram (PPG) in real time. Microelectrode was fabricated using Titanium nitride (TiN) as the potentiometric sensing material for pH variations. A reflectance optical sensor was used for SpO_2 monitoring. Both pH and SpO_2 probes are minimized and fabricated on flexible substrate (polyimide).

The most critical requirement of the pH sensor for fetal health monitoring is a precision of 0.01 in pH, with an appropriate miniaturized design. Potentiometric based pH sensors are the most favored electrochemical systems due to their simple design and possibility to be miniaturized. The first part of our work focuses on developing a TiN potentiometric pH micro-sensor in clean room with its complete characterization in vitro. The second part is an additional study, in which we present a prototype which is our first attempt to get continuous measurement of SpO_2 and provides a clear photoplethysmogram (PPG) in real time, considered as a complementary second line measurement on the foetus during labor. This work targets to make a SpO_2 sensor which can register raw pulse oximetry signals for biological research purpose. In addition, SpO_2 measurement is helpful to evaluate our pH measurement as correlation exists between low tissue oxygenation and lower pH.

The summaries below indicate the detail properties achieved on our designed pH and SpO_2 sensors.

Chapter 2 presented our study on designing and developing a flexible and micro pH sensor with a very high accuracy (below 0.06 in pH), a prototype fabricated on glass substrate could reach 0.02 in pH precision, which is close to the target of fetal health monitoring during labor and other biological applications related to human and animal health. Probe head size is designed with 1.2 mm x 1.5 mm (width x length) on single-probe design and 0.9 mm x 2.8 mm (width x length) on triple-probe design. In vitro results demonstrated a compatible sensitivity on several functional electrodes, ranging from 53.3 – 67.6 mV/pH in case of flat TiN, with a good reproducibility upon 3 loops of measurement. A specific treatment was applied to obtain nanoporous profile of TiN at the working electrode, instead of flat surface, to improve the precision of the sensor from 0.1 to 0.05 in pH. The precision of TiN porous was slightly reduced on the polyimide flexible substrate compared that of glass substrate (down to 0.02 in pH, see section 2.3.1) but still very low. A slight decrease in sensitivity of the porous TiN sensor after the in vivo test was observed, from 53.2 mV/pH down to 50 mV/pH, which however validates the consistency under insertion conditions. Reproducibility of the process to obtain porous TiN was evaluated, showing the variation of sensitivity in the range of 51-54mV/pH). A preliminary in vivo test was conducted on mice, recorded a stable OCV signal under anesthesia conditions.

Chapter 3 introduced our design of a reflectance SpO_2 sensor, employing two LEDs at 630 nm and 940 nm wavelengths with one wideband photodiode and was monitored by a MSP432 microcontroller. Several versions of the SpO_2 sensor were fabricated. Result recorded of the first prototype of the classical hard-type PCB shows close behavior to a commercial device. We optimized the analog front end (AFE) circuit and transferred it to a flexible PCB, fabricating a second prototype. Finally, we developed a prototype of miniature SpO_2 sensor

on a flexible substrate, which could register raw PPG signal and could be used as a supplementary measurement tool to validate our pH measurement.

At this stage, the sensors are separated but an integrated package is considered for the next step using both a flexible electronic circuit for SpO_2 and a flexible substrate fabrication for the pH sensor. This integration work is expected to provide a device embedding all above-mentioned sensors into a flexible solution for later in vivo testing but compatible with medical constraints (material biocompatibility, sterilization, easy manipulation of the final device by the medical staff…).

Main contributions and results:

- A microfabrication process developed and optimized on flexible polyimide
- A new working electrode material tested (TiN flat and porous)
- Several mask levels designed and implemented
- A full in vitro characterization protocol developed and used for all the probes (OCV, CV,PEIS, influence of the Temperature)
- A SpO_2 sensor developed allowing continuous PPG data recording
- Some in-vivo preliminary test done on mice showing the POC

4.2. Perspective and proposal

We are doing an evaluation for new pathologies or medical appications, for cardiac ischemia detection for instance. New tests are under going in animal facilities on different animal models at the Ecole Vétérinaire d'Alfort to complete the work in the near future.

As perspectives, in the final form of the device, the flexible pH electrodes could be considered to be attached into a specific needle, which is adaptable for clinical skin insertion. This pH sensing needle will be fixed with the SpO_2 sensing board using a flexible polyimide substrate in a customized package.

The important challenges to be considered for this work in the future are:

1) to find the best mechanical design to be easily used by the medical staffs and prevent any damage for the fetus and the mother;

2) to guarantee the sensitivity and accuracy in real use-case; including a full evaluation on the uniformity of the fabrication, complementary development on TiN material to have consistent sensitivity (in term of potential). For example, Paul Shylendra at all presented their study on adding a Nafion layer on Titanium Nitride for their pH Sensor, which can minimize the potential shift E0 value[32]. This aspect is important to improve performance of our sensor in high redox media for multiple application. A study to improve the potential

stability of the reference electrode and the integration technique of this reference electrode close to the working electrode of our pH sensor should also be considered.

3) to investigate a better control of the porosity of the porous TiN.

4) to establish a protocol for temperature correction, sterilization and storage of the pH sensing electrodes.

Further in vivo experiments are required to assess the proof of concept and find additional funding for the development of a future medical device, focusing on medical health mornitoring rather than only fetal scalp case. It is essential to acknowledge the multiple stages involved in progressing from research to a finalized product.

A study on the optical properties (reflectance and transmittance of TiN flat and porous material could be considered to further investigated, as we obtained some interesting result on this aspect (see annex).

Publications

1. T. Nguyen *et al.,* "pH and SpO_2 Miniaturized Sensors for Fetal Health Monitoring" in *Proceedings of the 15th International Joint Conference on Biomedical Engineering Systems and Technologies*, Online Streaming, Portugal, 2022, pp. 155–161.

2. T. Nguyen, B. Journet, H. Takhedmit, and G. Lissorgues, 'Porous Titanium Nitride electrodes on miniaturised pH sensor for foetal health monitoring application', in *2022 Symposium on Design, Test, Integration and Packaging of MEMS/MOEMS (DTIP)*, Pont-a-Mousson, France: IEEE, Jul. 2022, pp.

3. T. Nguyen, G. Lissorgues, B. Journet, H. Takhedmit, A. M. Ridoux and E. Lecarpentier, "Miniaturised flexible pH biosensor", Poster, in Conference Biosensors, Busan, Korea, Jul. 2023.

4. T. Nguyen, G. Lissorgues, L. Rousseau, B. Journet, H. Takhedmit, A. M. Ridoux and E. Lecarpentier, "Very Accurate Flexible pH Microsensor Based on Nanoporous Titanium Nitride Material ", under review, IEEE.

Annex

Annex 1. Literature review details.

Table 2. The introduction of optical fiber-based platform.

Types of Optical Fiber pH Sensor	Configuration	Specific Indicator Dyes	pH Range	Response Time	Accuracy	Reference
Fluorescent type	probe	Fluorescein	9–3	2.5 min	Not specified	[84]
			3–9	6 min		
Absorption type		Phenol red.	7.0–7.4	0.5 min	0.017	[85]
Reflection type		Bromothymol blue	7–12	2.5 min	Not specified	[86]

[29]

Table 3. The pH measuring characteristics of metal oxide-based pH electrodes.

Materials	Method	pH Range	pH Sensitivity	Stability	Reference
PbO_2	Thermal method	1.2–7.5	112 mV/decade	Only stable in the acid region,	Lima et al. [101] 2005
		Over 7.5	88 mV/decade	Non-linear behavior of the pH response	
OsO_2		2–11	51.2 mV/pH	were sensitive to oxidizing and reducing agents	William et al. [102] 1984
TiO_2		2–12	55 mV/pH		
PtO_2		5–10	46.7 mV/pH		
WO_3	Magnetron sputtering	2–12	41 mV/pH	High stability (over a month)	Zhang et al. [103] 2009
IrO_x	Electrochemical		63–82 mV/pH	The potential always stabilized in a few minutes.	Baur et al. [104] 1998
IrO_2	Electrospinning	3–12	67.1–70.15 mV/pH	stable in one week	Dong et al. [105]

[29]

Table 3 Properties of metal oxides based pH sensors for wearable/flexible electrochemical sensor fabrication

Material	Fabrication	Substrate	pH range	Response time	Sensitivity (mV pH^{-1})	Flexibility	Ref.
IrO_2	Sputtering	PET	4–7	—	61 ± 1	—	195
IrO_2	Electrodeposition	PI	4–9	0.5 s	69.9 ± 2.2	—	184
IrO_2	Sol–gel	PI	1.5–12	0.9 to 2 s	51	Tested in a tube with a 1 cm curvature radius	196
CuO nanorectangle	Hydrothermal synthesis	PET	5–8.5	—	0.64 μF pH^{-1}	Tested in a tube with a 5 mm curvature radius	22
ZnO nanowalls	Low temperature Polycrystalline silicon thin film transistor technology	PI	1–9	—	~59	—	197
IZO	Sputtering	PET	4–10	5 ms	105	Tested by bending around a cylinder with a 1.0 cm curvature radius	198
ITO	Radio frequency sputtering and a roll-to-roll process	PET	2–12	—	50.1	—	199
InGaZnO	Sputtering and thin film transistor technology	PI	3.3–11	—	51.2	Tested as a function of bending with up to 13 mm curvature radius	185
WO_3 nanoparticle	Electrodeposition	PI	5–9	23–28 s	−56.7 ± 1.3	—	186

[30]

Table 4 Properties of polymer and carbon-based pH sensors for wearable/flexible electrochemical sensor fabrication

Material	Fabrication	Substrate	pH range	Response time	Sensitivity (mV pH^{-1})	Flexibility	Ref.
PANi	Electrodeposition	a. PET b. PVC coated steel wire	1–13	A few seconds	58	—	125
PANi	Electrodeposition	PDMS	4–7	~60 s	—	Tested by mechanical friction and skin deformation	131
PANi	Drop-casting	PET-coated palette paper	4–10	Rise time 12 s Fall time 36 s (pH 6–8)	50–58.2 (pH 2–12)	—	206
PANi	Electropolymerization	Commercial adhesive bandage	5.5–8	20 s	58.0 ± 0.3	Tested by flexing the sensor and then releasing the device to return to its unperturbed state (100 iterations)	152
PANi	Electropolymerization	Commercially available temporary transfer tattoo paper	3–7	25 s	52.8–59.6 (dependent on bending/stretching conditions)	Tested using GORE-TEX under 50 bending (180°) and 40 stretching (10% in lateral extent) applications	210
PANi	Electrodeposition	Parylene C-coated newspaper	2–12	<10 s	58.2	Tested on a glass rod with respect to a bending radius of 7 mm	134
PANi	Dilute chemical polymerization	PET	3.9–10.1	12.8 s	62.4		7 and 126
PAA-CNTs	Electropolymerization	Si-chips	2–12	3 s	54.5	—	212
SWCNT	Vacuum filtration method	PET	3–11	30 s	59.71	Tested by measuring resistivity upon hard bending	8 and 211
G-PU	Printing	PDMS	5–9	8 s	11.13 ± 5.8	Tested by measuring resistance under 500 stretching cycles (30% strain), with the use of a stepper motor	8
G-PU	Printing	Cellulose-polyester blend cloth	6–9	5 s	47 ± 2	Demonstrated by hard crumpling Tested under 500 bending cycles at 11.40 mm bending radius	133

[30]

TABLE I
POTENTIOMETRIC PH SENSOR RESPONSE OF VARIOUS POLYMERS

Polymer	pH range	pH response (mV/pH)	reference
Polyaniline	3-11	-70	[42]
	2-12	-52	[43, 44]
Metal –tetraaminophthalocyanine	1-13	-55 ± 1	[45]
Linear Polyethylenimine (L-EPI)	3-10	-15 to -45	[43]
Linear Polypropylenimine(L-PPI)	2-11	-43	[44]
Polyaniline/Zeolite Conductive Blend	1-2.5	-310 ± 40	[46]
Polypyrrole/Zeolite Conductive Blend	1-2.5	-1300 ± 100	[46]
Polypyrrole	2-11	-48	[44]
Polyparaphenylenediamne	2-11	-34	[44]

[27]

Annex 2. Thermo-optical properties of TiN

We introduce an interesting additional result to be further investigated. We while measuring the reflectance on TiN sample, we saw a difference in spectra between the TiN flat sample and TiN porous sample.

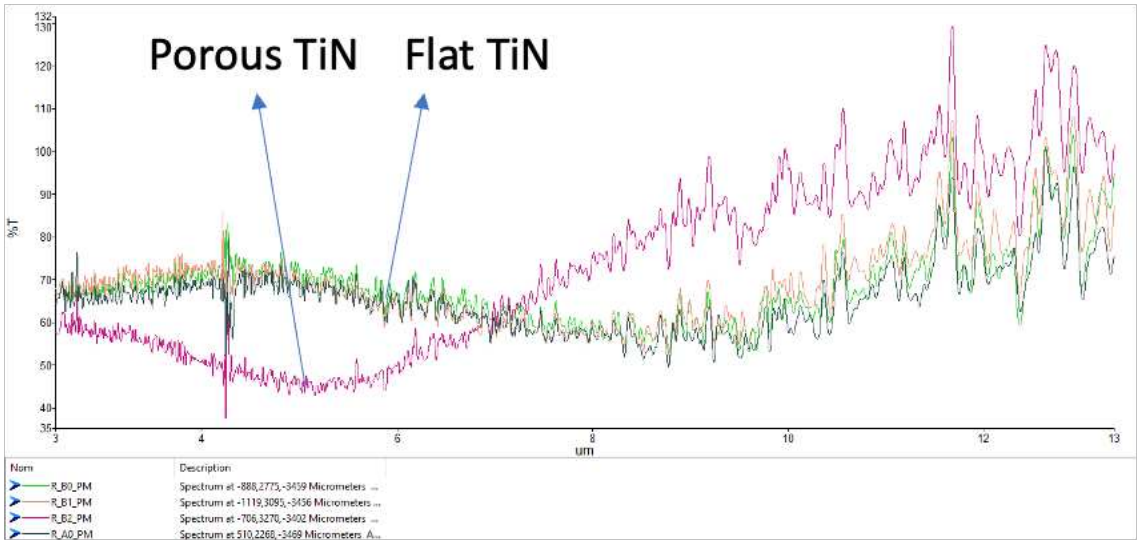

References

[1] B. Carbonne and A. Nguyen, "Surveillance fœtale par mesure du pH et des lactates au scalp au cours du travail," *J. Gynécologie Obstétrique Biol. Reprod.*, vol. 37, no. 1, pp. S65–S71, Feb. 2008, doi: 10.1016/j.jgyn.2007.11.012.

[2] David Daomin Zhou, "CHAPTER 10 - Microelectrodes for in-vivo determination of pH," in *Electrochemical Sensors, Biosensors and their Biomedical Applications*, 2008, pp. 261–305. [Online]. Available: https://www.sciencedirect.com/science/article/abs/pii/B978012373738050012X?via%3Dihub

[3] W. Aoi and Y. Marunaka, "Importance of pH Homeostasis in Metabolic Health and Diseases: Crucial Role of Membrane Proton Transport," *BioMed Res. Int.*, vol. 2014, pp. 1–8, 2014, doi: 10.1155/2014/598986.

[4] L. Gaohua, X. Miao, and L. Dou, "Crosstalk of physiological pH and chemical pKa under the umbrella of physiologically based pharmacokinetic modeling of drug absorption, distribution, metabolism, excretion, and toxicity," *Expert Opin. Drug Metab. Toxicol.*, vol. 17, no. 9, pp. 1103–1124, Sep. 2021, doi: 10.1080/17425255.2021.1951223.

[5] J. Zhang *et al.*, "Bio-responsive smart polymers and biomedical applications," *J. Phys. Mater.*, vol. 2, no. 3, p. 032004, Jul. 2019, doi: 10.1088/2515-7639/ab1af5.

[6] E. Proksch, "pH in nature, humans and skin," *J. Dermatol.*, vol. 45, no. 9, pp. 1044–1052, Sep. 2018, doi: 10.1111/1346-8138.14489.

[7] D. Ayres-de-Campos, S. Arulkumaran, and FIGO Intrapartum Fetal Monitoring Expert Consensus Panel, "FIGO consensus guidelines on intrapartum fetal monitoring: Physiology of fetal oxygenation and the main goals of intrapartum fetal monitoring," *Int. J. Gynecol. Obstet.*, vol. 131, no. 1, pp. 5–8, Oct. 2015, doi: 10.1016/j.ijgo.2015.06.018.

[8] G. Cummins *et al.*, "Sensors for Fetal Hypoxia and Metabolic Acidosis: A Review," *Sensors*, vol. 18, no. 8, p. 2648, Aug. 2018, doi: 10.3390/s18082648.

[9] E. Saling, "Erstmalige Blutgasanalysen und pH-Messungen am Feten unter der Geburt und die klinische Bedeutung dieses neuen Verfahrens," *Arch. Für Gynäkol.*, pp. 198, pages82-86 (1963.

[10] J. M. Giffei and E. Saling, "20. First experience with continuous pH measurements on fetus during delivery," *Arch. Gynecol.*, vol. 226, no. 1–2, pp. 133–139, Sep. 1978, doi: 10.1007/BF02116739.

[11] R. Hanwehr, M.-L. Smith, and B. K. Siesjö, "Extra- and Intracellular pH During Near-Complete Forebrain Ischemia in the Rat," *J. Neurochem.*, vol. 46, no. 2, pp. 331–339, Feb. 1986, doi: 10.1111/j.1471-4159.1986.tb12973.x.

[12] K. M. Busl and D. M. Greer, "Hypoxic-ischemic brain injury: Pathophysiology, neuropathology and mechanisms," *NeuroRehabilitation*, vol. 26, no. 1, pp. 5–13, Jan. 2010, doi: 10.3233/NRE-2010-0531.

[13] P. Kurzweil, "Metal Oxides and Ion-Exchanging Surfaces as pH Sensors in Liquids: State-of-the-Art and Outlook," *Sensors*, vol. 9, no. 6, pp. 4955–4985, Jun. 2009, doi: 10.3390/s90604955.

[14] O. Stamm, U. Latscha, P. Janecek, and A. Campana, "Development of a special electrode for continuous subcutaneous pH measurement in the infant scalp," *Am. J. Obstet. Gynecol.*, vol. 124, no. 2, pp. 193–195, Jan. 1976, doi: 10.1016/S0002-9378(16)33297-5.

[15] M. I. Khan, K. Mukherjee, R. Shoukat, and H. Dong, "A review on pH sensitive materials for sensors and detection methods," *Microsyst. Technol.*, vol. 23, no. 10, pp. 4391–4404, Oct. 2017, doi: 10.1007/s00542-017-3495-5.

[16] S. Paul Shylendra, W. Lonsdale, M. Wajrak, M. Nur-E-Alam, and K. Alameh, "Titanium Nitride Thin Film Based Low-Redox-Interference Potentiometric pH Sensing Electrodes," *Sensors*, vol. 21, no. 1, p. 42, Dec. 2020, doi: 10.3390/s21010042.

[17] M. Liu, Y. Ma, L. Su, K.-C. Chou, and X. Hou, "Titanium nitride nanotube array for potentiometric sensing of pH," p. 3.

[18] M. Nitzan, A. Romem, and R. Koppel, "Pulse oximetry: fundamentals and technology update," *Med. Devices Evid. Res.*, p. 231, Jul. 2014, doi: 10.2147/MDER.S47319.
[19] "ac041608j.pdf."
[20] F. Vivaldi *et al.*, "Recent Advances in Optical, Electrochemical and Field Effect pH Sensors," *Chemosensors*, vol. 9, no. 2, p. 33, Feb. 2021, doi: 10.3390/chemosensors9020033.
[21] M. Yuqing, C. Jianrong, and F. Keming, "New technology for the detection of pH," *J. Biochem. Biophys. Methods*, vol. 63, no. 1, pp. 1–9, Apr. 2005, doi: 10.1016/j.jbbm.2005.02.001.
[22] H.-F. Ji, K. M. Hansen, Z. Hu, and T. Thundat, "Detection of pH variation using modi®ed microcantilever sensors," 2001.
[23] Q. Y. Cai and C. A. Grimes, "A remote query magnetoelastic pH sensor," *Sens. Actuators B Chem.*, vol. 71, no. 1–2, pp. 112–117, Nov. 2000, doi: 10.1016/S0925-4005(00)00599-2.
[24] S. Cao *et al.*, "ISFET-based sensors for (bio)chemical applications: A review," *Electrochem. Sci. Adv.*, Mar. 2022, doi: 10.1002/elsa.202100207.
[25] S. Kumar and R. Thakur, "Soil pH Sensing Techniques and Technologies- A Review," vol. 4, no. 5.
[26] O. Korostynska, "Review on State-of-the-art in Polymer Based pH Sensors," 2007.
[27] O. Korostynska, K. Arshak, E. Gill, and A. Arshak, "Review Paper: Materials and Techniques for *In Vivo* pH Monitoring," *IEEE Sens. J.*, vol. 8, no. 1, pp. 20–28, Jan. 2008, doi: 10.1109/JSEN.2007.912522.
[28] P. Kurzweil, "Metal Oxides and Ion-Exchanging Surfaces as pH Sensors in Liquids: State-of-the-Art and Outlook," *Sensors*, vol. 9, no. 6, pp. 4955–4985, Jun. 2009, doi: 10.3390/s90604955.
[29] W. Xiao and Q. Dong, "The Recent Advances in Bulk and Microfluidic-Based pH Sensing and Its Applications," *Catalysts*, vol. 12, no. 10, p. 1124, Sep. 2022, doi: 10.3390/catal12101124.
[30] L. Manjakkal, S. Dervin, and R. Dahiya, "Flexible potentiometric pH sensors for wearable systems," *RSC Adv.*, vol. 10, no. 15, pp. 8594–8617, 2020, doi: 10.1039/D0RA00016G.
[31] L. Manjakkal, D. Szwagierczak, and R. Dahiya, "Metal oxides based electrochemical pH sensors: Current progress and future perspectives," *Prog. Mater. Sci.*, vol. 109, p. 100635, Apr. 2020, doi: 10.1016/j.pmatsci.2019.100635.
[32] S. P. Shylendra, M. Wajrak, K. Alameh, and J. J. Kang, "Nafion Modified Titanium Nitride pH Sensor for Future Biomedical Applications," *Sensors*, vol. 23, no. 2, p. 699, Jan. 2023, doi: 10.3390/s23020699.
[33] L. Wang, L. Li, T. Zhang, X. Liu, and J.-P. Ao, "Enhanced pH sensitivity of AlGaN/GaN ion-sensitive field effect transistor with Al2O3 synthesized by atomic layer deposition," *Appl. Surf. Sci.*, vol. 427, pp. 1199–1202, Jan. 2018, doi: 10.1016/j.apsusc.2017.09.072.
[34] C.-C. Chen, H.-I. Chen, H.-Y. Liu, P.-C. Chou, J.-K. Liou, and W.-C. Liu, "On a GaN-based ion sensitive field-effect transistor (ISFET) with a hydrogen peroxide surface treatment," *Sens. Actuators B Chem.*, vol. 209, pp. 658–663, Mar. 2015, doi: 10.1016/j.snb.2014.12.025.
[35] M. Liu, Y. Ma, L. Su, K.-C. Chou, and X. Hou, "A titanium nitride nanotube array for potentiometric sensing of pH," *The Analyst*, vol. 141, no. 5, pp. 1693–1699, 2016, doi: 10.1039/C5AN02675J.
[36] C. P. Constantin, M. Aflori, R. F. Damian, and R. D. Rusu, "Biocompatibility of Polyimides: A Mini-Review," *Materials*, vol. 12, no. 19, p. 3166, Sep. 2019, doi: 10.3390/ma12193166.
[37] J. del Valle, N. de la Oliva, M. Muller, T. Stieglitz, and X. Navarro, "Biocompatibility evaluation of parylene C and polyimide as substrates for peripheral nerve interfaces," in *2015 7th International IEEE/EMBS Conference on Neural Engineering (NER)*, Montpellier, France: IEEE, Apr. 2015, pp. 442–445. doi: 10.1109/NER.2015.7146654.
[38] P.-H. Yang, Y.-S. Chang, and C.-T. Chan, "ZnO and AZO Film Potentiometric pH Sensors Based on Flexible Printed Circuit Board," *Chemosensors*, vol. 10, no. 8, p. 293, Jul. 2022, doi: 10.3390/chemosensors10080293.

[39] L. Manjakkal, S. Dervin, and R. Dahiya, "Flexible potentiometric pH sensors for wearable systems," *RSC Adv.*, vol. 10, no. 15, pp. 8594–8617, 2020, doi: 10.1039/D0RA00016G.
[40] J. J. García-Guzmán, C. Pérez-Ràfols, M. Cuartero, and G. A. Crespo, "Toward *In Vivo* Transdermal pH Sensing with a Validated Microneedle Membrane Electrode," *ACS Sens.*, vol. 6, no. 3, pp. 1129–1137, Mar. 2021, doi: 10.1021/acssensors.0c02397.
[41] H.-J. Chung *et al.*, "Stretchable, Multiplexed pH Sensors With Demonstrations on Rabbit and Human Hearts Undergoing Ischemia," *Adv. Healthc. Mater.*, vol. 3, no. 1, pp. 59–68, Jan. 2014, doi: 10.1002/adhm.201300124.
[42] C. Zuliani, F. S. Ng, A. Alenda, A. Eftekhar, N. S. Peters, and C. Toumazou, "An array of individually addressable micro-needles for mapping pH distributions," *The Analyst*, vol. 141, no. 15, pp. 4659–4666, 2016, doi: 10.1039/C6AN00639F.
[43] G. K. Mani *et al.*, "Microneedle pH Sensor: Direct, Label-Free, Real-Time Detection of Cerebrospinal Fluid and Bladder pH," *ACS Appl. Mater. Interfaces*, vol. 9, no. 26, pp. 21651–21659, Jul. 2017, doi: 10.1021/acsami.7b04225.
[44] J.-X. Zhou *et al.*, "Monitoring of pH changes in a live rat brain with MoS2/PAN functionalized microneedles," *Analyst*, vol. 143, no. 18, pp. 4469–4475, 2018, doi: 10.1039/C8AN01149D.
[45] H.-J. Chung *et al.*, "Stretchable, Multiplexed pH Sensors With Demonstrations on Rabbit and Human Hearts Undergoing Ischemia," *Adv. Healthc. Mater.*, vol. 3, no. 1, pp. 59–68, Jan. 2014, doi: 10.1002/adhm.201300124.
[46] W.-D. Huang, H. Cao, S. Deb, M. Chiao, and J. C. Chiao, "A flexible pH sensor based on the iridium oxide sensing film," *Sens. Actuators Phys.*, vol. 169, no. 1, pp. 1–11, Sep. 2011, doi: 10.1016/j.sna.2011.05.016.
[47] T. Guinovart, G. Valdés-Ramírez, J. R. Windmiller, F. J. Andrade, and J. Wang, "Bandage-Based Wearable Potentiometric Sensor for Monitoring Wound pH," *Electroanalysis*, vol. 26, no. 6, pp. 1345–1353, Jun. 2014, doi: 10.1002/elan.201300558.
[48] H. J. Park, J. H. Yoon, K. G. Lee, and B. G. Choi, "Potentiometric performance of flexible pH sensor based on polyaniline nanofiber arrays," *Nano Converg.*, vol. 6, no. 1, p. 9, Dec. 2019, doi: 10.1186/s40580-019-0179-0.
[49] P. Malkaj, E. Dalas, E. Vitoratos, and S. Sakkopoulos, "pH electrodes constructed from polyaniline/zeolite and polypyrrole/zeolite conductive blends," *J. Appl. Polym. Sci.*, vol. 101, no. 3, pp. 1853–1856, Aug. 2006, doi: 10.1002/app.23590.
[50] L. Jiang and L. Gao, "Fabrication and Characterization of Carbon Nanotube-Titanium Nitride Composites with Enhanced Electrical and Electrochemical Properties," *J. Am. Ceram. Soc.*, vol. 89, no. 1, pp. 156–161, Jan. 2006, doi: 10.1111/j.1551-2916.2005.00687.x.
[51] H. Du, Y. Xie, C. Xia, W. Wang, and F. Tian, "Electrochemical capacitance of polypyrrole–titanium nitride and polypyrrole–titania nanotube hybrids," *New J. Chem.*, vol. 38, no. 3, p. 1284, 2014, doi: 10.1039/c3nj01286g.
[52] M. Stelzle, A. Stett, B. Brunner, M. Graf, and W. Nisch, "[No title found]," *Biomed. Microdevices*, vol. 3, no. 2, pp. 133–142, 2001, doi: 10.1023/A:1011450326476.
[53] T. Nguyen *et al.*, "pH and SpO2 Miniaturized Sensors for Fetal Health Monitoring:," in *Proceedings of the 15th International Joint Conference on Biomedical Engineering Systems and Technologies*, Online Streaming, --- Select a Country ---: SCITEPRESS - Science and Technology Publications, 2022, pp. 155–161. doi: 10.5220/0010867200003123.
[54] T. Nguyen *et al.*, "pH and SpO2 Miniaturized Sensors for Fetal Health Monitoring:," in *Proceedings of the 15th International Joint Conference on Biomedical Engineering Systems and Technologies*, Online Streaming, --- Select a Country ---: SCITEPRESS - Science and Technology Publications, 2022, pp. 155–161. doi: 10.5220/0010867200003123.
[55] P.-H. Yang, C.-T. Chan, and Y.-S. Zhang, "ZnO Film Flexible Printed Circuit Board pH Sensor Measurement and Characterization," *IEEE Access*, vol. 10, pp. 96091–96099, 2022, doi: 10.1109/ACCESS.2022.3205320.
[56] J. Zhou, L. Zhang, and Y. Tian, "Micro Electrochemical pH Sensor Applicable for Real-Time Ratiometric Monitoring of pH Values in Rat Brains," *Anal. Chem.*, vol. 88, no. 4, pp. 2113–2118, Feb. 2016, doi: 10.1021/acs.analchem.5b03634.

[57] M. Nedergaard, R. P. Kraig, J. Tanabe, and W. A. Pulsinelli, "Dynamics of interstitial and intracellular pH in evolving brain infarct," *Am. J. Physiol.-Regul. Integr. Comp. Physiol.*, vol. 260, no. 3, pp. R581–R588, Mar. 1991, doi: 10.1152/ajpregu.1991.260.3.R581.
[58] L. Gaohua, X. Miao, and L. Dou, "Crosstalk of physiological pH and chemical pKa under the umbrella of physiologically based pharmacokinetic modeling of drug absorption, distribution, metabolism, excretion, and toxicity," *Expert Opin. Drug Metab. Toxicol.*, vol. 17, no. 9, pp. 1103–1124, Sep. 2021, doi: 10.1080/17425255.2021.1951223.
[59] J. Zhang *et al.*, "Bio-responsive smart polymers and biomedical applications," *J. Phys. Mater.*, vol. 2, no. 3, p. 032004, Jul. 2019, doi: 10.1088/2515-7639/ab1af5.
[60] T. Nguyen, B. Journet, H. Takhedmit, and G. Lissorgues, "Porous Titanium Nitride electrodes on miniaturised pH sensor for foetal health monitoring application," in *2022 Symposium on Design, Test, Integration and Packaging of MEMS/MOEMS (DTIP)*, Pont-a-Mousson, France: IEEE, Jul. 2022, pp. 1–4. doi: 10.1109/DTIP56576.2022.9911738.
[61] K. Matthes., "Untersuchungen fiber die Sauerstoffs~ittigung des menschlichen Arterienblutes [Studies on the Oxygen Saturation of Arterial Human Blood]," *Naunyn-Schmiedebergs Arch. Pharmacol. Ger.*, vol. 13, no. 10, pp. 434–444, doi: doi:10.1063/1.1769941.
[62] J. W. Severinghaus, "Takuo Aoyagi: Discovery of Pulse Oximetry," *Anesth. Analg.*, vol. 105, no. 6, pp. S1–S4, Dec. 2007, doi: 10.1213/01.ane.0000269514.31660.09.
[63] T. Aoyagi, "Pulse oximetry: its invention, theory, and future," *J. Anesth.*, vol. 17, no. 4, pp. 259–266, Nov. 2003, doi: 10.1007/s00540-003-0192-6.
[64] W. Tin and M. Lal, "Principles of pulse oximetry and its clinical application in neonatal medicine," *Semin. Fetal. Neonatal Med.*, vol. 20, no. 3, pp. 192–197, Jun. 2015, doi: 10.1016/j.siny.2015.01.006.
[65] K. Miyasaka *et al.*, "Tribute to Dr. Takuo Aoyagi, inventor of pulse oximetry," *J. Anesth.*, vol. 35, no. 5, pp. 671–709, Oct. 2021, doi: 10.1007/s00540-021-02967-z.
[66] "Vital Sign Measurement Across the Lifespan".
[67] "American Lung Association. (2021). Pulse oximetry. Retrieved August 24, 2022, from https://www.lung.org/lung-health-diseases/lung-procedures-and-tests/pulse-oximetry (Level VII)".
[68] M. Nitzan, A. Romem, and R. Koppel, "Pulse oximetry: fundamentals and technology update," *Med. Devices Evid. Res.*, p. 231, Jul. 2014, doi: 10.2147/MDER.S47319.
[69] J. Park, H. S. Seok, S.-S. Kim, and H. Shin, "Photoplethysmogram Analysis and Applications: An Integrative Review," *Front. Physiol.*, vol. 12, p. 808451, Mar. 2022, doi: 10.3389/fphys.2021.808451.
[70] H. Lee, H. Ko, and J. Lee, "Reflectance pulse oximetry: Practical issues and limitations," *ICT Express*, vol. 2, no. 4, pp. 195–198, Dec. 2016, doi: 10.1016/j.icte.2016.10.004.
[71] M. Niwayama, H. Murata, S. Sone, and S. Shinohara, "Noncontact measurement of deep tissue absorption coefficient using Spatially Resolved Near-Infrared Spectroscopy," *IEEJ Trans. Electr. Electron. Eng.*, vol. 2, no. 4, pp. 485–487, Jul. 2007, doi: 10.1002/tee.20197.
[72] O. Y. Hay *et al.*, "Pulse Oximetry with Two Infrared Wavelengths without Calibration in Extracted Arterial Blood," p. 13.
[73] C.-C. Sun, K. Chun, T. T. Thai, and Y.-W. Yang, "Low-power microcontroller solution for measuring HBR using single reflection SpO2 Sensor," in *2015 IEEE International Conference on Consumer Electronics - Taiwan*, Taipei, Taiwan: IEEE, Jun. 2015, pp. 82–83. doi: 10.1109/ICCE-TW.2015.7217042.
[74] N. Kanayama and M. Niwayama, "Examiner's finger-mounted fetal tissue oximetry," *J. Biomed. Opt.*, vol. 19, no. 6, p. 067008, Jun. 2014, doi: 10.1117/1.JBO.19.6.067008.